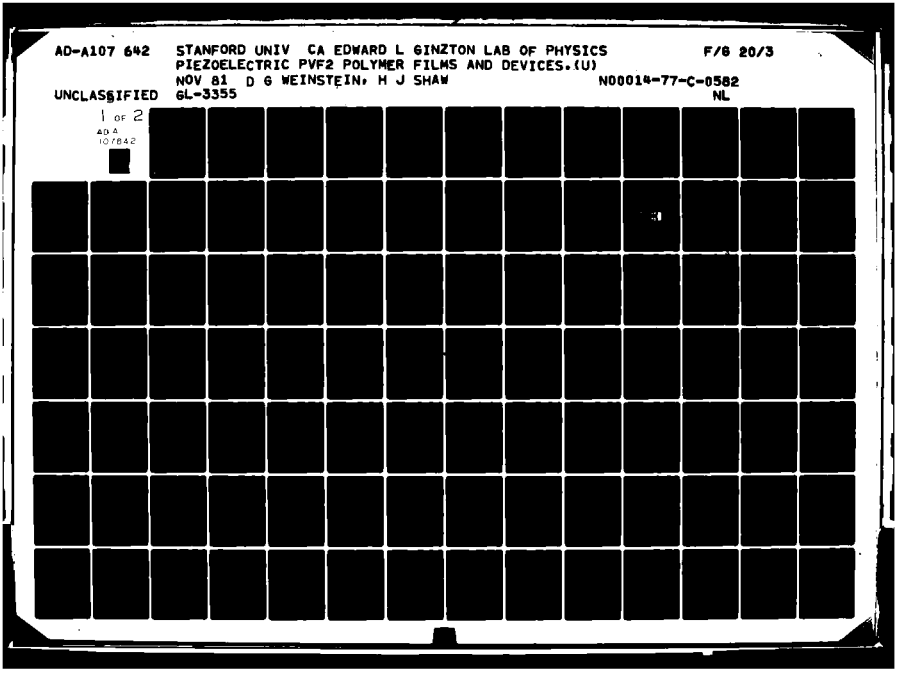
AD-A107 642
STANFORD UNIV CA EDWARD L GINZTON LAB OF PHYSICS
F/G 20/3
PIEZOELECTRIC PVF2 POLYMER FILMS AND DEVICES.(U)
NOV 81 D G WEINSTEIN, H J SHAW
N00014-77-C-0582
UNCLASSIFIED
GL-3355
NL
1 OF 2
AD A
107842

UNCLASSIFIED

SECURITY CLASSIFICATION OF THIS PAGE (When Data Entered)

REPORT DOCUMENTATION PAGE	READ INSTRUCTIONS BEFORE COMPLETING FORM
1 REPORT NUMBER	2 GOVT ACCESSION NO. / 3 RECIPIENT'S CATALOG NUMBER
4 TITLE (and Subtitle) PIEZOELECTRIC PVF_2 POLYMER FILMS AND DEVICES	5 TYPE OF REPORT & PERIOD COVERED Final Report 8-1-77 through 1-31-81
	6 PERFORMING ORG. REPORT NUMBER G.L. 3355
7 AUTHOR(s) D. G. Weinstein and H. J. Shaw	8 CONTRACT OR GRANT NUMBER(s) N00014-77-C-0582
9 PERFORMING ORGANIZATION NAME AND ADDRESS Stanford University Edward L. Ginzton Laboratory Stanford, California 94305	10 PROGRAM ELEMENT, PROJECT, TASK AREA & WORK UNIT NUMBERS NR 384-925
11 CONTROLLING OFFICE NAME AND ADDRESS Office of Naval Research Department of the Navy 800 N. Quincy St., Arlington, Virginia 22217	12 REPORT DATE November 1981
	13 NUMBER OF PAGES 126
14 MONITORING AGENCY NAME & ADDRESS (if different from Controlling Office)	15 SECURITY CLASS. (of this report) Unclassified
	15a DECLASSIFICATION DOWNGRADING SCHEDULE

16 DISTRIBUTION STATEMENT (of this Report)

Approved for public release; distribution unlimited.

17 DISTRIBUTION STATEMENT (of the abstract entered in Block 20, if different from Report)

18 SUPPLEMENTARY NOTES

19 KEY WORDS (Continue on reverse side if necessary and identify by block number)

Piezoelectric Films
Piezoelectric Transducers
Polyvinylidene Fluoride (PVF_2)
Phased Arrays
Nondestructive Testing
Acoustic Imaging
Monolithic Acoustic Arrays

20 ABSTRACT (Continue on reverse side if necessary and identify by block number)

Acoustic transducers and imaging arrays using PVF_2 piezoelectric film as the active element have been extensively explored. Thin disk PVF_2 bulk wave transducers were experimentally developed and studied using a computer model. Aspects of transducer behavior studied include bandwidth, impulse response, insertion loss, internal loss, impedance matching, and angular response. A monolithic multielement PVF_2 transducer array is described which uses photolithographic techniques to achieve a reproducible, inexpensive and highly accurate integrated device for ultrasonic imaging applications. This array was used to produce an

DD FORM 1 JAN 73 1473

81

UNCLASSIFIED

SECURITY CLASSIFICATION OF THIS PAGE When Data Entered

AD A107642

DTIC FILE COPY

DTIC ELECTE NOV 24 1981

electronically focused and scanned acoustic beam. Two-dimensional acoustic images of small test objects were performed, to investigate the beam shape and imaging ahcarateristics, which were found to be consistent with theoretical predictions. At a frequency of 2.25 MHz and an f/number of 5, a resolution in the range of 3 mm was observed.

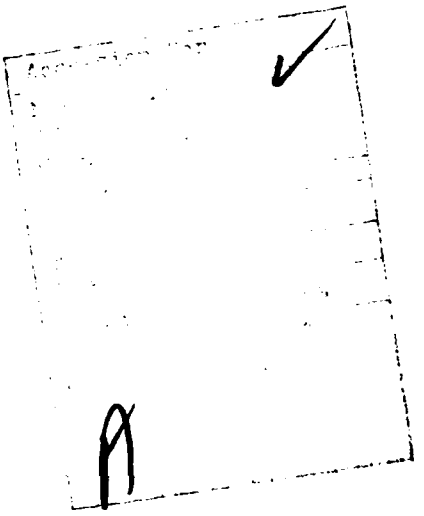

TABLE OF CONTENTS

		Page
I.	INTRODUCTION	1
II.	BACKGROUND MATERIAL	3
	A. PVF_2 BACKGROUND	3
	B. TRANSDUCER FUNDAMENTALS	10
III.	FABRICATION OF PVF_2 BULK WAVE TRANSDUCERS	14
	A. PVF_2 PROCESSING	14
	B. EXPERIMENTAL LABORATORY TRANSDUCERS	16
	C. IMPROVED DESIGN FOR APPLICATIONS	18
IV.	THEORY OF PVF_2 BULK WAVE TRANSDUCERS	20
	A. INTRODUCTION	20
	B. A TRANSDUCER MODEL	20
	C. TRANSDUCER ANALYSIS	30
V.	EXPERIMENTAL RESULTS WITH PVF_2 BULK WAVE TRANSDUCERS	46
	A. INTRODUCTION	46
	B. UNTUNED TRANSDUCER PERFORMANCE	47
	C. ELECTRICAL TUNING	53
	D. FOLDED PVF_2 TRANSDUCERS	58
	E COMPENSATION FOR LOW PIEZOELECTRIC ACTIVITY IN PVF_2	58
VI.	ANGLE RESPONSE OF PVF_2 TRANSDUCERS	68
	A. INTRODUCTION	68
	B. BASIC PROPERTIES OF ACOUSTIC FACEPLATES	69
	C. THEORETICAL STUDY OF PVF_2 FACEPLATES	73
	1. Single Layer Faceplates	73

Page

2. Multilayer Faceplates 76

3. Experimental PVF_2 Angle Response 80

VII. INVESTIGATION OF PVF_2 FILM PROPERTIES 82

A. INTRODUCTION 82

B. MEASUREMENT OF SPATIAL DEPENDENCE OF PIEZOELECTRIC ACTIVITY ACROSS FILM THICKNESS 82

C. EVALUATION OF PVF_2 FILMS BY TRANSDUCER TESTING 88

VIII. PVF_2 IMAGING ARRAYS 93

A. INTRODUCTION 93

B. TYPES OF IMAGING SYSTEMS 94

C. MATHEMATICS OF IMAGING 96

D. DESIGN AND CONSTRUCTION OF THE PVF_2 BULK WAVE IMAGING ARRAY 101

1. Description of the Physical Features of the Array 101

2. Design Considerations 103

3. Construction of the Array 109

4. Conclusion 110

E. EXPERIMENTAL IMAGING RESULTS 110

1. Array Electronic System 110

2. Calibration Tests 114

3. Imaging Test 115

4. Conclusion 122

REFERENCES 124

I. INTRODUCTION

In recent years acoustic techniques and methods have been increasingly applied in the field of nondestructive testing and evaluation (NDE) of materials and structures, and numerous types of acoustic testing devices have been developed. The importance of acoustics in NDE efforts is expected to increase in the future. Thus there is a continuing need for progress in the development of realiable, effective, and inexpensive ultrasonic devices. An important class of these devices consists of piezoelectric acoustic transducers and imaging arrays.

This is a report on the application of a new piezoelectric material, polyvinylidene fluoride (PVF_2), to acoustic transducers and arrays. We explore useful and novel features that these devices can possess.

PVF_2 is a relative newcomer to the field of acoustics. Usually, hard ceramic materials such as PZT (lead zirconate-titanate) are employed as the piezoelectric element in acoustic transducers. Many other solids such as quartz, bone, tendons and wood exhibit piezoelectricity, but in nearly all cases this piezoelectricity is extremely weak. In 1969, however, Kawai[1] in Japan showed that PVF_2 is strongly piezoelectric compared to other polymers.

PVF_2 has already found commercial applications outside the field of ultrasonic transducers and NDE. Among the strong piezoelectrics, it has a unique set of properties. Rather than being a hard ceramic material, it is flexible and can be made to conform to desired shapes including thin films for use as transducers at high frequencies. PVF_2 also has an unusual combination of acoustic and dielectric properties, aside from its piezoelectricity and its mechanical properties, which are very different from those of the standard piezoelectrics

and which have important consequences for ultrasonic transducers and imaging arrays, as will be shown.

This report describes our research on PVF_2. At the beginning of this research PVF_2 had just begun to be ivnestigated as an ultrasonic transducer material. We began by developing simple bulk wave PVF_2 transducers. Computer models were developed which allowed us to test and understand the behavior of many transducer designs. Following this work, we used the accumulated knowledge to design and construct a high quality multielement PVF_2 bulk wave imaging array of high accuracy and simple design, using reproducible, easily available techniques.

II. BACKGROUND MATERIAL

A. PVF_2 BACKGROUND

In this section we take a brief look at the structure and properties of PVF_2.

PVF_2, being a polymer, consists of long chains which repeat a basic molecular building block many times. The basic building block, or monomer, of PVF_2 is the group $-CH_2-CF_2-$.

Figure 1 shows part of a PVF_2 molecular chain. The polymer chain consists of a carbon backbone onto which pairs of alternating hydrogen or fluorine molecules are bonded. Dipole moments exist between the hydrogens and the carbons and between the fluorines and the carbons. It is these dipole moments which give PVF_2 most of its piezoelectricity.

In a bulk sample of PVF_2 an individual chain can take many forms and shapes. These various forms occur because the carbon backbone can twist and turn into a wide variety of stable states. There are also numerous ways in which these chains can be aligned with regard to one another. There are at least three possible crystalline phases - alpha, beta, and gamma, as well as an amorphous phase. These phases differ from each other in both the structures of their chains and the way these chains are arranged to form the crystal structure.

The beta phase has a higher piezoelectric constant than any other phase. The chain shown in Fig. 1 is a beta phase chain. The figure also shows (from an end on view) the arrangement of these chains in a unit cell of beta PVF_2. Beta phase PVF_2 belongs to the crystalline symmetry class orthorhombic 2mm. Unfortunately, when PVF_2 is crystallized from the melt

PLANAR ZIGZAG CONFORMATION

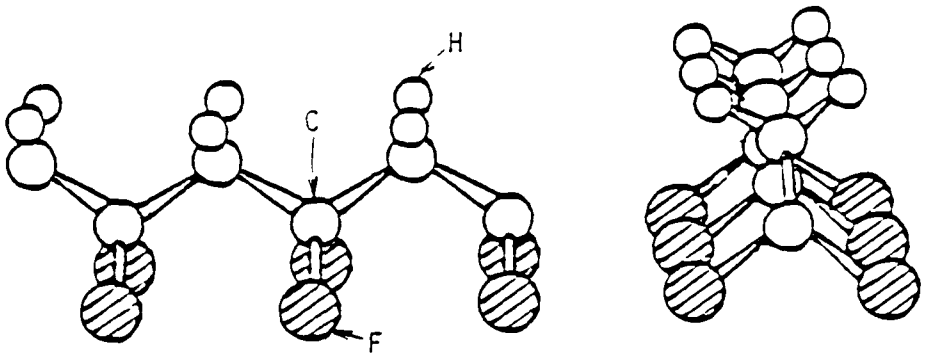

(a)

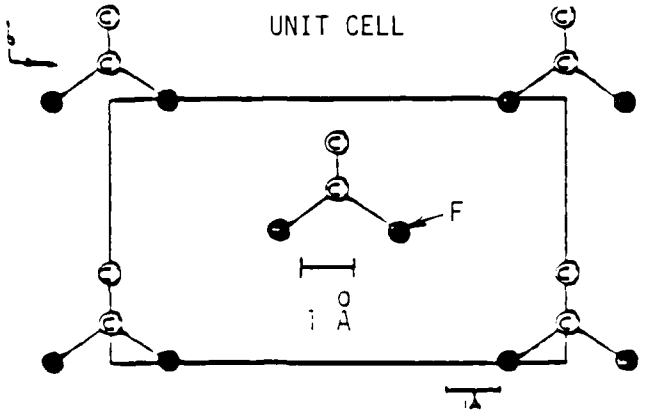

(b)

Fig. 1--(a) Planar zigzag (tttt) chain conformation for β-form PVF_2, (b) unit cell structure.

under standard laboratory conditions, the alpha phase is preferentially formed. Alpha phase film can be converted into the more active beta film by uniaxially stretching the PVF_2. This forces an untangling of any twisted molecular chains which are present, as well as a phase change. The film is generally increased in length by a factor of 3-5 during this process. Following this procedure the film is then poled in order to rotate and align the dipole moments all in the same direction. Poling fields are on the order of 80 volts/micron. The poling field is applied perpendicular to the film surface. This is usually defined as the z coordinate direction, while the stretching direction is taken as the x axis.

Since PZT-5A is a commonly used piezoelectric ceramic it is interesting and useful to compare its properties to those of PVF_2. The physical properties of PVF_2 are listed in Table I along with those of PZT-5A.

One very important difference is the piezoelectric strength of the two materials. Two of the values listed in Table I involve piezoelectric strength. One a is component of the piezoelectric stress constant tensor, e_{33}. The complete e tensor appears in the piezoelectric constitutive relations:

$$\underline{T} = -\underline{\underline{e}} \cdot \underline{E} + \underline{\underline{c}}^{E} : \underline{S} \qquad (1)$$

$$\underline{D} = \underline{\underline{\varepsilon}}^{S} \cdot \underline{E} + \underline{\underline{e}} : \underline{S}$$

where T is a 6 x 1 stress tensor,

S is a 6 x 1 strain tensor,

E is the electric field vector (3 x 1)

D is the displacement vector (3 x 1)

TABLE I

	PVF_2	PZT-5A
Density, (gm/cm^3)	1.78	7.75
Stiffened acoustic velocity (m/sec)	2150	4350
Elastic constant (N/m^2), C_{33}	9×10^9	11.1×10^{10}
Acoustic impedance (kg/m^2-S) $\times 10^6$	3.82	33.7
Relative dielectric constant, $\varepsilon^s_{33}/\varepsilon_o$	8	830
Piezoelectric stress constant e_{33} ($Coulombs/m^2$)	-.08 to -.165	15.8
electromechanical coupling constant	.01 to .04	.31

$\underline{\underline{c}}$ is the elastic stiffness matrix at zero $\underline{E}$ field (6 x 6)

$\underline{\underline{\varepsilon}}^S$ is the dielectric matrix at zero strain (3 x 3)

$\underline{\underline{e}}$ is the piezoelectric stress constant matrix (6 x 3)

If all components of $\underline{\underline{e}}$ are zero, Eqs. (1) and (2) reduce to two separate and uncoupled equations, one relating stress to strain, and the other relating $\underline{D}$ to $\underline{E}$. Thus, the larger the magnitude of $\underline{\underline{e}}$, the greater the coupling between elastic and electrical effects.

Because PVF_2 has a crystal symmetry of the class orthorhombic 2mm, symmetry arguments require that the $\underline{\underline{e}}$ tensor of PVF_2 must have the following form

$$\underline{\underline{e}} = \begin{bmatrix} 0 & 0 & 0 & 0 & e_{15} & 0 \\ 0 & 0 & 0 & e_{24} & 0 & 0 \\ e_{31} & e_{32} & e_{33} & 0 & 0 & 0 \end{bmatrix}$$

The most important component of the $\underline{\underline{e}}$ tensor is e_{33}. Remember that the z direction is defined parallel to the poling direction or, equivalently, perpendicular to the surface of the PVF_2 film. All our PVF_2 devices use the e_{33} component of the tensor. Components e_{31} and e_{32} are important in some situations, but they are generally secondary in importance to e_{33}. Components e_{24} and e_{15} are not used in the work presented here.

Table I gives a value of e_{33} between -.08 coulombs/m^2 and -.165 coulombs/m^2 for PVF_2. The lower value best fits the characteristics of our PVF_2 devices. However Ohigashi has reported larger values of e_{33}, up to -.165 coulombs/m^2 (ref. 2). These differences may be due to

variations in the processing parameters used in the fabrication of the PVF_2 samples tested.

A quantity which gives a better measure of the acoustic radiating power of a transducer is the dimensionless electromechanical coupling coefficient, k_t^2 . $K_t(33)^2$ is defined by the equation:

$$K_t(33)^2 = \frac{e_{33}^2}{C_{33}\varepsilon_{33}}$$

where C_{33} is a component of the elastic stiffness matrix that appears in Eq. (1) and e_{33} is a component of the dielectric constant matrix that appears in Eq. (2).

K_t^2 can often be used as a figure of merit. It can be defined in terms of energy in the following manner. Assume a transducer has electrodes covering the faces which are perpendicular to the z direction. Further assume that the thickness of the transducer in the z direction is small compared to the lateral size of the transducer. When an electric field parallel to the z direction is used to drive the transducer, $K_t(33)^2$ is approximately the ratio of the stored electrical energy in the piezoelectric to the stored elastic energy.

It is also a good measure of the acoustic insertion loss of an electrically driven piezoelectric, since the output of a transducer is often proportional to K_t^2 , rather than e_{33} . Table I lists the values of K_t^2 for PVF_2 and PZT. A range of values is given corresponding to the range of e_{33} values mentioned above. PVF_2 is about an order of magnitude weaker than PZT-5A in this regard. Clearly, this is a disadvantage of PVF_2 with respect to PZT-5A.

However, the acoustic impedance of PVF_2 (3.82) is much closer to that of water (1.48) than that of PZT-5A (34.3). When operating into a water load such a low impedance is a distinct advantage since it minimizes reflections at the water-transducer interface. This, in turn allows large frequency bandwidths and a clean impulse response without resorting to matching layers. This fact is important because water is a very convenient medium in which to test materials for flaws. Besides this, the human body, which is of prime importance in medical imaging, is largely water and thus matches well acoustically to PVF_2.

Furthermore, PVF_2 is thin and flexible while PZT is hard and difficult to work with in thin layers. Thus PVF_2 can conform to simple curved shapes if conditions demand such flexibility. Very thin films (on the order of 5 microns) have the prospect for use as fundamental mode transducers at frequencies near 90 MHz. Earlier work has shown that piezoelectric activity in PVF_2 persists up to 500 MHz.[3] In contrast to these figures, PZT is rarely used as an acoustic transducer above 10 MHz because of difficulties in working with the very thin and brittle PZT plates required to achieve resonant frequencies above 10 MHz.

The dielectric constant of PVF_2 shown in Table I is quite low when compared to that of PZT. It is helpful when receiving acoustic energy with PVF_2. The reasons for this will be explained in Section V-E which deals with methods of compensating for the low K_t^2 of PVF_2. The ability of PVF_2 to withstand high electric fields without breaking down or depoling will also be covered in Section V-E. The use of such large electric fields to drive PVF_2 transducers can also compensate for the low K_t^2 of the polymer.

B. TRANSDUCER FUNDAMENTALS

Practical ultrasonic transducers often approximate plane layered structures, consisting of a piezoelectric layer plus acoustic impedance matching layers, backing material and load material. Figure 2 shows such a device. When a voltage is applied across the piezoelectric layer, acoustic waves are radiated through any intervening matching layers present, into the load and backing materials.

If the applied voltage is sinusoidal in time, the power radiated by the transducer will depend on the frequency of the driving voltage. At a particular frequency, usually referred to as the resonant frequency, the power radiated into the load material will be a maximum. Most transducers using piezoelectric ceramics (such as lead zirconate titanate--PZT) will deliver maximum power to the load, or resonate, when the piezoelectric layer has a thickness equal to $\lambda/2$, where λ is the acoustic wavelength in the piezoelectric. This occurs because the ceramics have high acoustic impedances and thus are usually bounded by lower impedance materials when used in transducers. The phase shifts which occur when acoustic waves are reflected off the boundaries result in the $\lambda/2$ resonant condition mentioned above.

The shape of the resonant power peak as a function of frequency also depends on the relative acoustic impedances of the system. The reflection coefficient, R , for acoustic waves incident on a plane boundary is

$$R = \frac{Z_2 - Z_1}{Z_2 + Z_1} \qquad (3)$$

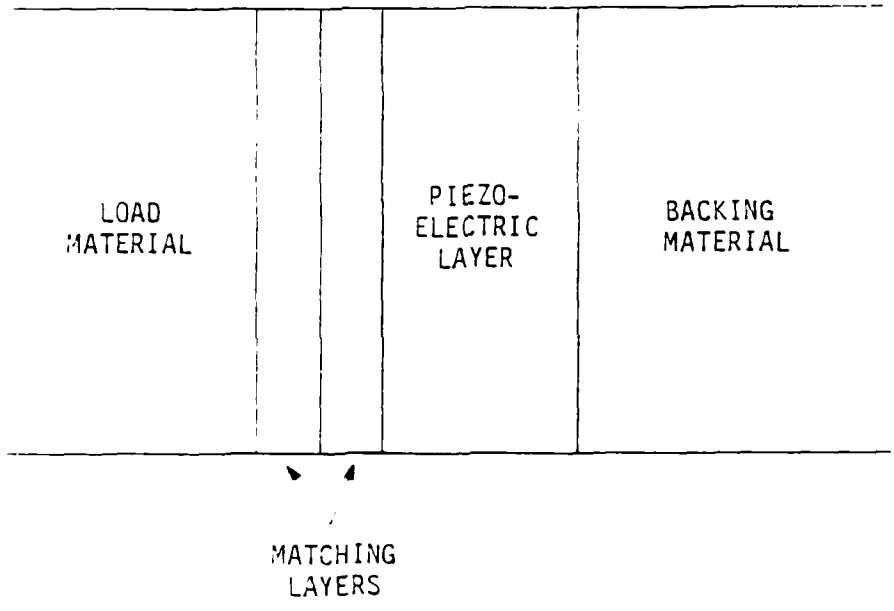

Fig. 2--Transducer with matching layers.

where Z_1 and Z_2 are the acoustic impedances of the reflecting material and the propagation material, respectively. The closer the impedance match between the two materials, the less the reflection. Ceramic transducers have an impedance ~ 34 x 10^6 kg/m^2-sec, while the most common and convenient load material, water, has an impedance of 1.48. Therefore, waves attempting to leave the ceramic and enter the water are highly reflected. This causes complex reverberations in the ceramic leading to (1) a very sharp resonant power peak, i.e., narrow bandwidth when operated with cw or long tone pulse excitation, (2) poor impulse response when operated with short pulses, and (3) inefficient power transfer even at the resonant frequency. For these reasons, matching layers of intermediate impedances are generally placed between the ceramic and the water.

Currently, most PZT transducers employ matching layers in order to increase the transducer efficiency. For instance, a half inch diameter PZT-5A transducer with a resonant frequency of 3.5 MHz will typically have a power conversion efficiency of ~ 5% when driven from a 50 ohm source. The addition of two carefully chosen matching layers and an electrical matching network between the power source and the transducer will raise the conversion efficiency to ~ 60%.[4]

Many of our PVF_2 transducers are different than those just described. We usually construct PVF_2 transducers by bonding electroded PVF_2 onto the flat face of a brass cylinder. As the acoustic impedance of PVF_2 is ~ 4 while brass has an impedance of ~ 32, acoustic reflections at the brass-PVF_2 boundary have a 180° phase shift relative to reflections occurring in transducers using ceramic piezoelectric elements. It turns out therefore,

that these PVF_2 transducers resonate in a $\lambda/4$ thickness mode, not a $\lambda/2$ mode as is normally the case. However, when a PVF_2 transducer is backed by a material having an acoustic impedance lower than that of PVF_2, the device will resonate in a $\lambda/2$ mode.

There are other consequences of the low impedance of PVF_2. The large impedance mismatch at the brass interface reflects most of the acoustic energy toward the load, where it is needed. The relatively good impedance match between the PVF_2 and water results in efficient transfer of acoustic energy and a broadband resonance curve. PVF_2 transducers radiate a bipolar acoustic wave when excited by a voltage impulse. Such an impulse response is more desirable than the many-cycled ringing impulses response often experienced with piezoelectric ceramics because shorter (in time) transducer impulse responses allow better resolution (in space) when used in time domain reflectometry and acoustic imaging.

At the start of this research PVF_2 had been previously studied as a transducer material by several researchers. In 1973, Sussner[3] reported on the generation of acoustic waves at frequencies up to 500 MHz using PVF_2. PVF_2 transducers were first fabricated at our laboratory by Bui.[6] He measured the spectral response of the transducers and found it to be extremely broadband. Later he measured both the acoustic loss factor (the Q) and the piezoelectric coupling coefficient using a resonance method which was applied to an air-backed PVF_2 film.[6]

III. FABRICATION OF PVF_2 BULK WAVE TRANSDUCERS

A procedure devised for fabricating simple, thin disk PVF_2 bulk wave transducers useful for laboratory experiments will be presented. The process of electroding and poling the PVF_2 film will be described in detail. A more rugged and practical version of PVF_2 bulk wave transducers will also be described.

A. PVF_2 PROCESSING

The PVF_2 used in this work was obtained through two sources. One was the Kureha Corp. of Japan. The Kureha PVF_2 was either 9 or 25 microns thick. As received, it was uniformly electroded on both sides with an aluminum covering of approximately 500 angstroms, and had been stretched uniaxially and poled normal to its face.

The other source was the Stanford Center for Materials Research. Films in various thicknesses fabricated under an NSF MRL program were made available for use in device research.

We found that for most of our applications a gold electrode covering on the PVF_2 was preferable to an aluminum electrode. Aluminum electrodes tend to disintegrate after even brief exposures to water. Furthermore, the electrical conductivity of the aluminum electrodes is not as high as that of gold.

We fabricated gold electrodes on the film samples by vacuum deposition. In the case of Kureha films, the aluminum electrodes were first removed using sodium hydroxide.

After cleaning the film, a thin ($\sim$ 50 angstrom) layer of chromium was evaporated on the PVF_2 using an electron gun deposition system. Immediately after the chromium was deposited, a 1000 angstrom layer of gold was evaporated on top of the chromium. A chromium-gold electrode is preferable to a pure gold electrode because chromium usually adheres better to the substrate than gold. Care must be taken, however, that the chromium does not oxidize before the gold is applied. If this occurs, the gold layer will not be very durable. Nor will it be possible to selectively etch miniature electrode patterns in the chromium, because the oxide resists etching.

The deposition of the electrode layers heats the PVF_2. Most of the heat is released by the recrystallization of the gold layer. The amount of heat released by this process can be estimated as equal to the heat needed to vaporize the gold originally. It takes 84 kilocalories to vaporize one mole of gold. Assuming a 1000 Å thick layer of gold is deposited, and taking the specific heat of PVF_2 to be .2 cal/gm°C,[7] we find that the temperature rise is on the order of 100°C degrees for a 25 micron film. A 9 micron film will experience a temperature change about three times this value. This temperature increase can be large enough to deform and melt the PVF_2. The Curie temperature of PVF_2 is believed to be near the melting temperature, which is $\sim$ 180 degrees. As room temperature is 25 degrees, we see that increases of $\sim$ 150 degrees might allow the film to rise above the Curie temperature, resulting in massive disordering of the film structure and loss of piezoelectric activity. As expected, 9 micron films were much more prone to suffer damage than 25 micron films. In order to keep the film as cool as possible the PVF_2 was stretched across a slightly domed aluminum surface during the evaporation procedure. An o-ring was used to provide

radial tension in order to keep the film against the aluminum heat sink. We often used a mask to produce many circular electrodes on one piece of film rather than covering the entire film area with gold. This also seemed to keep the temperature rise down and resulted in less damage to the films during evaporation.

After the electrodes had been applied, the PVF_2 was poled. Typical poling parameters were an applied voltage of 2000 volts across the 25 micron PVF_2 (a field strength of 800,000 volts/cm or 80 volts/micron) for two hours at a temperature of 80 degrees centigrade. The poling took place either in an oil bath or an air oven.

The poling parameters listed above were standardized on because they produced a film with near maximum piezoelectricity with a high yield. Up to a point, higher applied poling fields at higher temperatures result in a more piezoelectrically active film. Beyond this point however, a plateau is reached, and increases in the poling parameters will not significantly increase the piezoelectricity of the finished product. Further increases in the poling parameters will at some point actually destroy the film.

B. EXPERIMENTAL LABORATORY TRANSDUCERS

PVF_2 bulk wave transducers can be constructed quite easily. We bonded poled, electroded PVF_2 onto smooth brass rods, as seen in Fig. 3. The size of the film ranged from a 1/4 inch diameter circle up to a 1/2 inch by 1/2 inch square. Some care was taken to achieve a thin, uniform bond. The surfaces to be bonded were fully cleaned and the epoxy was mixed carefully to avoid producing bubbles. The film was pressed against the brass with a

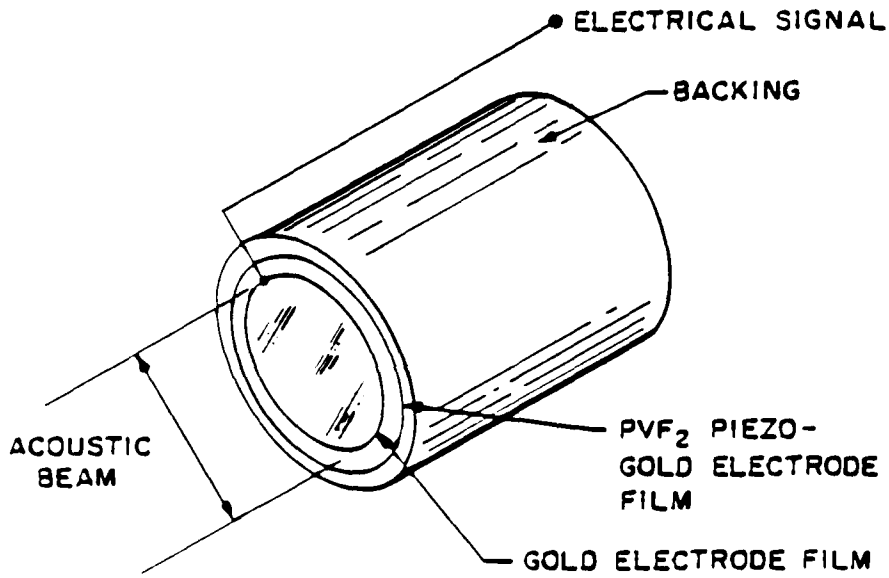

Fig. 3--Schematic of simple experimental transducers.

firm rubber sphere. This insures that the epoxy is spread radially away from the center of the film so that no air pockets form.[8] In order to obtain thin, uniform bonds we used a relatively non-viscous epoxy, Epotek V-6. This required curing times of $\sim$ 5 hours at 60 degrees centigrade.

Electrical contact was established to the top electrode using silver paint and a thin wire. The back electrode of the film is quite possibly in contact with the brass rod at several points due to imperfections in the epoxy layer between the brass and the gold In any case, the back electrode will be capacitively coupled to the brass. This is sufficient for operation of the transducer. In fact, transducers constructed without the back electrode work as well as those with a back electrode.

C. IMPROVED DESIGN FOR APPLICATIONS

While the transducers of Fig. 3 offer a very simple vehicle for testing films, and are also useful as transmitters and receivers for laboratory systems, a more rugged design is needed for general practical applications. An encapsulated design we developed is shown in Fig. 4. The backing material is tungsten loaded epoxy, which was chosen because of its high acoustic impedance, low electrical conductivity and ability to absorb delayed acoustic reverberations. The outer electrode of the PVF_2 film is grounded at the case, and a thin gold foil strip, embedded in the epoxy, is used for the hot electrical contact to the inner electrode of the film. The aluminum case produces detectable low level spurious echoes. The use of a plastic (e.g., delrin) case would probably reduce these echoes substantially.

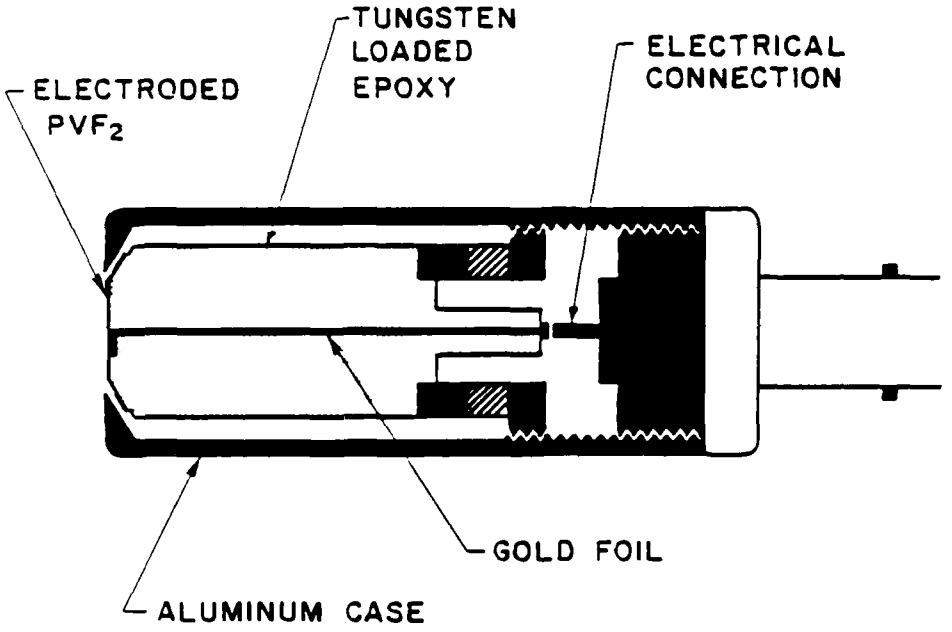

Fig. 4--Encapsulated PVF_2 transducer.

IV. THEORY OF PVF_2 BULK WAVE TRANSDUCERS

A. INTRODUCTION

A matrix impedance model will be presented and applied to PVF_2 thin disk bulk wave transducers. We have extended the model so that the performance of transducers consisting of any number of matching layers besides the piezoelectric layer can be calculated. The model has also been extended to include the effects of small acoustic losses (proportional to frequency squared) through the use of a complex elastic constant. Dielectric losses have also been included through the use of a complex dielectric constant.

The above transducer model is then used to examine and understand the effects that the many different transducer parameters have on transducer performance. Criteria examined in evaluating transducer performance include insertion loss, bandwidth, and frequency response. Parameters studied include electrode thickness, transducer epoxy bond thickness, PVF_2 acoustic Q, PVF_2 dielectric loss, transducer backing acoustic impedance, and electrical source impedance.

B. A TRANSDUCER MODEL

The bulk wave devices used in this work had lateral dimensions many times larger than their thickness. A typical transducer was at least 6000 microns wide while being less than 50 microns thick. These transducers were driven by a voltage applied across their thickness. Therefore they were longitudinal wave, thin disk transducers. For such a device, one can safely

assume that there is no lateral motion in the transducer and thus all acoustic and electric field variables are independent of lateral position. Thus a one dimensional model can be used to accurately describe the device. Figure 5 shows the geometry of the model.

The thin disk model we used was based on a matrix impedance model.[9] In electrical circuit theory one can write down a system of linear impedance equations relating voltage and current at different points of the circuit. These equations are conveniently written in matrix form.

Analogous to that, one can derive a system of linear equations relating the acoustic variable, stress, to the acoustic variable, particle velocity, at the boundaries of the transducer. These relations are obtained by satisfying the acoustic and electric boundary conditions of the transducer. In this model the terminal variables are F_1, F_2, V_1, V_2, I and ϕ as shown in Fig. 5.

F_1 and F_2 are the stresses on the two faces of the transducer, V_1 and V_2 are the particle velocities and ϕ is the voltage across the device.

We first calculate the total current in the transducer. Since we have assumed a one dimensional model E, D, V, T and ϕ are functions of z only. Thus $E_z = -(\partial\phi/\partial z)$. As there are no free charges present

$$\vec{\nabla} \cdot \vec{D} = 0 \quad \text{or,} \quad \frac{\partial D_z}{\partial z} = 0 \quad \text{and} \quad D_z = \text{a constant in space.} \qquad (4)$$

If we take the divergence of Maxwell's equation

$$\vec{\nabla} \cdot \vec{H} = \frac{\partial \vec{D}}{\partial t} + \vec{J}_c + \vec{J}_s$$

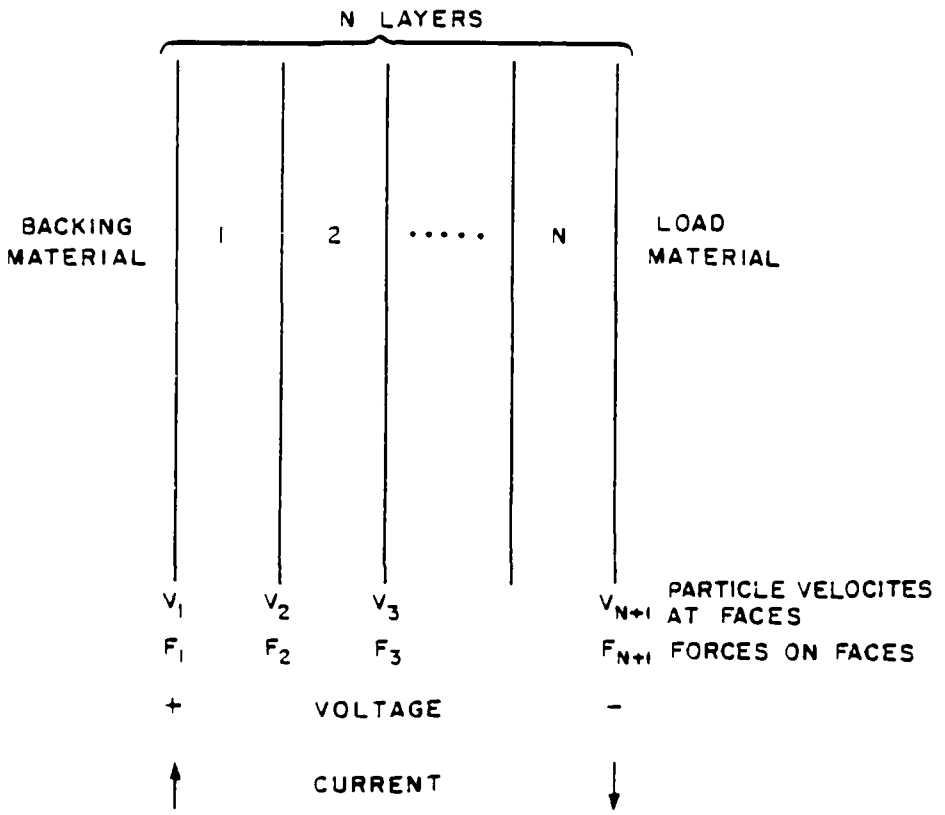

OTHER PARAMETERS - E_{zz}, Z, velocity, ε, tanδ, Q, THICKNESS, CROSS-SECTION AREA A

Fig. 5--Multiple thin layer transducer model.

and assume no source current is present, we have

$$\vec{\nabla} \cdot \left(\frac{\partial \vec{D}}{\partial t} + \vec{J}_c \right) = 0 \tag{6}$$

If we integrate this equation over a surface surrounding one electrode of the transducer (shown in Fig. 6), and assume D_z varies as $e^{j\omega t}$, we have

$$I = J_c A = j\omega D_z A \tag{7}$$

Because D_z is constant, the same current flows at the right hand boundary.

We now look at a piezoelectric medium in detail. It is useful to consider a material that belongs to the crystal symmetry group orthorhombic 2mm, since this includes PVF_2 and can also apply to materials belonging to the symmetry group hexagonal 6mm. This includes the useful piezoelectric materials CdS and ZnO. We write the constitutive relations in the usual manner:

$$\begin{aligned} \underline{D} &= \underline{\underline{\varepsilon}}^S : \underline{E} + \underline{\underline{e}} : \underline{S} \\ \underline{T} &= -\underline{\underline{e}} \cdot \underline{E} + \underline{\underline{c}}^E : \underline{S} \end{aligned} \tag{8}$$

Acoustic bulk waves traveling in the plus and minus z directions set up a velocity field of the form:

$$V_z = a \sin \left| \frac{\omega z}{V_{a'}} \right| + b \cos \left| \frac{\omega z}{V_{a'}} \right| \tag{9}$$

where a and b are constants, and $V_{a'}$ is the stiffened acoustic velocity.

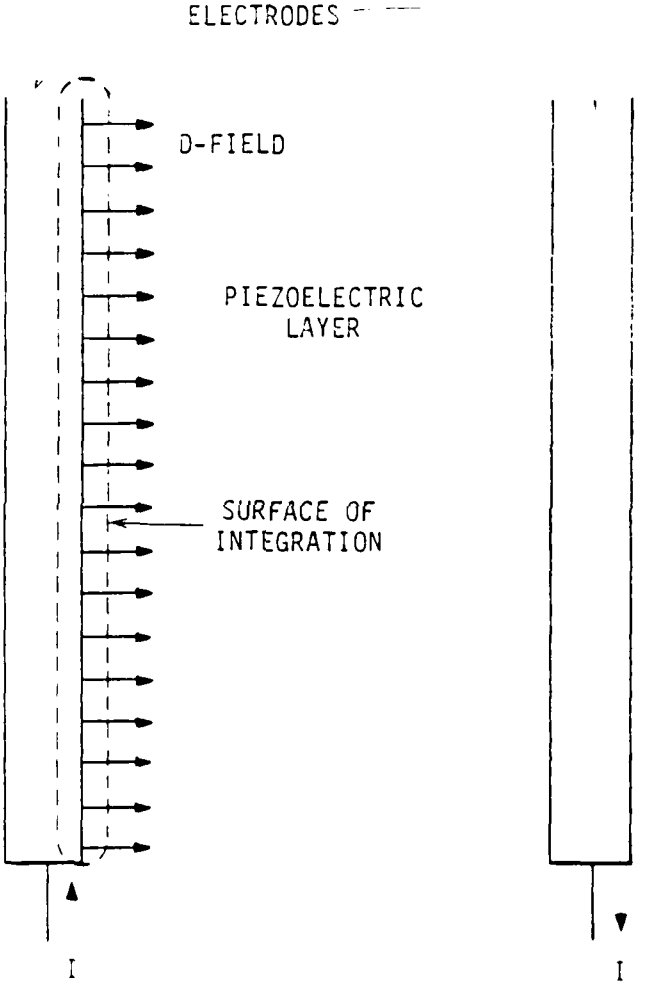

$I = j\omega D_z A$

A = CROSS-SECTIONAL AREA

Fig. 6--Location of surface of integration used to obtain Eq. (7).

There is also an associated $\underline{D}$ field that is constant in space. So we set $D_z = c$, where c is also a constant. Using this we can calculate the strain the rewrite parts of the constitutive relations as:

$$E_z = \frac{c}{\varepsilon_{33}^S} + \left(\frac{j}{V_a'}\right)\left(\frac{e_{33}}{\varepsilon_{zz}^S}\right)\left[a\cos\left(\frac{\omega z}{V_a'}\right) - b\sin\left(\frac{\omega z}{V_a'}\right)\right]$$

$$T_3 = -e_{33}/\varepsilon_{33}^S - j\left(\frac{C_{33}}{V_a'}\right)\left[a\cos\left(\frac{\omega z}{V_a'}\right) - b\sin\left(\frac{\omega z}{V_a'}\right)\right] \tag{10}$$

where we have used the equations

$$D_z = \varepsilon_{33}^S E_z + e_{33} S_3$$

$$T_3 = -e_{33} E_z + C_{33}^E S_3 \tag{11}$$

which are taken from Eqs. (8)

We now define $V_2 \equiv V_z(d)$; $V_1 \equiv V_z(0)$; $F_1 \equiv -AT_3(0)$; $F_2 \equiv -AT_3(d)$; $I \equiv i\,D_z A$; $b\int_0^d E_z dz$. With these definitions we can solve for the parameters a , b , and c and write the set of 3 x 3 impedance equations below.

$$F_1 = jAz_o\left(V_1 \cot(kd) + V_2 \csc(kd)\right) + \frac{e_{33}I}{j\omega\varepsilon^S_{33}}$$

$$F_2 = jAZ_o\left(V_1 \csc(kd) + V_2 \cot(kd)\right) + \frac{e_{33}I}{j\omega\varepsilon^S_{33}} \qquad (12)$$

$$\phi = \frac{e_{33}}{j\omega\varepsilon^S_{33}}(V_1 + V_2) + \frac{I}{j\omega C_o} \quad .$$

We then extended this model to a system with n layers. The terminal variables must be supplemented by variables at each of the $n + 1$ boundaries between the layers of the system. So we introduce the variables F_3 to F_{n+1} and V_3 to V_{n+1}. I_i is defined as the current entering the ith face. As total current (which includes displacement current) is conserved, $I_1 = I_2 = I_n = I$. We define voltage potentials ϕ_1 to ϕ_{n+1} to take the place of the variable ϕ. Next, the 3x3 set of linear equations is rearranged (using simple linear algebra) into a set of 4x4 equations of this form:

$$F_2 = Z_{11}F_1 + Z_{12}V_1 + Z_{13}\phi_1 + Z_{14}I$$

$$V_2 = Z_{21}F_1 + Z_{22}V_1 + Z_{23}\phi_1 + Z_{29}I \qquad (13)$$

$$\phi_2 = Z_{31}F_1 + Z_{32}V_1 + Z_{33}\phi_1 + Z_{34}I$$

$$I_2 = Z_{41}F_1 + Z_{42}V_1 + Z_{43}\phi_1 + Z_{44}I$$

The Z_{ij}'s can be found in terms of the previous matrix elements. The matrix above relates the acoustic and electrical variables at the two boundaries of layer 1. A similar matrix can be found for every layer in the system. We then multiply the matrices together in the following form:

$$\begin{bmatrix} F_{n+1} \\ V_{n+1} \\ \phi_{n+1} \\ I_{n+1} \end{bmatrix} = \begin{bmatrix} Z_{ij} \\ \text{for} \\ \text{layer} \\ n \end{bmatrix} \begin{bmatrix} Z_{ij} \\ \text{for} \\ \text{layer} \\ n-1 \end{bmatrix} \cdots\cdots \begin{bmatrix} Z_{ij} \\ \text{for} \\ \text{layer} \\ 1 \end{bmatrix} \begin{bmatrix} F_1 \\ V_1 \\ \phi_1 \\ I_1 \end{bmatrix} \tag{14}$$

After this is completed we are left with a set of four linear equations relating the values of the sets of variables of F, V, ϕ, and I at the two ends of the n layers to each other. Given a complete set of transducer parameters and the load and backing impedances, the output power of the device can be calculated for a given drive voltage applied across the transducer. The output power radiated into the material bordering interface 1 is given by the expression

$$P_{ave} = 1/2\ V_1^2\ Z_1\ A \tag{15}$$

where Z_1 is the acoustic impedance of the load material and A is the cross sectional area of the transducer. By calculating the ratio V_1/voltage , the power output can be obtained.

This model can be further extended to account for small acoustic and dielectric losses. For small acoustic losses the stress-strain relation

$$\underline{T} = \underline{\underline{c}} : \underline{S} \tag{16}$$

can be modified to include losses due to viscosity to obtain

$$\underline{T} = \underline{\underline{c}} : \underline{S} + \underline{\underline{\eta}} \frac{d\underline{S}}{dt} \tag{17}$$

where η is a 6x6 *viscosity tensor*.

For harmonic fields varying as ωt, we can write the above equation as

$$\underline{T} = (\underline{\underline{c}} + j\omega\underline{\underline{\eta}}):\underline{S} \tag{18}$$

If the acoustic equations of motion are solved using this modified c matrix, it is found that the k vector of acoustic waves propagating in the z direction of the lossy material is given by the equation:

$$k^2 = \left(\frac{\omega}{V_a}\right)^2 + j\omega\eta_{33} \tag{19}$$

where V_a = the acoustic wave propagation velocity in the z direction .

Thus the k vector has an imaginary component due to the introduction of the small viscous losses. The real and imaginary parts of the k vector are found by solving Eq. (19). We find that if

$$k = \beta + j\alpha \quad .$$

Then

$$\beta \approx \frac{\omega}{V_a} \tag{20}$$

and

$$\alpha = \frac{\beta\omega\eta_{33}}{2C_{33}} \quad . \tag{21}$$

Thus the total k vector can be written as

$$k = \beta\left(1 + \frac{j\omega\eta_{33}}{2C_{33}}\right) \tag{22}$$

Now the mechanical Q, or quality factor of the material is defined as[9]

$$Q = C_{33}/\omega\eta_{33} \quad . \tag{23}$$

Thus the modified k vector can be written as

$$k = \frac{\omega}{V}\left(1 - \frac{j}{2Q}\right) \quad . \tag{24}$$

Besides this modification, C_{33} is converted into

$$C_{33}\,(1 + j\omega\eta_{33})$$

$$= C_{33}\left(1 + \frac{j\omega\eta_{33}}{C_{33}}\right)$$

$$= C_{33}\left(1 + \frac{j}{Q}\right) \quad .$$

This change occurs in Eqs. (10).

These changes were incorporated into the computer model. When a value of Q is given in this paper, it refers to the Q at the quarter wave resonant frequency of the transducer. The Q value at other frequencies is calculated from Eq. (23), which says that Q is inversely proportional to frequency. This is equivalent to modeling losses as being proportional to the square of the frequency.

Dielectric losses are included through the use of a complex dielectric constant. The imaginary part of the dielectric constant represents electrical heating losses occurring in the PVF_2. If the dielectric constant is written as

$$\varepsilon = \varepsilon' + j\,\varepsilon'' \tag{25}$$

the ratio $\varepsilon''/\varepsilon'$ is called the loss tangent. When a complex dielectric constant is used in the program, the impedance arising from the capacitance of the transducer $(1/\omega C_o)$ acquires a real part which represents the ohmic heating losses occurring.

The loss tangent of PVF_2 has been measured by Sussner, et al.[10] and Callerame, et al.[11] Although their results were not identical, both measured the loss tangent to be between .2 and .3 over the range 3-12 MHz. In our calculations we used a value of .3, in order to be on the safe side.

The parameters used are all assumed to be frequency independent in the program, (except for the acoustic losses, as explained above). The effects of electrical matching through the use of external lumped elements can be included in the model by appropriate modification of the equation which couples the total voltage across the transducer to the current flowing in the transducer, the third of Eqs. (13).

C. TRANSDUCER ANALYSIS

The model described above was implemented on a computer and used to examine the behavior of PVF_2 transducers. Table II gives a list of the parameters used in obtaining the results presented in this section along with the values assigned to these parameters. Any change from these values will be noted on the appropriate figure.

Figure 7 shows the basic theoretical insertion loss (one-way) of PVF_2 longitudinal wave transducers of the type shown in Fig. 3. Here it is assumed that the transducer is connected to external electrical circuits of 50 ohms impedance. This is a rather ideal case in which there are no losses (either mechanical or electrical) in the PVF_2 and zero thickness

TABLE II

ε_{33}	-.08	Coulombs/m^2
$\varepsilon_{33}/\varepsilon_o$	8	
Acoustic Impedance	3.82 x 10^6	kg/m^2-sec
Acoustic Velocity	2200	m/sec
Film Thickness	25	microns
tan δ	-.3	
Acoustic Q	10	
Film Area	1	cm^2

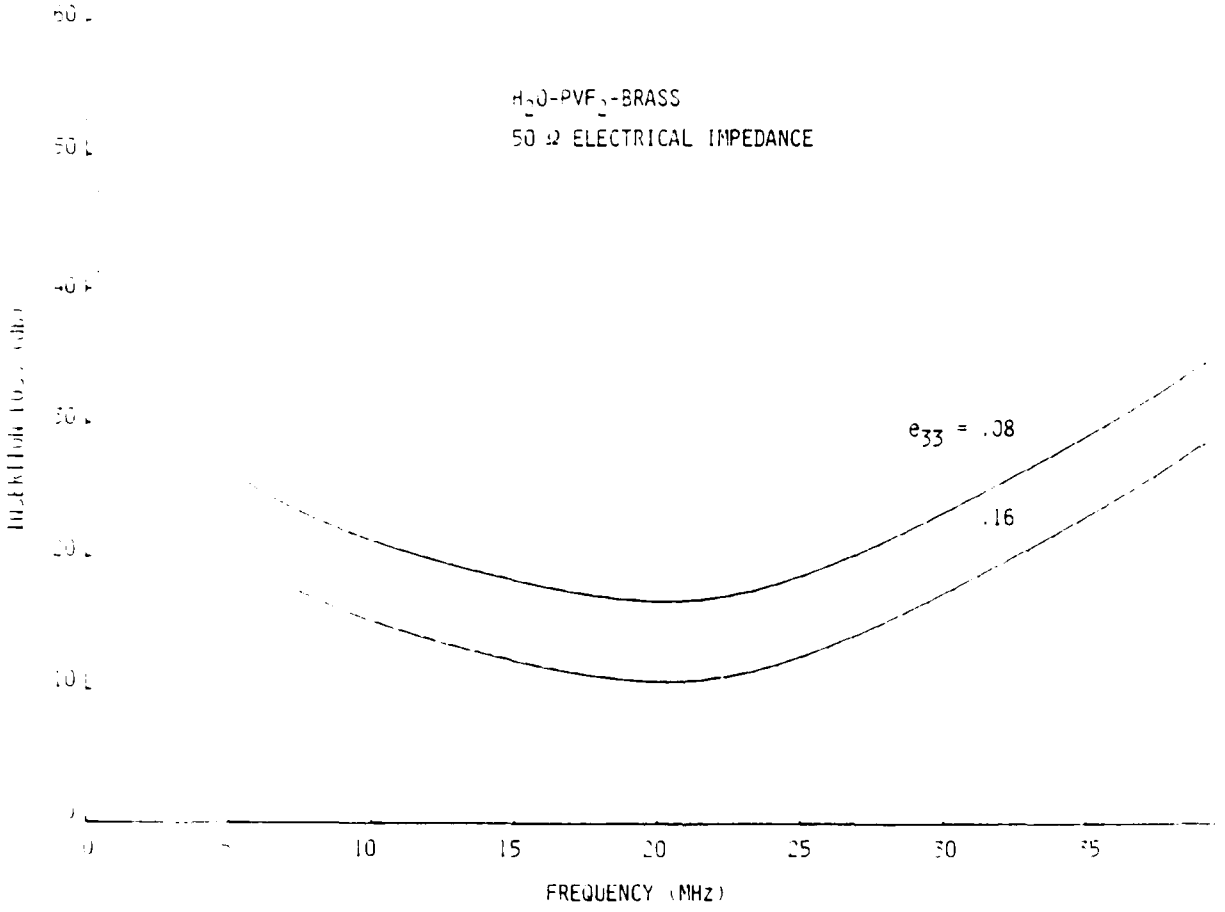

Fig. 7--Theoretical insertion loss of idealized bulk wave transducers. Backing material brass; PVF_2 film thickness 25 μ; film area 1 cm; film $\kappa/\varepsilon_0^2 = 8$.

bonds and electrodes are assumed. The backing in this case is brass, which has a higher acoustic impedance than PVF_2. Therefore the transducer is resonant when the PVF_2 layer is approximately 1/4 of a wavelength thick. The minimum insertion loss occurs at $\sim$ 17 MHz for 25 micron thick film. The upper curve is for a piezoelectric stress constant $e_{33} = -.08$ coulombs/m^2, corresponding to a readily available range, and the lower curve is for higher activity material reported by some workers in the field.[2] The curve for $e_{33} = -.08$ exhibits a bandwidth of $\sim$ 75% and a minimum insertion loss of $\sim$ 20 dB. The bandwidth is defined as $\frac{\Delta\omega}{\omega_o}$ where ω_o is the frequency of minimum insertion loss.

The practical effects referred to above have relatively small effects on the transducer insertion loss. Figure 8 shows the theoretical effect of varying the loss tangent of PVF_2 from 0 to the rather high value of -.3. Recall that $\tan \delta = \varepsilon''/\varepsilon'$ where $\varepsilon = \varepsilon' + j\varepsilon''$. The introduction of this dielectric loss increases the insertion loss by about 1 dB, and does not significantly alter the shape of the curve. However, this high dielectric loss will severely limit the minimum insertion loss that can be achieved through inductive tuning of the transducer. It also adversely affects the signal-to-noise ratio of the transducer when it is used as a receiver.[12]

We can understand the effect of the dielectric loss by examining a rather simple equivalent circuit, shown in Fig. 9. In this circuit the transducer is modeled as a series capacitor, resistance and reactance. (The resistance is broken up into two parts, R_a and $R_$.) The correct values for these parameters are found by solving the transducer equations of Section IVB. The capacitance is just that due to the electrodes of the

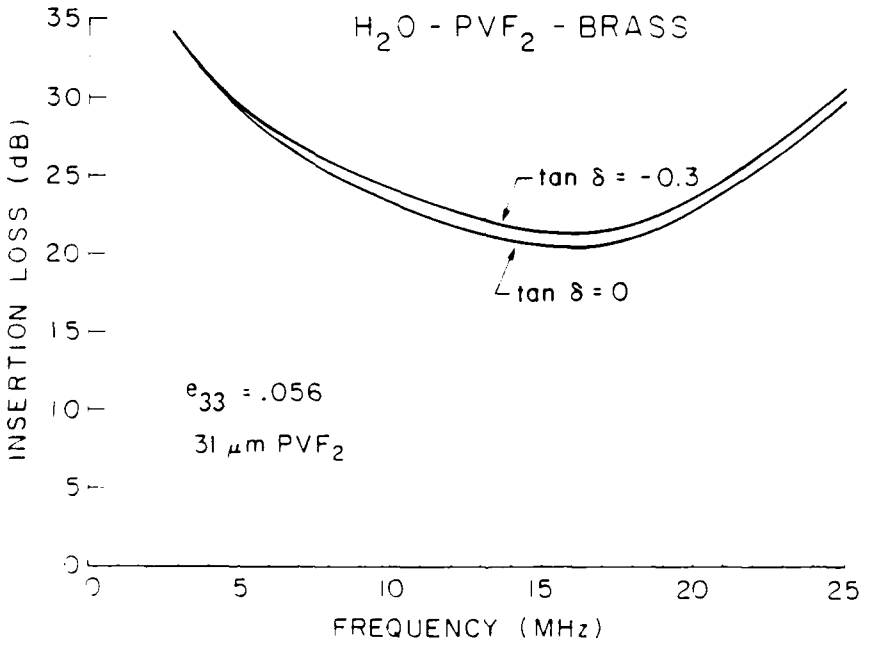

Fig. 8--Theoretical effect of dielectric loss. Backing material brass; electrical impedance 50 Ω; PVF_2 film thickness 31 μ; film area 1 cm^2; film $\varepsilon/\varepsilon_0^2$ = 7; e_{33} = .056.

SERIES EQUIVALENT CIRCUIT

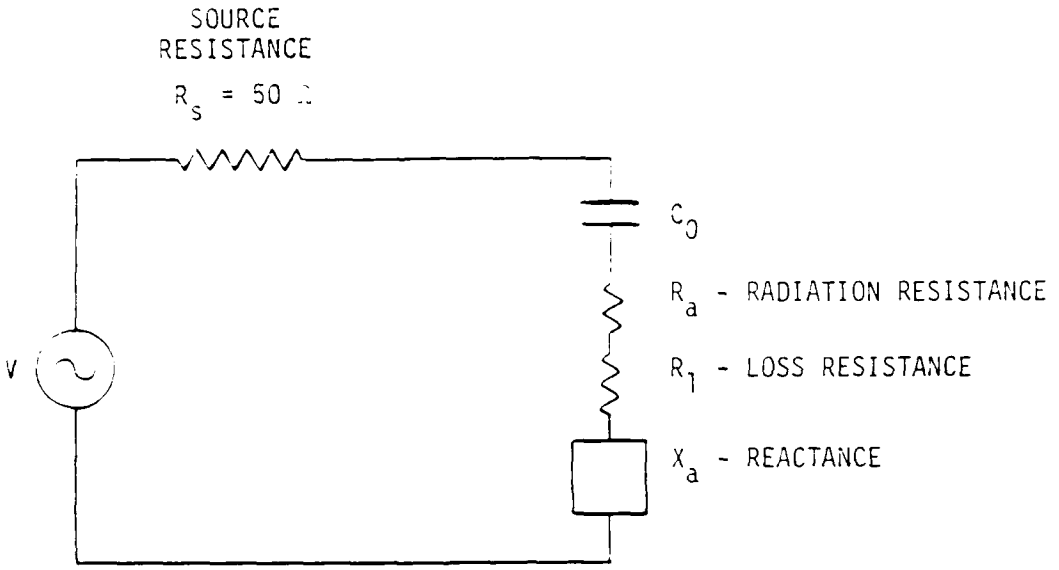

Fig. 9--Series equivalent circuit
for a lossy transducer.

transducer. The resistance R_a, known as the radiation resistance, accounts for power converted to acoustic radiation by the transducer. The resistance R_ℓ accounts for power losses in the transducer. Both R_a and the reactance, X_a, are brought about by piezoelectric coupling of the acoustic and electrical fields of the device. If the piezoelectric stress constant were to drop to zero, both R_a and X_a would disappear. Also included in the circuit is the resistance of the voltage source, R_s. R_s is taken to be 50 ohms in this analysis.

Using the parameters of Table II and the approximate physical dimensions of the transducers detailed in Section IIIB, the components of the circuit are found to have the following impedances (approximately) near resonance, $\sim$ 17 MHz:

$$\frac{1}{j\omega C_o} = -30j \text{ ohms}$$

$$R_a = .5 \text{ ohms real}$$

$$X_a = .5j \text{ ohms} \quad .$$

Therefore the power radiated into the acoustic loads when no losses are present (and hence $R_\ell = 0$), is

$$\frac{1}{2} I^2 R_a = \frac{1}{2} V^2 \left| (R_s + R_a)^2 + (X_a + 1/\omega C_o)^2 \right|^{-1} R_a$$

$$\approx \frac{1}{2} V^2 R_a \left| R_s^2 + 1/\omega^2 C_o^2 \right|^{-1} = V^2 \left| 1.47 \times 10^{-4} \right| \text{watts} \quad .$$

The introduction of dielectric loss introduces a series loss resistance. The magnitude of this resistance is found by replacing epsilon by its complex value $\varepsilon \rightarrow \varepsilon' + j\varepsilon''$. Thus $1/j\omega C_o = \frac{d}{j\omega A\varepsilon}$ becomes

$$\frac{\varepsilon' d}{j\omega A(\varepsilon'^2 + \varepsilon''^2)} + \frac{\varepsilon'' d}{\omega A(\varepsilon'^2 + \varepsilon''^2)} \quad ,$$

where $\varepsilon''/\varepsilon' = \tan \delta$.

The inclusion of this component in the equivalent circuit reduces the power radiated to

$$\frac{1}{2} V^2 R_a \left[(50+9)^2 + 30^2 \right]^{-1} = V^2 (1.14 \times 10^{-4}) \text{ watts} \quad .$$

Thus the dielectric loss increases the insertion loss by about only 1 dB. This result is slightly misleading however. The calculation above used a standard 50 ohm source resistance. The introduction of the dielectric loss resulted in an 8 ohm loss resistance being placed in series with the 50 ohm resistance. The current in the equivalent circuit was only marginally reduced, and as R_a was not altered, the power radiated, $1/2\ R_a I^2$, was not significantly changed However, in a practical situation the source resistance, R_s , might be much less than 50 ohms. If it is desired to radiate large amounts of acoustic power R_s will be made as small as possible so that power is not wasted heating up R_s . In this case the introduction of $\tan \delta$ will increase the insertion loss appreciably.

The acoustic Q of the film is another loss mechanism included in the program. However, the insertion loss curve changes by only a small fraction of a dB as the Q goes from 10 to 100,000.

This can be quantitatively explained by calculating the loss experienced by an acoustic wave traveling once across the thickness of the transducer. As explained in Section IVB, acoustic losses were introduced in our transducer model through the use of a complex k vector. The usual lossless k vector was simply multiplied by a factor of $(1-j/2Q)$. Thus an acoustic wave propagating across the transducer thickness, d , will be attenuated by a factor

$$\exp[-2\pi d/2Q\lambda]$$

At the resonant frequency, where $d = \lambda/4$, we find a loss factor of

$$\exp[-\pi/4Q]$$

In decibels, this equals 6.8/Q dB. Therefore, Q values larger than 10 will have only a minor impact on the transmission of acoustic waves through the PVF_2, and will not significantly alter the transducer characteristics.

In Fig. 10 the effect of an epoxy bond between the PVF_2 film and the brass backing can be seen to be minimal. A 1/2 or 1 micron bond only slightly degrades the transducer performance. Because PVF_2 has an acoustic impedance (3.8) very close to that of the epoxy (3.1), the thickness of the bond is not as critical as in the case of PZT transducers backed by a high impedance. Then the thickness of the epoxy between the PZT and the backing must be thin in order for proper performance. This is a consequence of the large impedance mismatch between the epoxy and the PZT. But in PVF_2 transducers, the main effect of the bond is to marginally lower the resonant frequency of the transducer.

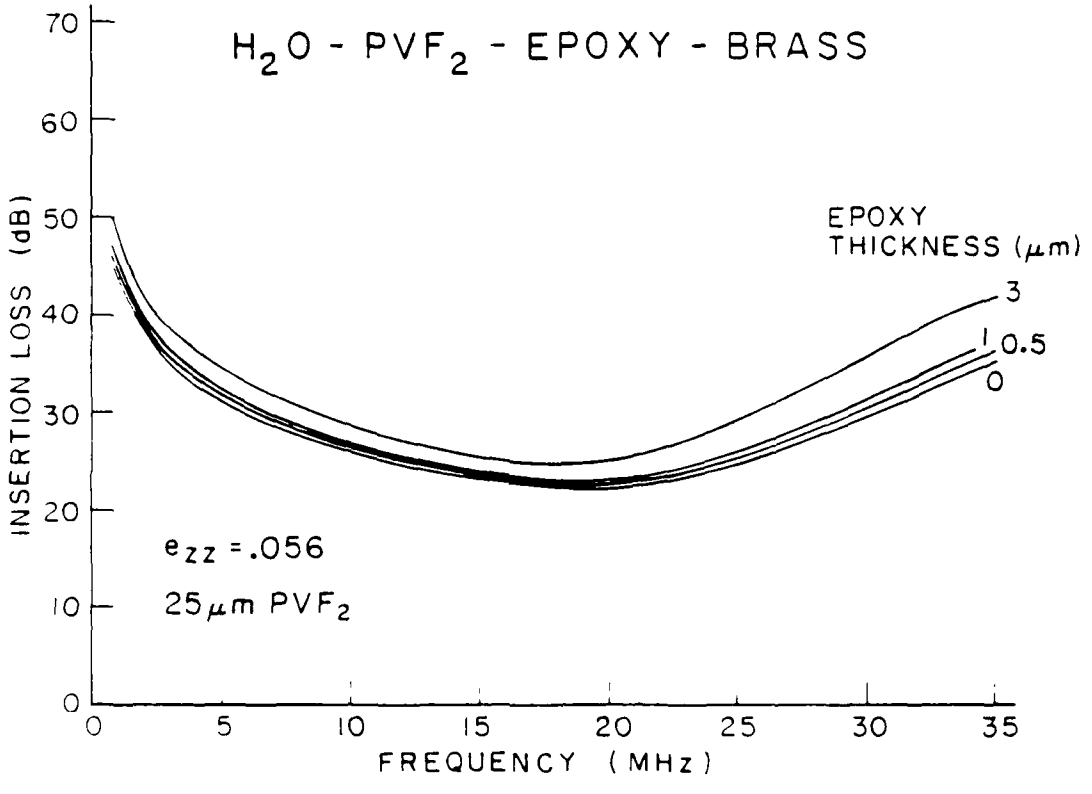

Fig. 10--Theoretical Calculation showing the effect of epoxy bond thickness on a 25 μm PVF_2 brass backed transducer. Electrical impedance 50 Ω, $\varepsilon/\varepsilon_0$ = 7, film area - 1 cm^2.

Figure 11 shows the mass loading effect of the gold electrodes on the film. For a 9 micron film with 1000 angstrom Au electrodes, the ratio of the mass of the gold to the mass of the PVF_2 is about 1:4. The graph shows the resonant frequency of the transducer lowered from 53 MHz to 44 MHz.

The absolute shift in the resonant frequency of a free acoustic resonator due to mass loading is proportional both to the unloaded resonant frequency and the ratio of the mass of the perturbing load to the mass of the bare resonator.[13] Assuming that these two proportionalities hold for our brass-backed PVF_2 transducers, we can estimate the frequency downshift caused by mass loading for our 25 micron transducers.

The 25 micron transducers have a resonant frequency lower by a factor of $\sim$ 9/25 relative to the 9 micron devices. They also have a lower ratio of electrode mass to PVF_2 mass. This reduces $\Delta\omega/\omega$ by another factor of 9/25 compared to the 9 micron case. Therefore, the absolute frequency shift for our 25 micron transducers should be around 9 MHz x (9/25) x (9/25) = 1.1 MHz. A shift of this magnitude was not significant given our measurement accuracy and research goals. Thus the frequency shift was not investigated further.

Now consider the effects of changing the electrical impedance level. Figure 12 shows theoretical insertion loss for a low electrical impedance (10 ohms, compared to the $\sim$ 30 ohms capacitive impedance of the transducer at the resonant frequency) and a high acoustic impedance backing.

Figure 13 shows the effect of a high (600 ohms) electrical impedance. One of the curves corresponds to a brass backing (acoustic impedance $\sim$ 31), and the other is for a low impedance (nearly matched) backing. The low impedance backing moves the resonance out to a higher frequency, near the value for half-wave film thickness. Notice that the high electrical

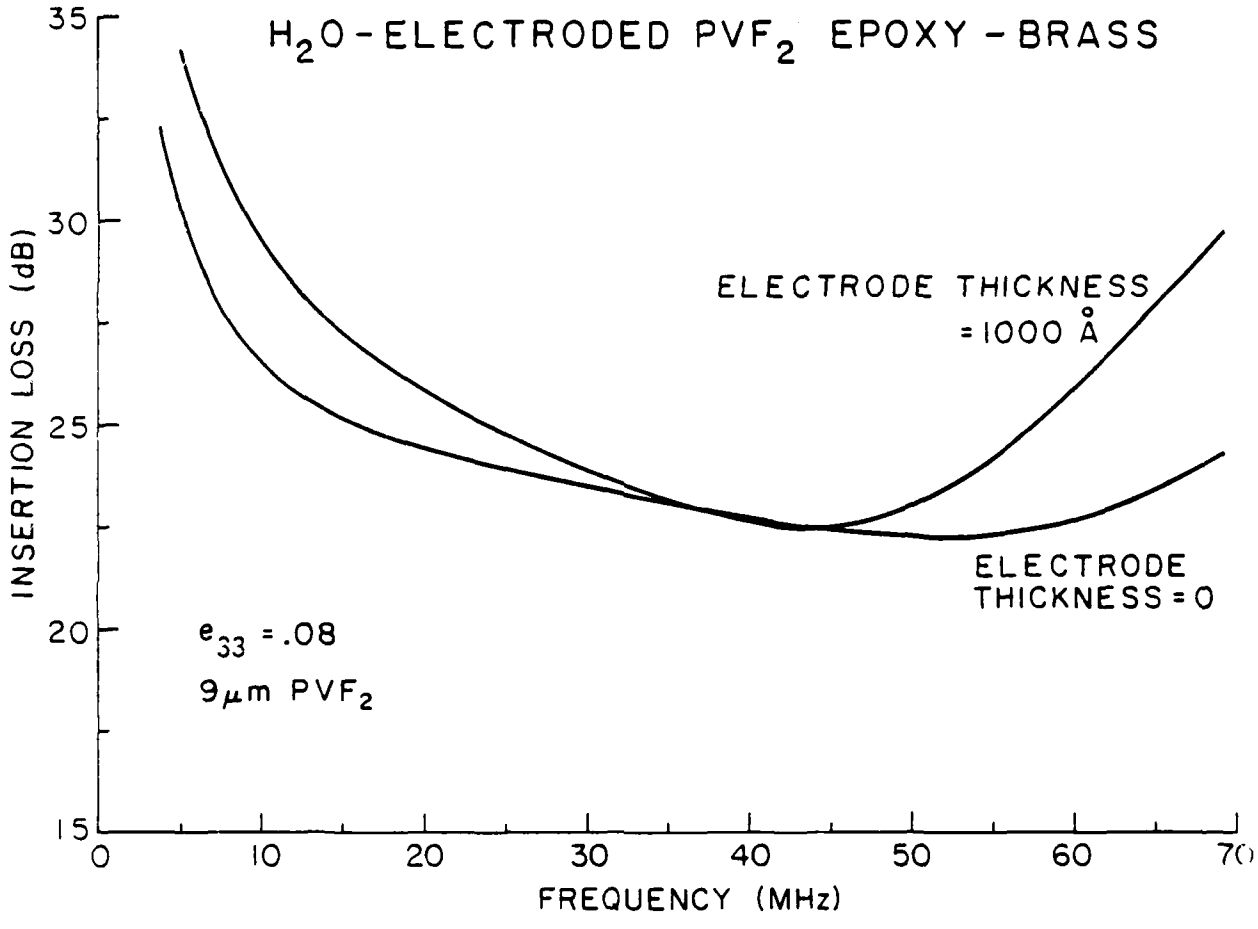

Fig. 11--Theoretical effect of electrode loading. Backing material brass; electrical impedance 50 Ω; PVF_2 film thickness 9 μ; film area 1/2 cm^2; film $\varepsilon/\varepsilon_0$ = 7; e_{33} = .08; epoxy bond thickness 1/2 μ.

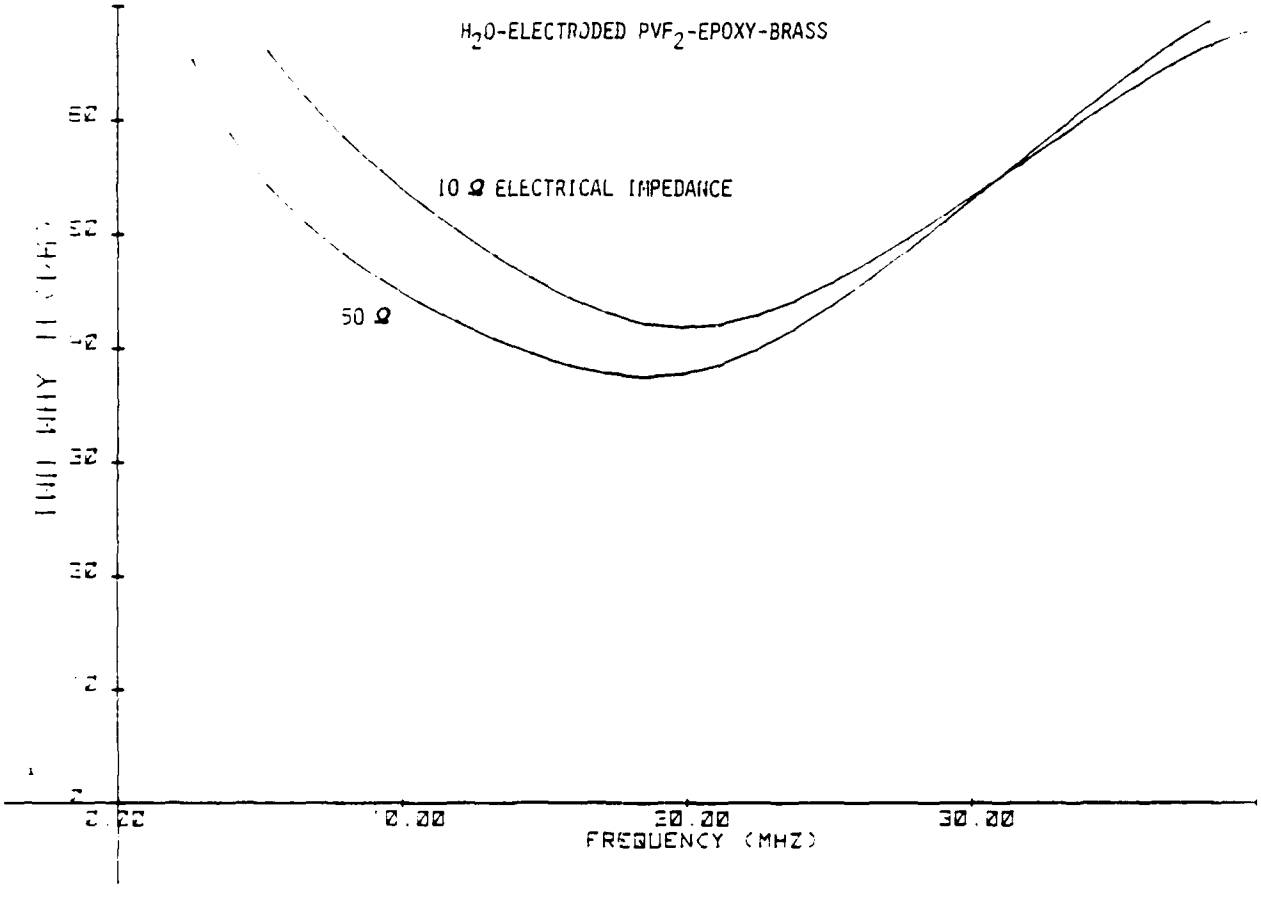

Fig. 12--Theoretical insertion loss of bulk wave transducers with low electrical impedance. PVF_2 film thickness 25 μ; film $\varepsilon/\varepsilon_0$ = 7; e_{33} = .08; film tan δ = .3; film acoustic Q = 10; Au electrode thickness = 1000 Å; epoxy bond thickness = .5 μ.

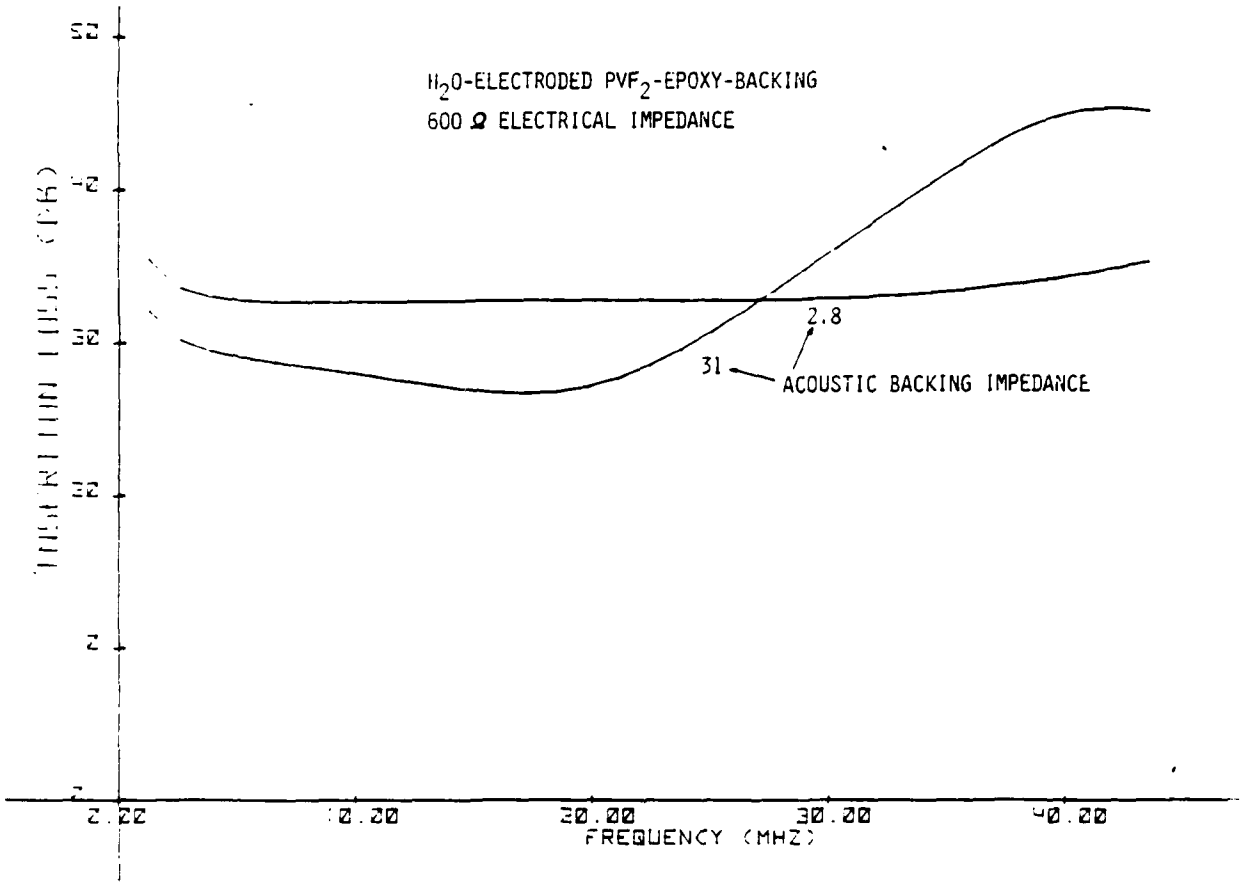

Fig. 13--Theoretical insertion loss of bulk wave transducers with high electrical impedance; PVF_2 film thickness 25 μ; film area 1 cm^2; film $\varepsilon/\varepsilon_0$ = 8; e_{33} = .08; film tan δ = -.3; film acoustic Q = 10. Au electrode thickness = 1000 Å; epoxy bond thickness = .5 μ.

impedance increases the insertion loss but also results in an enormous bandwidth. The response can be flat to within a dB over the range of 2 MHz to 40 MHz.

The large bandwidths obtainable with PVF_2 transducers imply that short time duration impulse responses are also obtainable. Figure 14 shows a picture of the experimental impulse response of a PVF_2 transducer. The response is basically bipolar, with a small amount of ringing. Such a response is desired in a pulsed acoustic imaging system since the axial resolution is determined by the length of the impulse response.

Figure 14 also shows the calculated impulse response. This was derived by taking a discrete Fourier transform of the transfer function of the transducer. The transfer function is calculated during the execution of the thin disk insertion loss program. The figure demonstrates good agreement between theory and experiment.

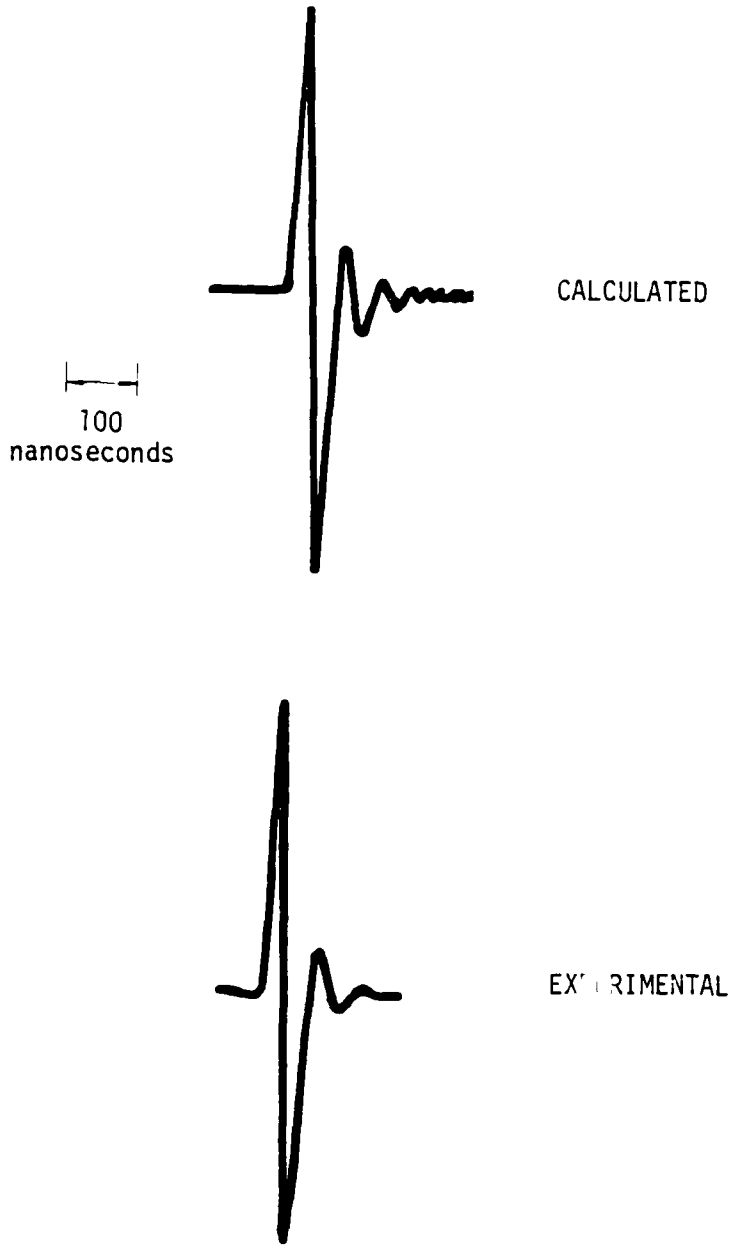

Fig. 14--Comparison of calculated and experimental PVF_2 transducer impulse response. The transducer was brass-backed and operated into a water load. Film area = 1 cm^2, film thickness = 25 μm.

V. EXPERIMENTAL RESULTS WITH PVF_2 BULK WAVE TRANSDUCERS

A. INTRODUCTION

Insertion loss versus frequency measurements were performed on six 25 micron PVF_2 transducers. The results are compared with a theoretical calculation of insertion loss based on the transducer model of Section IV-B. The model calculation was fitted to the experimental result by slight adjustment of the PVF_2 material parameters. Good agreement between theory and experiment is shown when we assume a value of e_{33} slightly lower than some published values. All six transducers gave nearly identical results, showing that our fabrication procedure gave repeatable results. Transducers using 9 micron PVF_2 were also tested. These had minimum insertion losses near 40 MHz. A comparison between the experimental and calculated insertion loss versus frequency curves is shown to give a close fit over the range 10 - 50 MHz. The transducer model is found to successfully predict the performance of several PVF_2 transducers, showing it can be used in designing PVF_2 transducer devices.

Electrical tuning of PVF_2 transducers is also discussed. Tuning using one inductor, either in parallel or in series with the transducer, is explored. A tuning network consisting of a transformer and an inductor in parallel with our standard transducers produces good results with a minimal amount of difficulty. Tuned PVF_2 transducers had measured insertion losses as low as 14 dB (one-way). The minimum insertion loss achievable with the PVF_2 film now available was calculated to be approximately 12 dB one-way.

The ability of PVF_2 transducers to operate as effective acoustic transmitters when driven with large electric fields is demonstrated. This property of PVF_2 has been compared with that of PZT. It has been shown that using large electric fields to drive PVF_2 transducers can compensate somewhat for the lower piezoelectric activity of PVF_2 relative to PZT. The advantages of the low dielectric constant of PVF_2 are also discussed. When used as an acoustic receiver, this property can also compensate for the lower piezoelectric activity of PVF_2.

B. UNTUNED TRANSDUCER PERFORMANCE

We used the theoretical model described above to predict the performance of some of the basic bulk wave devices we had constructed. Six identical transducers had been made in conjunction with the experiment to be described in Section VII-B. The average measured two way insertion loss of these devices is compared with the theoretical calculation.

The insertion loss was measured using the set-up of Fig. 15. The sine wave oscillator, the pulser and the two mixers produced a tone pulse of variable frequency and duration. This signal was amplified by the ENI power amplifier. That device has an internal source resistance of 50 ohms across the frequency range of interest, next, the signal was split using a 4-port quadrature hybrid. This device will divide a signal entering the hybrid into two equal parts, and send the split signals to the two side ports of the hybrid. (Ports 2 and 3 are side ports relative to port 1.) For instance, a signal entering port 1 will be equally divided between ports 2 and 3. Port 4 will not receive any of the incoming signal. All 4 of the ports act in this manner.

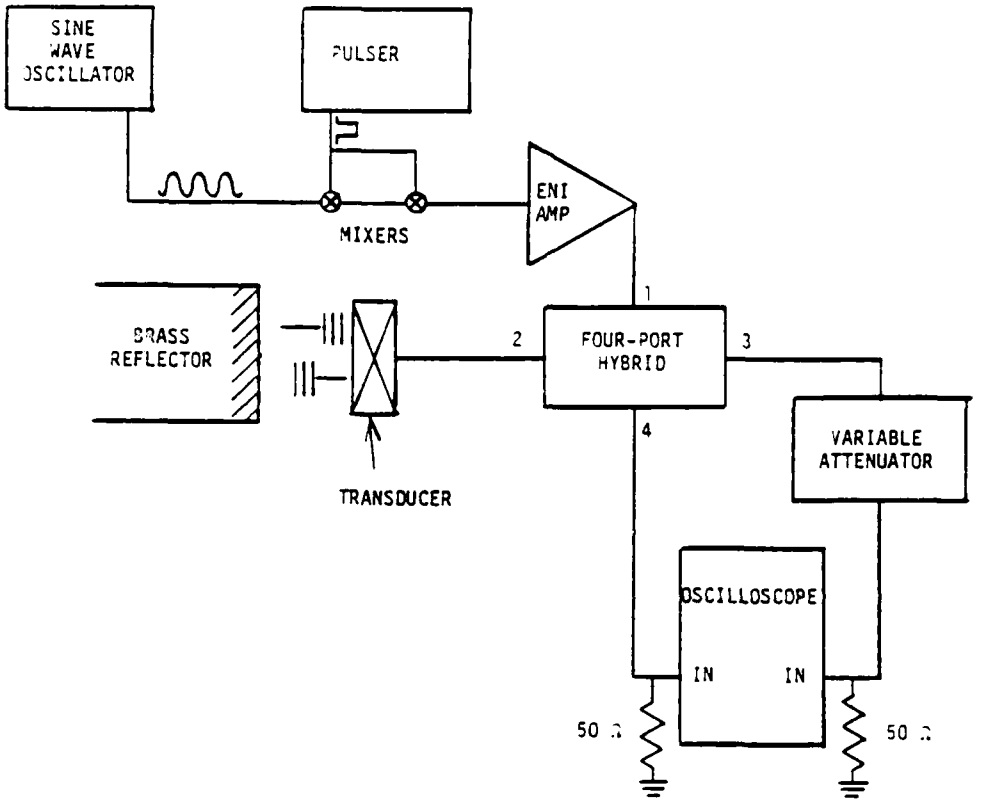

Fig. 15--Experimental set-up for the measurement of transducer insertion loss.

Figure 15 shows that one half of the incoming signal is sent through reference attenuators and thence into a 50 ohm load connected across an oscilloscope. The other half is used to drive the transducer under test. The transducer then excites an acoustic wave in the water which impinges on the smooth brass surface. Most (~90%) of the acoustic signal is reflected back to the transducer. The transducer is held in an adjustable jig which allows the system to be aligned so that the faces of the brass and the transducer are quite close to parallel.

The two surfaces must be aligned very accurately because the acoustic beam pattern of the transducer is quite narrow. If the distance between the reflector and the transducer varies by $\sim\lambda/2$ across the cross section of the acoustic beam the reflected wave incident on the transducer will not uniformly excite the transducer face. (λ is the acoustic wavelength in the water.) This will result in a greatly reduced signal and an inaccurate measurement. Given the particular dimensions and operating frequencies of our devices, we required the faces of the transducer and the reflector to be within abut .3° of parallel. The adjustable jig allowed us to achieve this degree of alignment.

Thus the reflected wave uniformly excited the transducer. The voltage produced across the transducer creates a signal that enters the hybrid through port 2. Half the signal leaves by way of port 1 and is completely absorbed by the 50 ohm internal resistance of the amplifier. The other half of the signal leaves the hybrid through port 4 and appears across a 50 ohm load connected across an oscilloscope. The variable attenuators can then be adjusted so as to equalize the two signals appearing on the scope. The insertion loss is then equal to the amount of loss

introduced by the variable attenuators plus a 3 dB correction due to the splitting of the return signal from the transducer as it passes through the hybrid. The final result is the two-way insertion loss of the transducer relative to 50 ohm electrical impedances at both the source and the receiver.

Insertion loss versus frequency measurements were made by manually changing the frequency of the sine wave oscillator and measuring the insertion loss point by point across the frequency range of interest.

Figure 16 shows the results. The calculation was obtained by curve fitting, using values for the various electrical and acoustic parameters (shown in the figure) that produced a good match while at the same time lying within reasonable ranges (these were estimated from published values). The value of e_{33} (0.054) is quite low. We consider this due to only partial poling of the film from which these transducers were made. Due to technical difficulties the poling field was removed from the film while the PVF_2 was at 80 degrees. It is considered best to allow the film to cool to room temperature while the poling field is still being applied. This procedure freezes in the changes produced by the electric field.[14]

Figure 17 shows an example of higher frequency operation using thinner (9 micron) film, suitable for operation in the 40 MHz range. At these frequencies the measured loss must be corrected for acoustic loss in water (5 dB/cm at 50 MHz) to arrive at the insertion loss. This was done in the figure. This loss skews the uncorrected loss curve toward lower frequencies. Good agreement between the curves is seen, with the performance of the transducer being unexpectedly good near 60 MHz.

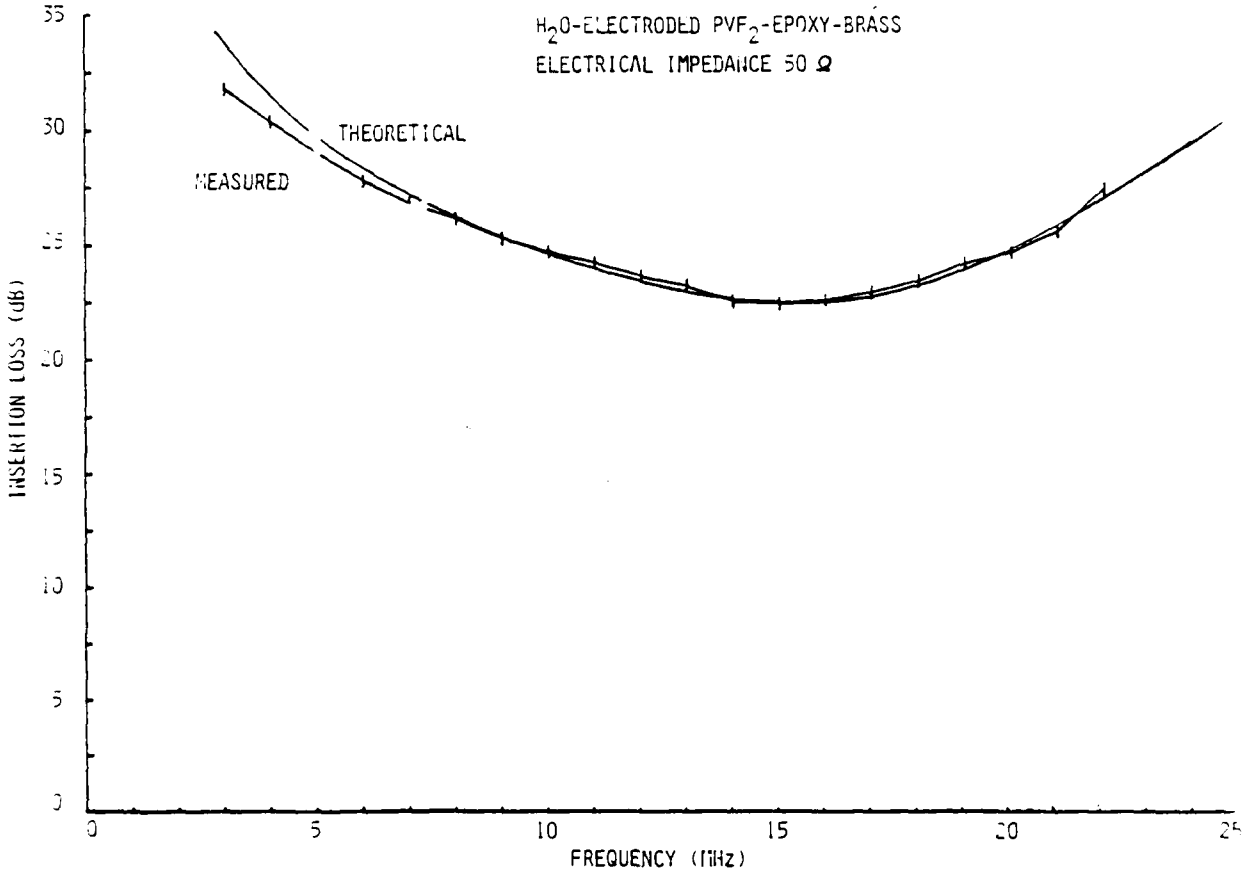

Fig. 16--Experimental and theoretical insertion loss of bulk wave transducers with 29.5 μ PVF_2 film thickness. Backing material brass; electrical impedance 50 Ω; film area 1.6 cm^2. Measured curve; average of six identical units. Theoretical curve parameters: film e_{33} = .054; film $\varepsilon/\varepsilon_0$ = 7; film tan δ = -.3; film acoustic Q = 10; film acoustic impedance = 3.82; film acoustic velocity = 2150 m/s.

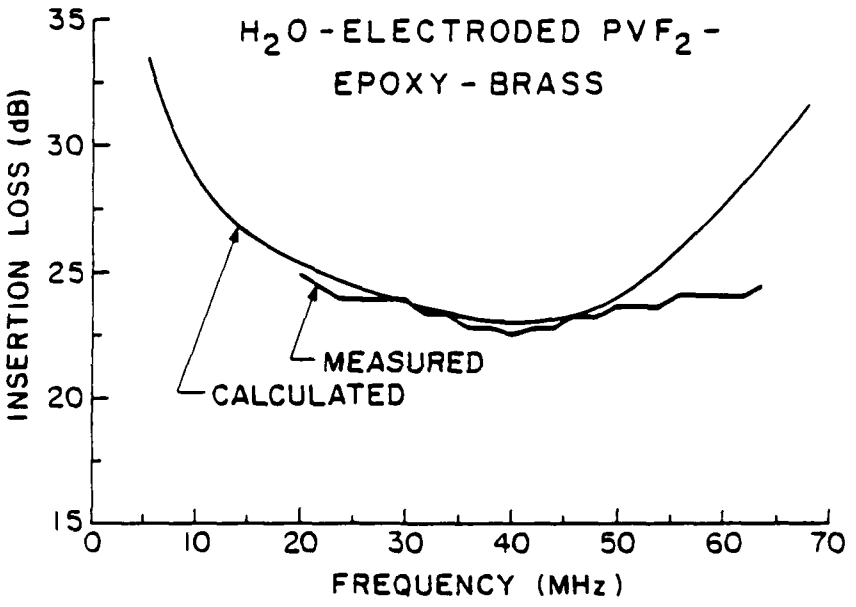

Fig. 17--Experimental and theoretical insertion loss of bulk wave transducers with 9 μ PVF_2 film thickness. Backing material brass; electrical impedance 50 Ω; film area 1/2 cm^2. Theoretical curve parameters: film e_{33} = .08; film $\varepsilon/\varepsilon_0$ = 7; film tan δ = 0.3; film acoustic Q = 5; Au thickness = 1000 Å; epoxy bond thickness = 1/2 μ.

We would like to add at this point that other aspects of the behavior of these PVF_2 transducers also conform rather uniquely to classical thin layer behavior, and so are accurately calculable, allowing ultrasonic measurements to be corrected for transducer effects. Using some of the above transducers, Kino and Stanke[15] have shown that one can accurately calculate acoustic beam diffraction effects and subtract them from raw data, in the measurement of small changes of acoustic attenuation in materials.

This last result, together with the fact that we were able to obtain a good fit between theory and experiment shows that the material properties of PVF_2 are fairly well known and that the theoretical model does a good job of predicting the properties of PVF_2 transducers.

C. ELECTRICAL TUNING

Often the insertion loss (IL) of a transducer can be dramatically improved by electrical tuning. Frequently the power delivered to the transducer by the voltage source of the system is transmitted over a line having a characteristic impedance of 50 ohms real. Tuning is used to convert the electrical impedance of the transducer to a value closer to 50 ohms.

Transducers can be represented by the clamped capacitance of their electrodes (C_o), plus a term explicitly caused by piezoelectricity. The real part of the impedance represents the power radiated by the transducer as well as the power lost by the transducer due to acoustic Q and dielectric losses.

One method of tuning involves placing an inductor and transformer in series with the transducer. The inductor is chosen so that it cancels out the reactance due to C_o at the frequency of interest - this is usually the resonant frequency (ω_o) of the device. Then the turn's ratio of the transformer is chosen to bring the now purely real impedance up (or down) to 50 ohms.

This results in a reduced bandwidth, since the impedance of the inductor ($\propto \omega L$) and the impedance of C_o ($\propto 1/\omega C_o$) are rapidly diverging when they cross at ω_o. The reduced bandwidth of the tuned device depends on the relative values of C_o, L, and the radiation resistance. A weak transducer will have a small radiation resistance. Then tuning results in a greatly reduced bandwidth since the transducer impedance will be dominated by C_o and L.

Furthermore, practical transformers have intrinsic losses and series and shunt inductances. Often the inductances are not a big problem; the shunt inductance will be large and the series one small. If this is so, the shunt has negligible effect and the series can be incorporated into the discrete, lumped, tuning inductance of the circuit. However the resistive losses of the transformer may be large enough to offset its benefits.

An alternative is to tune using only an inductor, which may be placed either in series or in parallel with the transducer. If it is placed in series the impedance of the transducer (Z_t) at ω_o is equal to the radiation resistance plus the resistance due to losses. So we have

$$\omega_o^2 C_o L = 1$$

and

$$Z_t = R_a + R_\ell$$

PVF_2 transducers of the type described then have Z_t from 5 to 10 ohms with most (~ 90%) of that due to the loss tangent.

If the inductor is placed in parallel with the transducer the impedance at resonance is (assuming $\omega_o^2 C_o L = 1$)

$$Z_t \approx \left(\frac{1}{\omega_o C_o}\right) \left(\frac{1}{\omega_o C_o R} + j\right)$$

where R equal $R_a + R_\ell$.

This equals

~ 100 ohms + j20 ohms

for a typical PVF_2 transducer.

This is a better match than that which is achieved with a series inductor. Since only one matching component is used, the two components of the impedance (real and imaginary) can not both be adjusted independently. Nevertheless, this type of matching can be quite useful.

Other methods of tuning which use two or more components are capable of creating a perfect impedance match at one frequency. An example of this type of circuit is the combination of a parallel and series inductor tuning circuit. If more than two components are used, the characteristics of the tuned device can be modified over a specified frequency range, or the time domain impulse response of the device can be optimized.[16]

Several transducers were tuned using inductors and transformers. The best results were obtained using one inductor placed in parallel with the transducer. Table III shows the results. The one-way insertion loss of 14 dB is 5 dB better than the best untuned transducer.

TABLE III

Tuned PVF_2 Transducers

Inductor (μH)	Minimum IL	Frequency (MHz)
.18	14 dB	18
.18	14.5 dB	20
.18	15.5 dB	16
.27	15.5 dB	18
.27	15.5 dB	20
.20	15 dB	20

This result can be compared to an estimate of the best IL obtainable from a tuned PVF_2 transducer. For this estimate we will assume that at one frequency the tuning circuit completely eliminates reactance from the circuit. Also, it is assumed that the tuning circuit raises (or lowers) the magnitude of the impedance to the best possible level, namely 50 ohms. Thus using this idealized tuning circuit the transducer impedance (at one particular frequency) is $R_a' + R_\ell' = 50$ ohms, where R_a' is the tuned radiation resistance and R_ℓ' is the tuned loss resistance.

The ratio of $R_a' + R_\ell'$ will be the same as the ratio of R_a and R_ℓ (for the untuned transducer). It was calculated previously that our untuned transducer had $R_a = .5$ ohms. Taking $\tan \delta = -.3$, using the values of Table I and assuming a transducer area of 1 cm^2, we calculate $R_\ell = 9$ ohms. Thus the power lost across R_ℓ' will be 9/.5 or 18 times the power taken up (or acoustically radiated) by R_a'. Then it can easily be shown that the insertion loss is 1/(1+18) or 12.5 dB. This calculation is only an estimate because many of the parameters used are not extremely well known.

However the major point of the calculation is that the dielectric loss of PVF_2 limits the lowest possible tuned insertion loss to about 10 dB one-way. This figure could be reduced either by an increase in the piezoelectric strength (e_{33} or K_t^2) of PVF_2, or a decrease of the loss tangent. But at present very efficient PVF_2 acoustic transducers are not yet possible.

D. FOLDED PVF_2 TRANSDUCERS

Multilayer PVF_2 transducers also have been investigated. By folding and bonding an electroded film as shown in Fig. 18, a multilayer transducer is constructed in which the voltages of the individual layers are in parallel while their acoustic fields are in series. This provides two advantages. First, the transducers can be driven with high electric fields without requiring a high voltage level. Also, this provides a way of obtaining lower resonant frequencies with a given film thickness. This last point is of interest because piezoelectrically active films with thicknesses much greater than 50 microns are more difficult to produce than thinner tilms.

Folded transducers were constructed and used to observe the movement of the mitral valve of the human heart via acoustic waves reflected from the valve. The transducer was excited with a tone pulse of center frequency 2 MHz and length 1 microsecond.

E. COMPENSATION FOR LOW PIEZOELECTRIC ACTIVITY IN PVF_2

In comparing PVF_2 and PZT transducers, we ask the question of how much power per unit area can be generated by both materials at a given frequency. This question is important because it can directly affect the dynamic range of a system.

As stated previously, PVF_2 has a much lower piezoelectric strength than PZT. Generally, this means that PVF_2 transducers will not be as powerful as PZT transducers, either as transmitters or receivers. Of

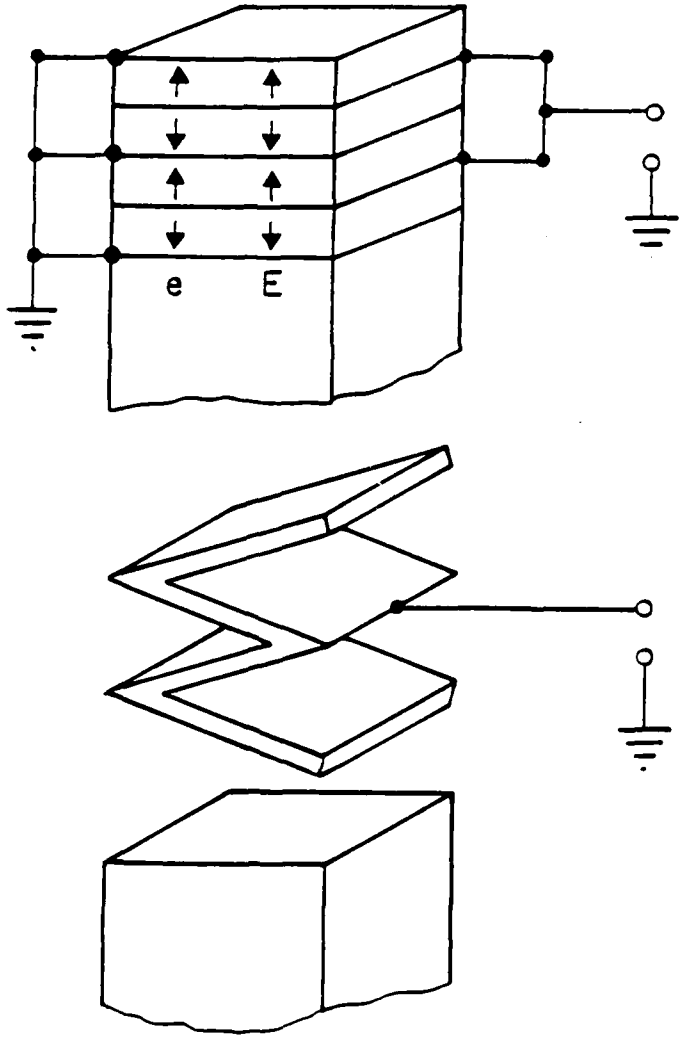

Fig. 18--Diagram of a folded multilayer transducer showing the application of a driving electric field parallel to the poling direction in all layers.

course, impedance load conditions have a crucial impact on the acoustic performace of a transducer. The fact remains however, that one can radiate a larger power density into water from a PZT transducer than from a PVF_2 device, assuming equal driving voltages.

We have examined the possibility of a compensating for the low K_t^2 of PVF_2 by driving a transducer with a higher voltage than can be commonly applied to a PZT transducer. This would allow larger output powers, although the transducer efficiency would not be improved.

The voltage that can be applied to PVF_2 or PZT is limited by a depoling of the material that occurs when the voltage strength passes a certain level. It has been shown by J.G. Linvill of Stanford Electronics Research Laboratories, working at low frequencies, that PVF_2 can stand some 100 times the applied electric fields of PZT, namely some 30 volts per micron as compared to .3 volts per micron for PZT, without depoling.[17] Therefore, in order to test the power generating capabilities of PVF_2, we wished to drive the film with fields on the order of ~ 20-30 volts/micron.

Figure 19 shows the result of an experimental measurement performed by W. Chen showing the output of a PVF_2 transducer remaining linear at rf applied voltages up to 30 volts/micron (750 volts across a 25 micron film). A high power CW rf generator was used to excite a broadband PVF_2 transducer, and the acoustic energy radiated into a water load was monitored with an electrostatically shielded receiving transducer. The radiated field is seen to be a linear function of applied voltage over the entire range, which extends to the limit of the power source, namely 750 volts.

This experiment was difficult to perform due to the large CW voltage being applied to the transmitting transducer. There was a large amount of

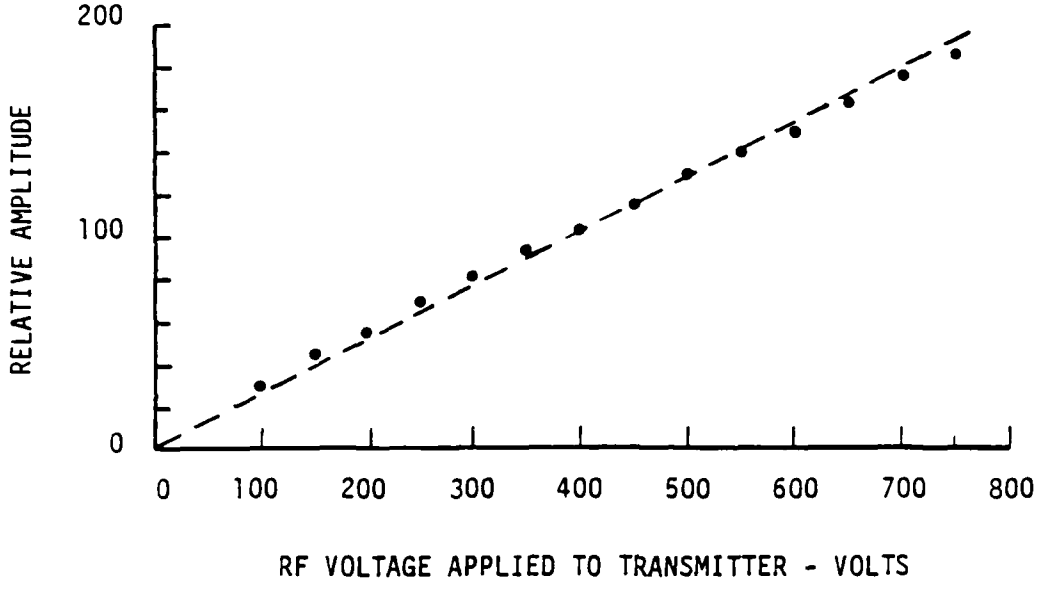

Fig. 19--Relative output of a PVF_2 transducer versus voltage applied across the transducer. The plot shows the linearity of the output up to 700 volts applied across the 25 μm film.

electronic feedthrough pick-up at the receiving transducer. The shielding employed only partially solved this problem. Nor was it feasible to produce tone pulses of 700 volts peak amplitude, since the instruments needed to gate the CW signal could not withstand 700 volts. Because of these problems it was decided to continue our research using voltage pulses as the applied signal. We made this decision because (1) we had the equipment to produce high strength voltage pulses, and (2) the time delay due to the acoustic wave propagation time in the water would eliminate all electrical feedthrough problems.

The transducers used in this portion of the experiment differed from some earlier models in that the electrode covering was etched back away from the edges of the polymer in order to prevent arcing around the edge of the film.

An input pulse was applied to the transducers while they were immersed in water. The input pulse was roughly triangular in shape with a width of 150 nanoseconds. A resistive network was constructed to better match the generator's 200 ohm real impedance to the transducer.

The drive pulse produced a bipolar stress wave in the water which was incident on a fixed PVF_2 transducer terminated by a high impedance electrical load. The peak to peak voltage signal observed across the receiving transducer was measured along with the peak voltage of the driving signal.

Figure 20 shows one of the resulting curves. We see that the strength of the signal increases in a roughly linear manner as the applied field is increased to 600 volts (24 volts/micron). At this point the pulse

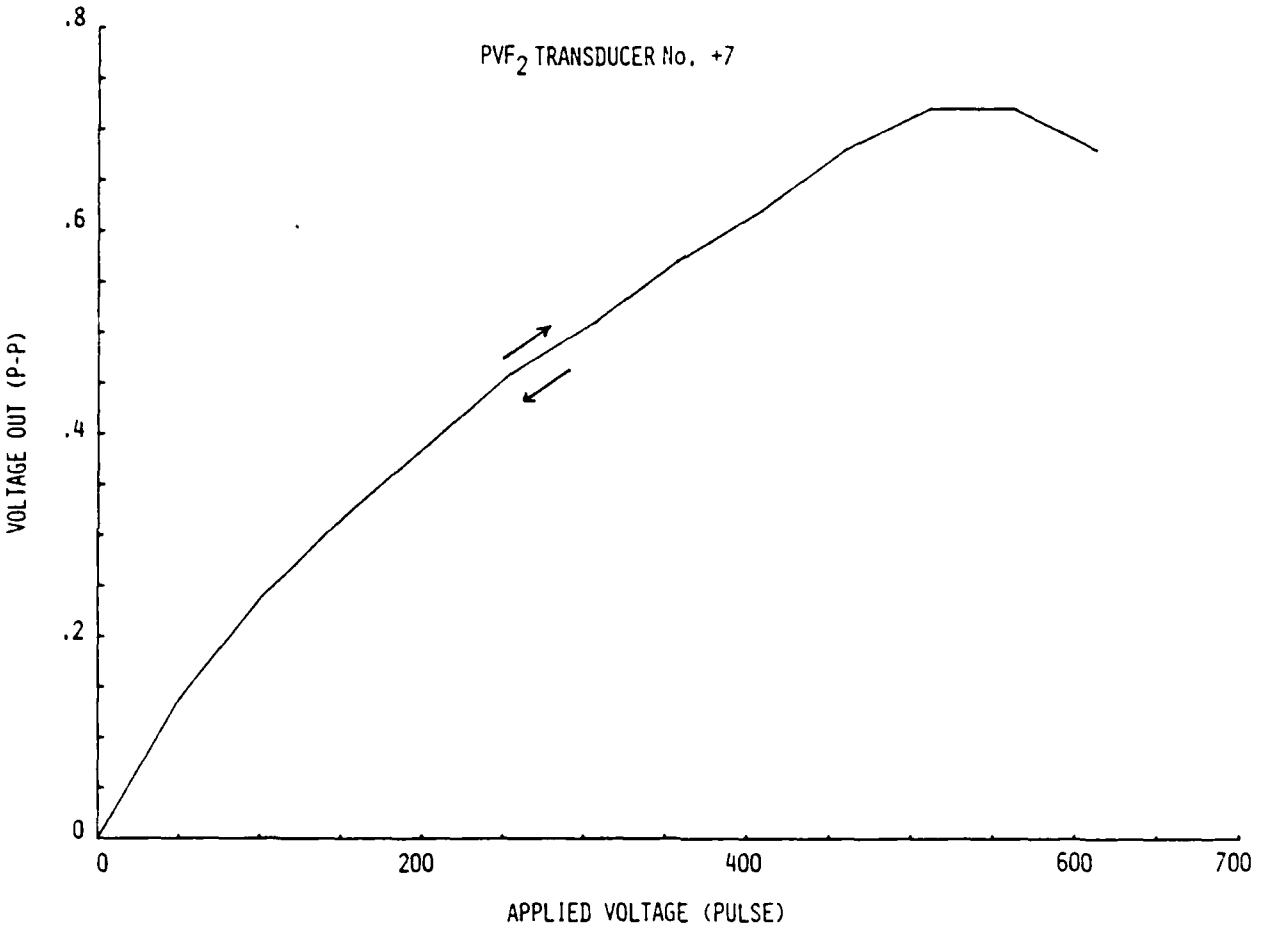

Fig. 20--Plot of the voltage measured across the PVF_2 receiving transducer versus the amplitude of the voltage pulse applied to the PVF_2 transmitter. Arrows indicate the curve was reproducible.

generator could not supply a larger amplitude output pulse unless the pulse width was increased. This pulse widening shifted the pulse energy from high to low frequencies, where the transducer output is weaker. Therefore, it is not clear if the output leveled off due to the high voltage being applied to the transducer, or due to the pulse widening.

This experiment was repeated using the same transducer, and similar results (within the experimental error limits) were obtained. This shows that PVF_2 transducers can withstand ~ 25 volts/micron without damage (in a pulsed mode) while still operating well.

We also used the generator to drive transducers with pulses as high as 1500 volts (60 volts/micron). In order to get voltages this large no resistive matching between the source and the transducer was used. The width of the applied pulse was larger than 250 nanoseconds and was increased during the experiment in order to allow the peak voltage level to be increased.

In this case the transducer response changed with time. Figure 21 shows how the output of the device varied. The edges of the gold electrodes on the PVF_2 exhibited damage after this trial.

In this case, applied fields of 80 volts/micron damaged the transducer. This is interesting since poling fields of this magnitude are common and these do not harm the PVF_2. Possibly rough spots on the brass backing result in local regions of the transducer that have thicknesses less than 25 microns. This could lead to dielectric breakdown at lower than expected fields.

We should like to point out that Omoto[18] et al. have recently driven PVF_2 with high voltage pulses in medical imaging experiments. A focused,

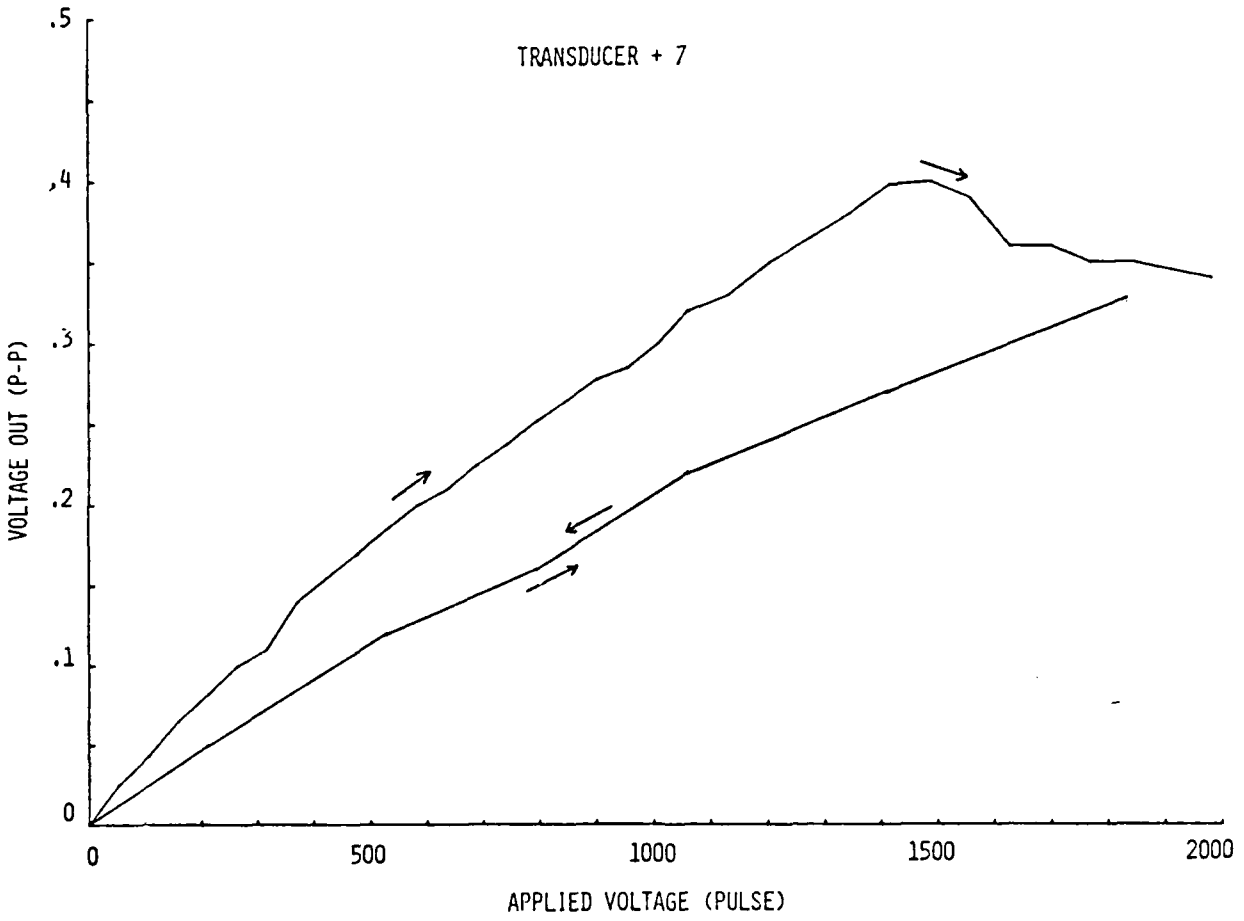

Fig. 21--Plot of the voltage developed across the PVF_2 receiver versus the amplitude of the voltage pulse applied to the PVF_2 transmitter. Arrows indicate that after raising the applied peak voltage to 2000 volts the output signal was reduced permanently.

tuned PVF_2 transducer was used to obtain B-scan images of the livers, breasts and thyroid glands of several patients. The transducers were excited with voltages as high as 300 volts in order to image deep into the body. Thus, the idea of applying high voltage to PVF_2 transducers is useful and feasible.

This is a good time to explore a significant difference between PVF_2 and PZT that was mentioned in passing in Section II-A. The relative dielectric constant of PVF_2 is 8, while it is ~ 850 for PZT-5A. This difference gives PVF_2 an advantage over PZT when used as an acoustic reciever connected across a large electrical impedance.

This comes about mainly as a result of the fact that voltage = charge/capacitance.

Consider a receiving transducer connected to a high impedance load. The load might be a passive component, or an active op-amp. This type of receiver attempts to generate the highest possible voltage across the high impedance in order to maximize the dynamic range of the device.

We now consider three general areas which effect the voltage output level. First, the charge developed will be proportional to $K_t(33)$, the electromechanical coupling constant. In this regard PVF_2 is much weaker than PZT. Secondly, purely acoustical resonances in the receiver will have a direct bearing on the charge that accumulates on the transducer electrodes. The transducer thickness, load impedance, backing impedance and frequency of operation will determine the strength of the resonances. When used in water, the low acoustical impedance of PVF_2 gives it a significant edge over PZT in regard to the effects just mentioned. The low impedance of PVF_2 does not reflect as much energy back into the water as PZT does (unless matching layers are used on the PZT). Thirdly, the low relative

dielectric constant of PVF_2 (~ 8 to ~ 800 for PZT) also gives PVF_2 an advantage over PZT. The fact that capacitance of a transducer is proportional to epsilon implies that the voltage developed across the transducer is inversely proportional to epsilon. Thus a low epsilon is desired if a large voltage signal is desired.

When all these factors are taken into account, it appears that PVF_2 underwater receivers are superior to PZT receivers. Several PVF_2 hydrophones have been reported on in the literature. These hydrophones basically consist of a PVF_2 sheet backed and loaded by water, with a high electrical impedance amp located quite close to the PVF_2. The frequency response of these devices closely matches that of Fig. 13, which modelled a PVF_2 transducer with a matched backing, a water load, and a high electrical impedance termination.

When 9 μ film is used the resonant frequency occurs at ~ 120 MHz. In concurrence with Fig. 13, bandwidths of 100 MHz have been reported.[19,20]

VI. ANGLE RESPONSE OF PVF_2 TRANSDUCERS

A. INTRODUCTION

In all of the transducer investigations reported in Section V, the propagation direction of the acoustic waves has been perpendicular to the transducer face. Another property of transducers, which is important in applications such as acoustic imaging, is their response to acoustic radiation at other angles.

In most single-transducer applications only normal incidence operation is involved. However, in high-resolution, phased-array type acoustic imaging, such as will be described in Section VIII, a transducer array is required which can accommodate acoustic waves traveling at a wide range of angles with regard to the normal to the face of the array. For instance, in a phased array operating with an f-number equal to one, a line from the end element of the array to the focal spot forms an angle of 26 degrees with the face of the array.

To obtain large angle bandwidth, a periodic electrode structure is needed on the transducer. A device of this kind, containing a uniform piezoelectric layer with a periodic electrode structure, is an example of a so-called acoustic face plate. We have investigated the properties of PVF_2 face plates, because this sheds light on the behavior of PVF_2 which is useful in imaging applications.

The results of this section served as a guide in the design of the PVF_2 imaging array in Section VIII. The array is monolithic, and not composed of small discrete elements which allow wide angles response in

usual arrays. It was possible to choose the backing impedance and frequency of operation to provide adequate angular response.

B. BASIC PROPERTIES OF ACOUSTIC FACEPLATES

When an ultrasonic wave strikes a transducer at an angle to its face normal, the behavior differs in essentially three ways from that under the usual operation at normal incidence. One is that the resonance characteristics of the transducer film are different from those for normal incidence, resulting in an alteration in the transducer response. Another is that different piezoelectric tensor elements are brought into play than those which are active for the case of normal incidence again bringing about a change in the transducer response. The third is that while for normal incidence the electric field generated piezoelectrically within the transducer film is uniform over the plane of the film, for the case of oblique incidence it is *nonuniform* (periodically varying) as a function of distance in the plane of the film. Furthermore, the period of this variation decreases monotonically as the incidence angle increases. The first two of the above factors affect the angle response of the transducer independently of the electrode structure, while the third factor, the characteristics of the electrode structure are very much involved in the angle response characteristic.

It can be shown theoretically that the angle bandwidth of a transducer, at a given frequency, is proportional to its frequency bandwidth at a given angle.[21] This refers to the angle bandwidth as influenced by the first two of the three factors listed above which affect the angle response,

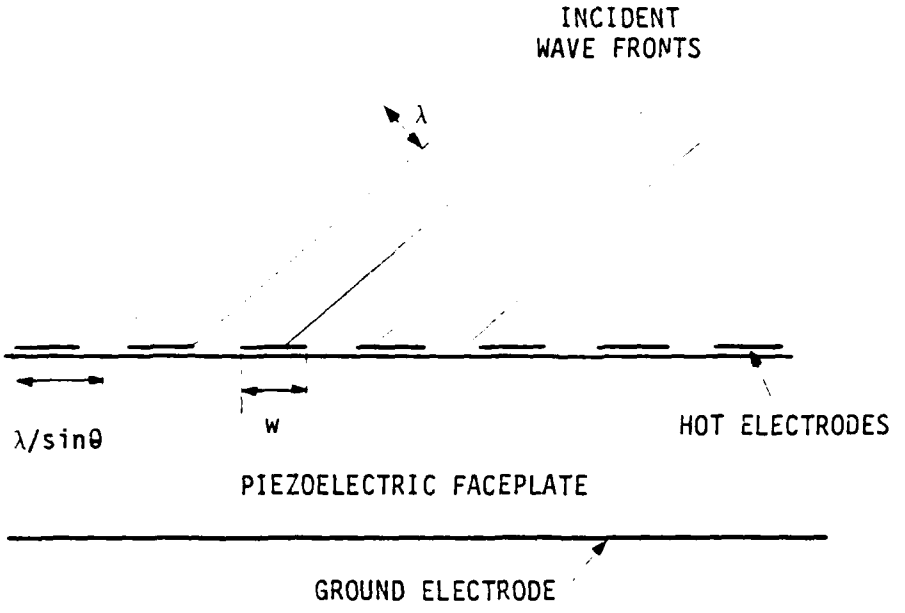

Fig. 22--Representation of wave fronts incident on faceplate.

i.e., the material-dependent factors. Thus PVF_2, which we have shown in earlier sections can have extremely large bandwidths at normal incidence, are expected to be capable of very large angle bandwidths. The third factor affecting angle response which was listed above is controlled by the design of the electrode structure, as will be discussed below.

Figure 22 shows a face plate, which in its simplest form is a slab of material insonified by acoustic waves. Several imaging schemes have used such structure.[22,23] If the faceplate is not piezoelectric the incoming acoustic wave simply deform the boundaries of the faceplate. The magnitude of the deformation can be measured in various ways. For instance, a laser beam may be scanned across the faceplate and the deflection of the beam related to the deformation of the faceplate boundary. This information can be used to produce an image of the object scattering the acoustic waves toward the faceplate.

In the case of a piezoelectric faceplate, such as PVF_2, the information contained in the incoming waves would be read off the faceplate by monitoring the voltage produced across the PVF_2. To do this it would be necessary to place small discrete electrodes on the film. These electrodes would not significantly change the voltage generated across the film if the electrical impedance across the electrodes was large compared to the impedance of the transducer.

The width of these electrodes would effect the response of the faceplate. If the electrodes were too large the electric field developed by the received radiation would be undersampled, and information carried in spatial harmonics above a certain frequency would be lost. Figure 22 illustrates this effect. It shows an acoustic wave incident on a faceplate.

The wave creates a periodic stress pattern along with an accompanying voltage pattern on the faceplate surface. The spatial repeat distance of this pattern is $\lambda/\sin\theta$. If $\lambda/\sin\theta$ becomes too small the incident waves will produce regions of excess of both positive and negative charge on one individual electrode. This will occur when $\lambda/2\sin\theta$ is less than w . As the electrode is a conductor, positive and negative charges on the same electrode will move to cancel each other. When this phenomenon occurs, the voltage developed across the electrodes is strongly dependent on the electrode width, as well as the acoustic properties of the faceplate. This problem can be avoided however, if the electrodes can be made small enough.

Another important effect present involves acoustic resonances in the faceplate. The incoming waves generally produce both shear and longitudinal waves at the surface of the faceplate. These travel across the faceplate and are partially reflected and transmitted at the back face of the faceplate. The reflection coefficient at this boundary is a function of the angle of incidence of the wave, the shear and longitudinal impedances of both the backing and the faceplate, and the shear and longitudinal wave velocities. At certain specific angles of incidence either the shear or longitudinal waves that are present will experience a resonance in the faceplate layer.

C. THEORETICAL STUDY OF PVF_2 FACEPLATES

1. Single Layer Faceplates

We have studied the problem of designing faceplates having large angle bandwidths. The resolution of a particular piezoelectric faceplate can be calculated by analyzing the response of the faceplate to an incident bulk acoustic plane wave as a function of the incidence angle of the wave, θ , as shown in Fig. 22. That is to say, one calculates the voltage developed across the piezoelectric faceplate as a function of θ . This calculation is analogous to calculating the angular aperture of the system. Just as a wide aperture optical lens has better resolution than a narrow aperture lens, a broad angular response transducer will lead to better resolution than a receiver with relatively narrow response. Therefore, good faceplate characteristics will include a voltage versus θ curve that is broad. It is also desirable that the curve be fairly flat, so as to minimize distortions caused by unequal voltage outputs for different incidence angles.

The calculation was performed using a computer program developed in 1974 by Auld, Drake and Roberts.[21] We modified the program so that faceplates consisting of several layers could be treated.

Figure 23 shows the relative open-circuit voltage for PVF_2 receiving transducers having backing impedances both high compared to PVF_2 and matched PVF_2. We see that PVF_2 is capable of very large angle bandwidths, extending to values beyond 30 degrees. The piezoelectric coefficient e_{31} is specified in the figure because when the angle of wave incidence is

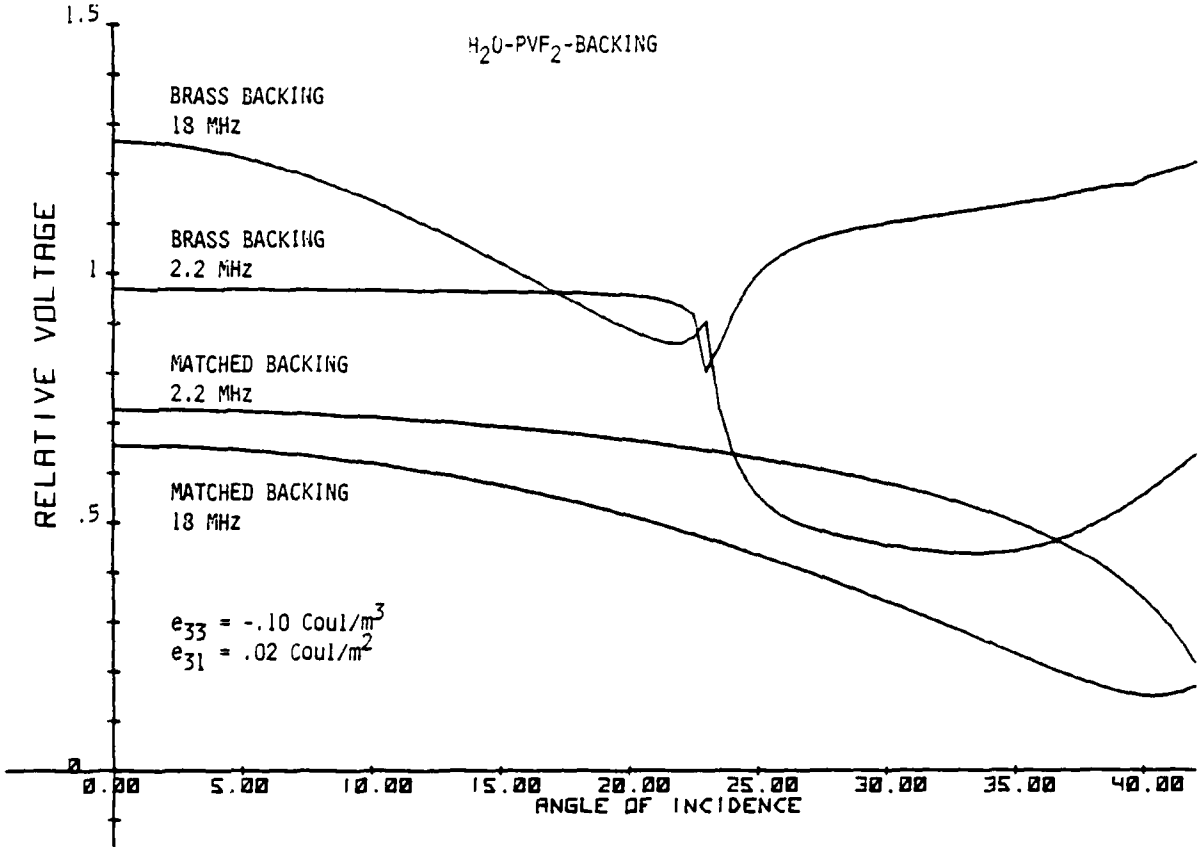

Fig. 23--PVF_2 transducer response versus angle of incidence of plane waves. PVF film thickness = 25 μ; shear w : G

nonzero this coefficient, as well as e_{33}, effects the transducer response. (Here we assume for purposes of the calculation that the electrode strips run perpendicular to the x axis -- the stretch direction -- of the film.) The sign of e_{31} relative to e_{33} is such as to cause a decrease in output voltage as the angle of incidence increases.

Shear waves are also excited in the transducer when the angle of incidence is nonzero, and so shear wave Q is specified on the figure, although it has little effect except in the vicinity of $\theta = 52$ degrees where a shear wave resonance occurs. The sharply peaked behavior seen on the curves for brass backed devices occurs near the critical angle for acoustic longitudinal plane waves propagating from water into brass (23 degrees).

These results show large angular bandwidths comparable to those obtained with PZT faceplates, which must employ matching layers to achieve useful bandwidths.[24]

Our work in this area indicates several things. First, it is best to operate at a frequency slightly lower than the bulk wave resonant frequency of the transducer. Therefore, in this type of operation, the system is off resonance at $\theta = 0$. As θ increases however, the system moves toward, and through a bulk wave resonance. This results in the flattest voltage curves.

Secondly, we found that the best acoustic Q value is in the range $Q = 10$. If Q is too large, resonant peaks will destroy the uniformity of the curve. On the other hand, very low values of Q will impair the sensitivity of the device.

Thirdly, it was discovered that the relative sign of the piezoelectric constants was not in our favor. In PVF_2 a material compression in the z direction will produce a positive voltage across the film (measured with respect to the poling direction of the film). A material compression in the x direction will produce a negative voltage output across the film. These two effects work counter to one another. As θ increases, the film, which is deformed only in the z direction when $\theta = 0$, starts to deform more and more in the x direction (and less and less in the z direction). As e_{31} and e_{33} are producing voltages of opposite sign, the voltage output drops rapidly as θ increases. This is demonstrated in Fig. 24 which shows voltage versus θ curves for several values of e_{31}. (In this graph shear wave effects have been suppressed in order to simplify understanding of the result.) The plot shows that as $|e_{31}|$ increases the width of the main lobe of the plot decreases from $\theta \sim 35'$ to $\theta \sim 25'$.

2. Multilayer Faceplates

One possible direction of attack at this problem might be the fabrication of PVF_2 films with e_{31} and e_{33} having the same sign. This may not be possible, and as our program was not directly concerned with PVF_2 fabrication we attempted to devise a scheme to improve the faceplate response with the material available.

We developed a method of exercising control over the acceptance angle of a PVF_2 faceplate by separately controlling the effective longitudinal and transverse coupling coefficients. This idea involves the use of uniaxially stretched PVF_2 films in a layered structure of more than one

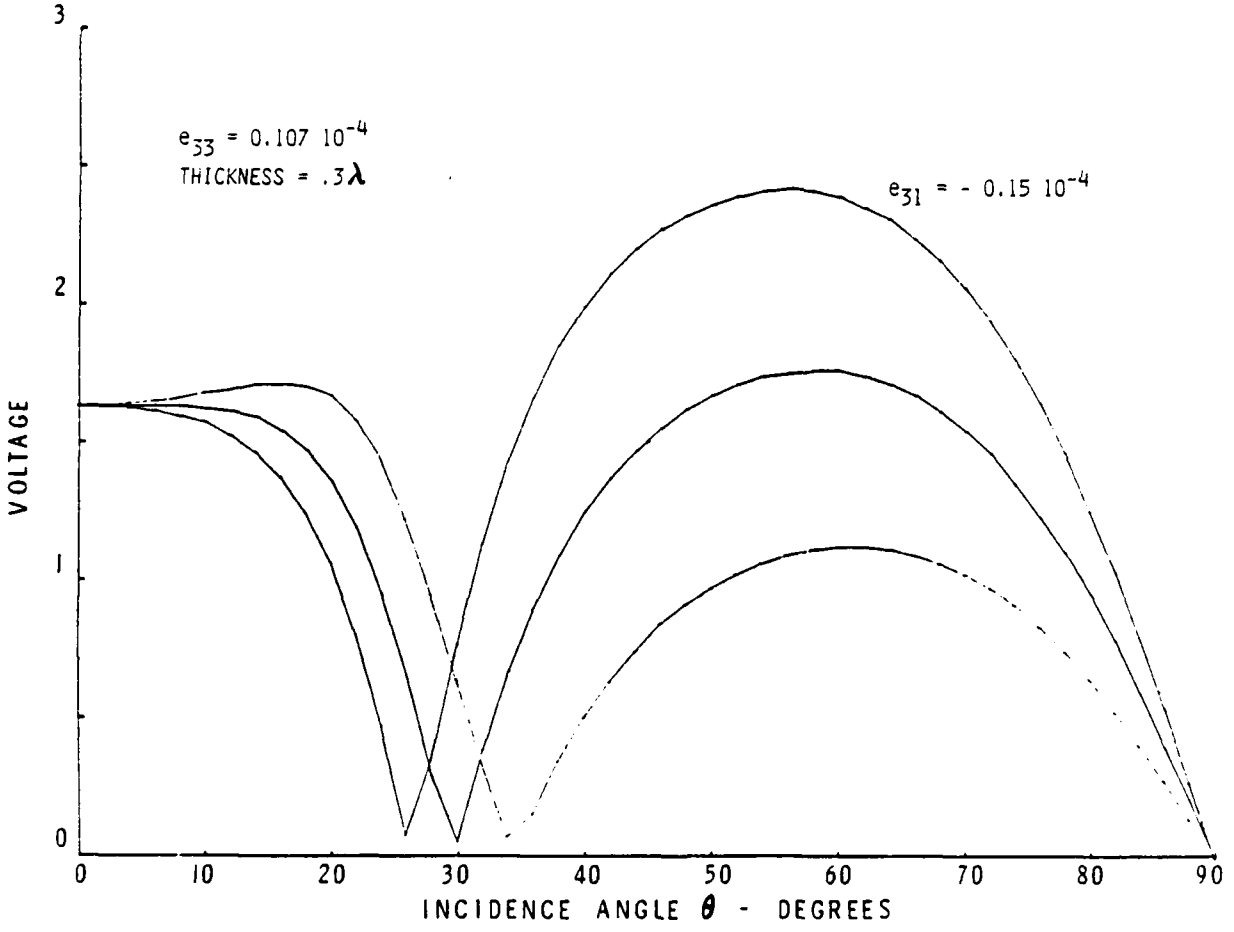

Fig. 24--Angular response of PVF_2 faceplate for several values of e_{31}.

film. The process takes advantage of the anisotropy which exists in such films, and involves rotating the films in their own plane to vary the acceptance angle.

To illustrate this, consider a stack of three PVF_2 films. Imagine the films stacked one on top of each other in the same orientation. Assume each film has $e_{33} = -.107$ coulombs/m^2 and $e_{31} = .1$. The value of e_{33} was chosen based on our experimental work and the value of e_{31} was taken from reference 2. Now the stretch direction of the film is along the x axis. Thus there is a clear anisotropy between the x and y axis of the film (each of which lie in the plane of the film). Therefore e_{31} is not necessarily equal to e_{32} . Let e_{31} be about five times as large as e_{32} . If we rotate the two lower films 90° about an axis perpendicular to the film surface we produce a stack in which all the films have $e_{33} = -.107$ and the top film has $e_{31} = .10$, while the other films have $e_{31} = .02$. By next flipping the bottom two films upside down, we reverse the signs of all the piezoelectric constants of that layer (relative to the top layer). The effective piezoelectric stress constants (in coulombs/m^2) are now shown below.

	e_{31}	e_{33}
Layer 1	-1.0	+1.07
Layer 2	.2	-1.07
Layer 3	.2	-1.07

Now if we disregard the positions of the layers in the stack, we see that overall e_{31} is positive and e_{33} is also positive. Thus at first

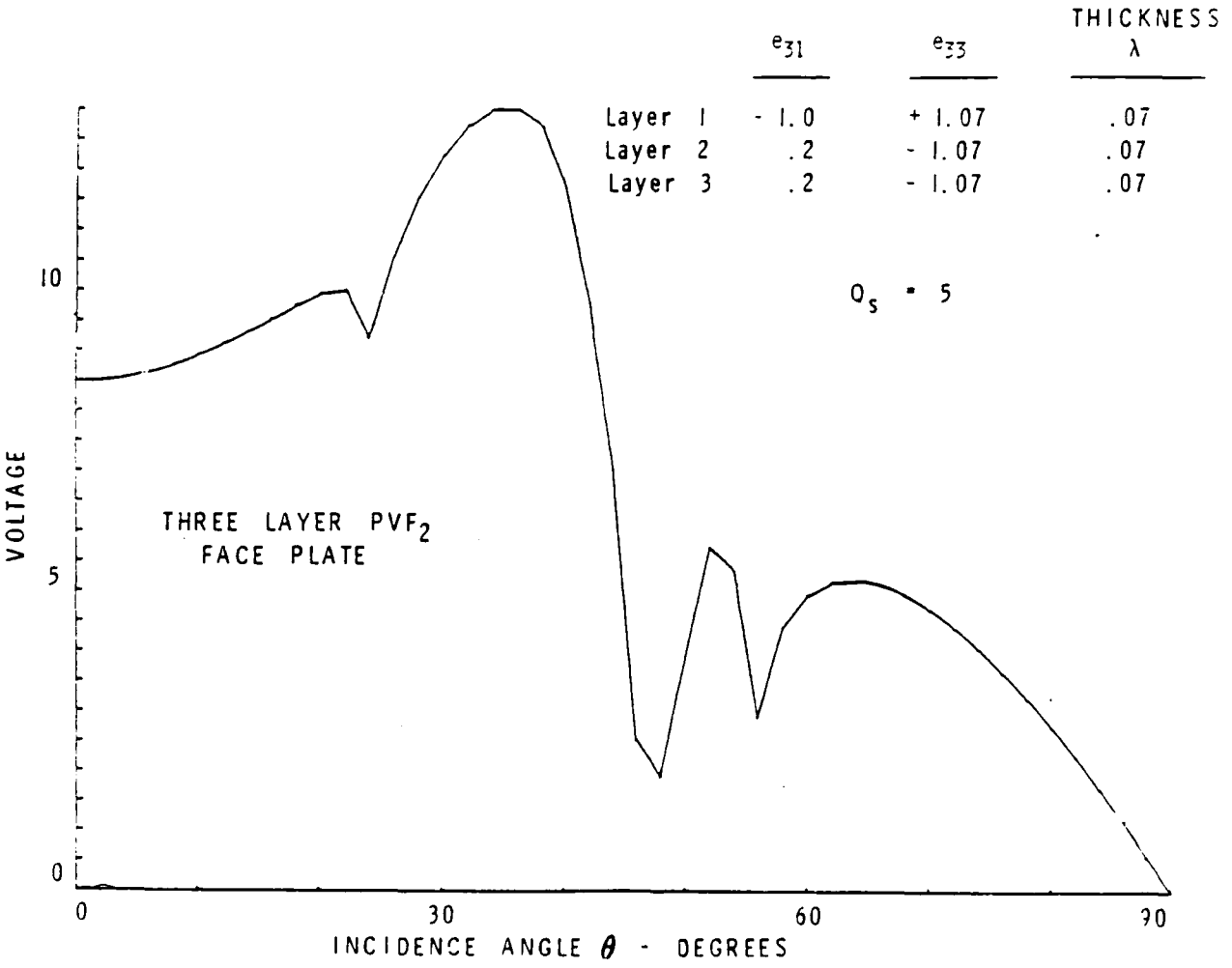

Fig. 25--Angular response of three layer PVF_2 faceplate.

glance, this stack of films might perform as if it were a single film with e_{31} and e_{33} having the same sign.

We calculated the voltage versus θ curve for the stack of films described above along with the two other stacks that can be derived from the first stack by rearrangement of the film stacking order. The calculation was performed slightly below the 1/4 wave resonant frequency.

One of the graphs obtained is shown in Fig. 25. We see that the curve obtained is promising. In Figure 23 the voltage versus θ curve of a one layer PVF_2 brass backed faceplate is given. The output decays almost monotonically from 0° to 32° with a variation of 8 dB.

By contrast the graph of Fig. 24 has a maximum to minimum variation of only 2.3 dB out to 36°, with a fast drop off at that point. True, the valley in the curve near 22° is not a good feature. However overall, the curve for the stacked model exhibits better response prospects than single layer models. Furthermore, improvements of the theoretical angular response may be possible by rotating the film layers not 90° with respect to each other, but rather some angle living between 0° and 90°. Thus we see that multilayer PVF_2 faceplates can have their characteristics altered, and to some extent, tailored by careful orientation of the layers.

3. Experimental PVF_2 Angle Response

We performed an experiment in an attempt to measure the angular response of a PVF_2 brass backed transducer.[25] In order to avoid the problems concerning electrode size described above, we selectively etched the exposed gold electrode of one of our standard PVF_2 transducers, producing an isolated gold strip 1 inch long and 25 microns wide. This

transducer was placed in oil and insonified with acoustic waves at 18 MHz. Oil was used as the test medium because water tended to short the electrode to grounded portions of the remaining parts of the top electrode. The voltage produced across the strip was recorded as a function of the angle of incidence of the acoustic waves. The angular response of the transducer extended out to 40 degrees, without any large variations in response becoming evident. However, difficulties in producing a continuous, unbroken 1 inch long, 25 micron wide electrode on the surface of the PVF_2, as well as the low signal to noise ratio of the experiment, made further measurements unproductive.

VII. INVESTIGATION OF PVF_2 FILM PROPERTIES

A. INTRODUCTION

Along with the device work performed, we also devised and carried out two series of experiments designed to reveal information about the PVF_2 film at our disposal. This section will report on these experiments. The first series was concerned with spatial uniformity of piezoelectric activity across the PVF_2 film thickness. The second was a large scale test of the piezoelectric strength of many transducers made using PVF_2 films fabricated, from many different PVF_2 resin sources, in the Stanford Center for Materials Research.

B. MEASUREMENT OF SPATIAL DEPENDENCE OF PIEZOELECTRIC ACTIVITY ACROSS FILM THICKNESS

It has been reported that the value of the piezoelectric stress constant, e_{33} , of PVF_2 is dependent upon position in a PVF_2 film. Several experiments[26] implied that e_{33} was a function of the coordinate position z within the film. Furthermore, these experiments indicated that e_{33} was largest near the surface of the film that had been charged positive during the DC electric field poling that activates the film. It was hypothesized that these results were due to the development of a polarized surface layer of PVF_2, occurring only at the side of the film next to the positive poling electrode.

These findings were interesting for two reasons. First, the reported asymmetry of e_{33} was a clue to the piezoelectric mechanism of PVF_2. The origin of piezoelectricity in PVF_2 was not well understood at that time (and in fact is not completely understood at this time). So the question of the asymmetry of PVF_2 was of interest to those desirous in improving the performance of the material.

Secondly, a transducer made with highly asymmetric PVF_2 might behave quite differently from standard transducer models. There might be advantages or disadvantages to the use of such a piezoelectric.

Therefore we probed the spatial dependence of e_{33} through a simple experiment. The plan was to take some PVF_2 and construct two sets of brass backed transducers. Half of the devices were to have the positive side of the film (positive during the poling procedure) bonded next to the brass, while the other half were to have the negative side of the film bonded next to the brass. Measurement and comparison of the insertion loss versus frequency curves of the two sets of transducers would yield information on the spatial dependence of e_{33}.

Before performing the experiment we made numerous calculations on theoretical PVF_2 transducer models that had a spatially varying e_{33}. These calculations convinced us that if the piezoelectricity of PVF_2 were concentrated near either side of the film, the proposed experiment would yield easily detectable differences in the insertion loss curves.

The calculations performed used two models. One model was the distributed source excitation mode. This method is an analytic way of considering each point across the thickness of the transducer as an acoustic radiator in the z direction.[27]

By performing an appropriate integral and matching boundary conditions at the edges of the PVF_2 one can calculate the energy radiated per volt across the transducer. This method is not ideal in that the electrical impedance of the transducer was not calculated. Therefore, one can not calculate the voltage that would appear across the transducer if it were to be driven by say, a 50 ohm source. However, the electrical impedance of the transducer can be approximated by simply looking at the transducer as a capacitor. This is not strictly correct since the piezoelectricity of the PVF_2 will result in an effective complex impedance that will add to the pure capacitance of the transducer. But for the case of PVF_2, which is only weakly piezoelectric, this approximation is good.

In order to perform the integrals necessary to the calculation one must be able to integrate $e_{33} \exp[ikz]$. To simplify matters and allow a closed form solution e_{33} was modeled as (1) an exponential function, and (2) a linear function. Both cases predicted that the power radiated by the transducer would be smaller when the most active side of the PVF_2 was adjacent to the load material, water.

We also performed a similar calculation using the thin disk model described earlier. We could model inhomogeneous PVF_2 by imaging a transducer made up of many (say 10) equally thick PVF_2 layers in which the layers had different intrinsic values of e_{33} while otherwise being identical.

Shown in Fig. 26 is the result obtained when the PVF_2 was modelled as ten 3.1 micron thick layers. The PVF_2 layers were given e_{33} values of .1, .05, .025, .0125, .00625, .003125, 0, 0, 0, and 0 in order across

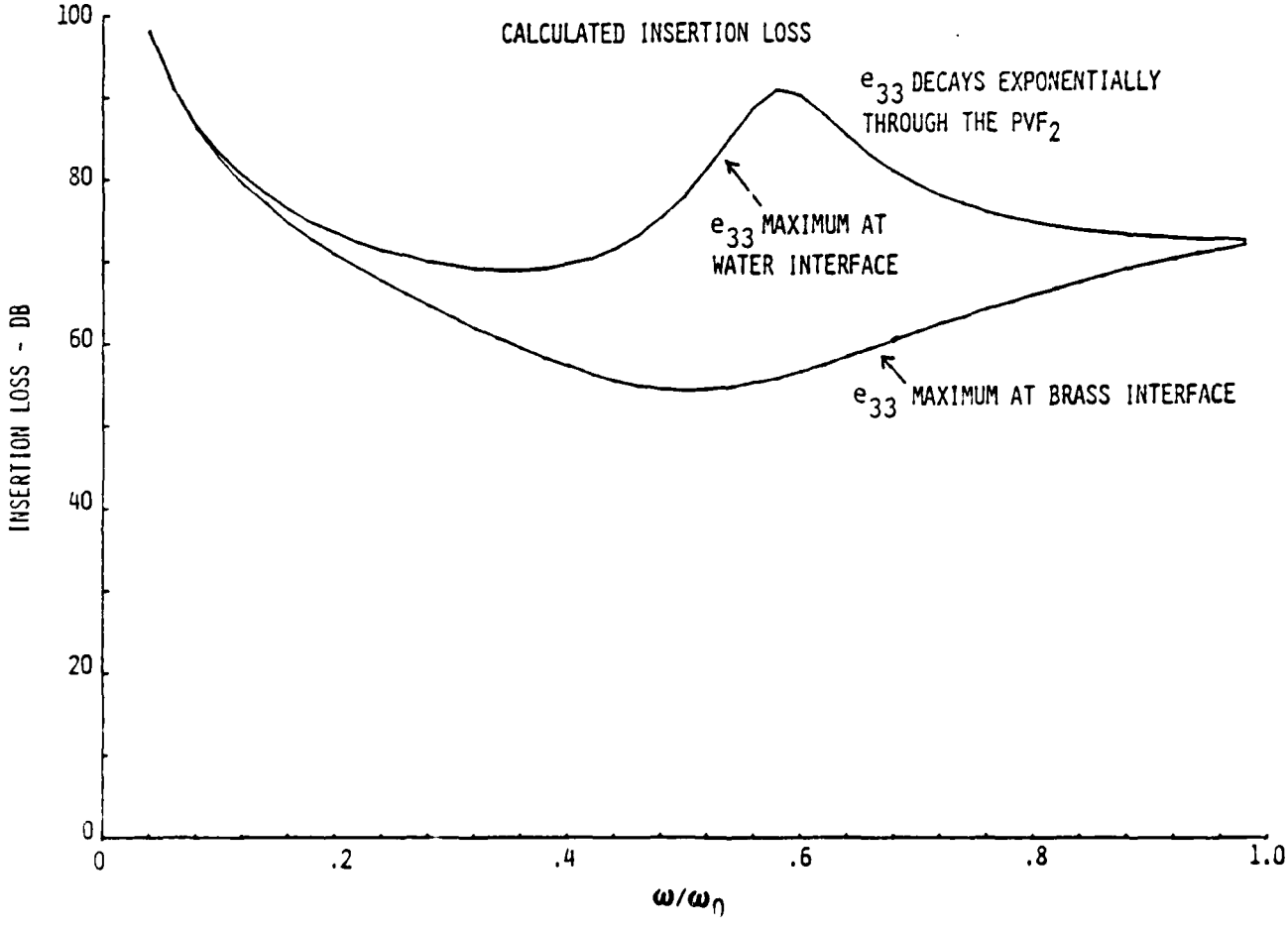

Fig. 26--Calculated insertion loss curves for PVF_2 with non-homogenous value of e_{33}.

the ten layers. The top curve shows the calculated insertion loss when e_{33} is a maximum at the water-PVF_2 interface, while the bottom curve shows the result for e_{33} maximum at the brass-PVF_2 interface. The top curve has a resonance valley around $\omega = .6\omega_o$ due to the layers of non-piezoelectric PVF_2 trapped between the active PVF_2 and the brass. The graph shows that large insertion loss differences (up to 40 dB) are present if e_{33} is strongly inhomogeneous as modelled.

Next, these predictions were experimentally tested. Six brass-backed PVF_2 transducers were fabricated using film obtained through the Kureha Corp. of Japan. The fabrication process followed the procedure described in Section III-B, with the PVF_2 being cut into 1/2" x 1/2" squares.

Three of the transducers were constructed so that the side of the PVF_2 that had been charged negative during poling was epoxied against the brass backing. (These will be referred to as transducers +1, +2, and +3.) The other three were bonded so that the positive side during poling was epoxied against the brass (referred to as transducers -1, -2, and -3).

Two-way IL measurements were taken on all six transducers. Reflection mode measurements in which the same transducer was both transmitter and receiver were accomplished through the use of a quadrature hybrid and a brass reflector as described earlier. The input to the transducer was a tone pulse of 5 microsecond duration. IL versus frequency measurements were taken by changing the output of the sine wave generator manually. The experiment was carried out in a water tank.

The data collected on all six devices is shown in Fig. 27. The plots are quite uniform and consistent. There is no large variation

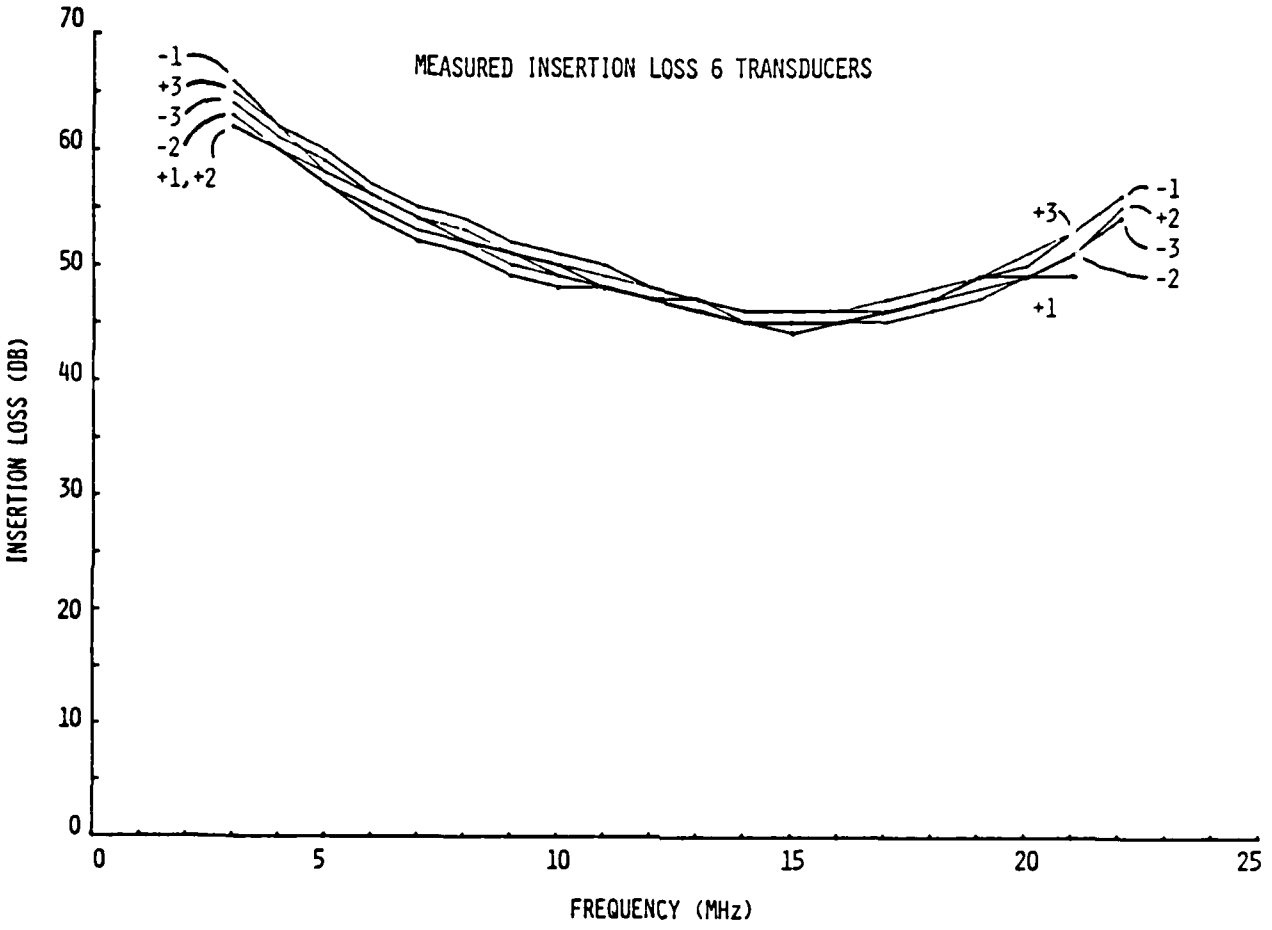

Fig. 27--Measured insertion loss curves for the six test transducers (-1, -2, -3, +1, +2, +3).

between the curves, certainly not the striking differences predicted by the previous calculation.

Thus we concluded that the PVF_2 used in our experiment at least had a symmetrical value of e_{33}. Our results also strongly imply that e_{33} is constant across the film because the earlier experiments mentioned above found that e_{33} was highly concentrated near one side of the film. Reference 26 estimated that most of the polarization of the film was confined to at most 1/2 the film thickness. We believe that the nonuniformity found by other researchers was the result of their using weaker poling conditions. In contrast to our poling parameters given before, the PVF_2 used in the earlier experiments was poled at only 50 volts/micron for just 45 minutes.

As an experimental check we made several two-way IL measurements using transducer -1 as the receiver and the other transducers as the transmitter. The results obtained were consistent with the reflection mode measurements. Besides demonstrating that PVF_2 can be made piezoelectrically homogeneous, this experiment showed that the transducer construction procedure gives uniform, repeatable results.

C. EVALUATION OF PVF_2 FILMS BY TRANSDUCER TESTING

The experiments described above were performed using commercial film obtained from the Kureha Corporation, re-electroded and repoled as detailed. We now turn to an experimental evaluation of PVF_2 films carried out here, using films fabricated in the Stanford Center for Materials Research by R. Route and R. DeMattei, under the direction of R. Feigelson.

The films were made from bulk PVF_2 resins available commercially from various suppliers.[28] The first step in producing the PVF_2 films involves melt pressing the bulk PVF_2 (which is in the form of pellets or powder) into thin sheets. The film is pressed between two smooth plates at 1250 psi for five minutes at a temperature of ~ 160°C.

The film is then stretched using a motor driven lead screw located in an oven heated to ~ 60°C. The film is stretched to a length 3-5 times the original length. This stretching is done in order to align the polymer chains of the film so as to produce a high dipolar orientation in the film. Next, the film is annealed at 120°C for fourteen hours to heal any damage caused by the stretching process. Finally, the film is poled in order to rotate the dipoles of the film into a highly ordered state.

The entire fabrication procedure uses inexpensive and easily obtainable equipment, and is therefore quite easy to set-up.

After this step the films are ready to be used as transducers. Some 70 transducers of the type of Fig. 3 were constructed and tested for minimum insertion loss as an indication of the effectiveness of the various film samples. The testing set-up was as shown in Fig. 15. Some ranges of mechanical and thermal parameters were involved in the pressing and processing of different film samples from a given starting material, but poling parameters were standardized at nominal values to limit the number of variables in these comparative measurements. The poling parameters were identical to those given in Section III-A.)

A general conclusion from this work is that the film quality is quite independent of the source of the starting resin. During the above survey the lowest two-way insertion loss measured was 2 dB higher than

that obtained with the best commercial piezo films. Since that time however, processing changes have resulted in films which are more active than the commercial samples. These changes include a higher film stretching rate (~ 2000 mm/min) and annealing under tension.

Figure 28 shows insertion loss curves of transducers made using both CMR and commercially produced film. The figure indicates the close match between the relative piezoelectric strengths of the different films.

These results show that other workers in ultrasonics, using simple, inexpensive and readily available equipment can fabricate state-of-the art piezoelectric films from commercially available resin. PVF_2 resin is obtainable from many sources, and thus laboratories which can produce PVF_2 piezoelectric films do not have to depend on the unpredictable commercial market for piezoelectric films.

At present there is also a program based in the Stanford Chemical Engineering Department under the direction of Professor Curt Frank that is synthesizing PVF_2 starting from monomer. Like the film fabrication program described in other sections of this report, this work receives support from NSF under the MRL program. This program is studying in detail the structure of PVF_2 synthesized under various conditions.

Currently there is interest in a particular defect often found in PVF_2 molecular chains. This is the so-called head-to-head defect formed when two carbon molecules adjacent to each other in the chain both have fluorines attached to them, instead of one carbon being attached to fluorines and the other carbon attached to hydrogens. The relative occurrence of this defect is measured using high resolution 19F nuclear magnetic resonance. It has been found that head-to-head defects occur between 5 and 9 of the ti

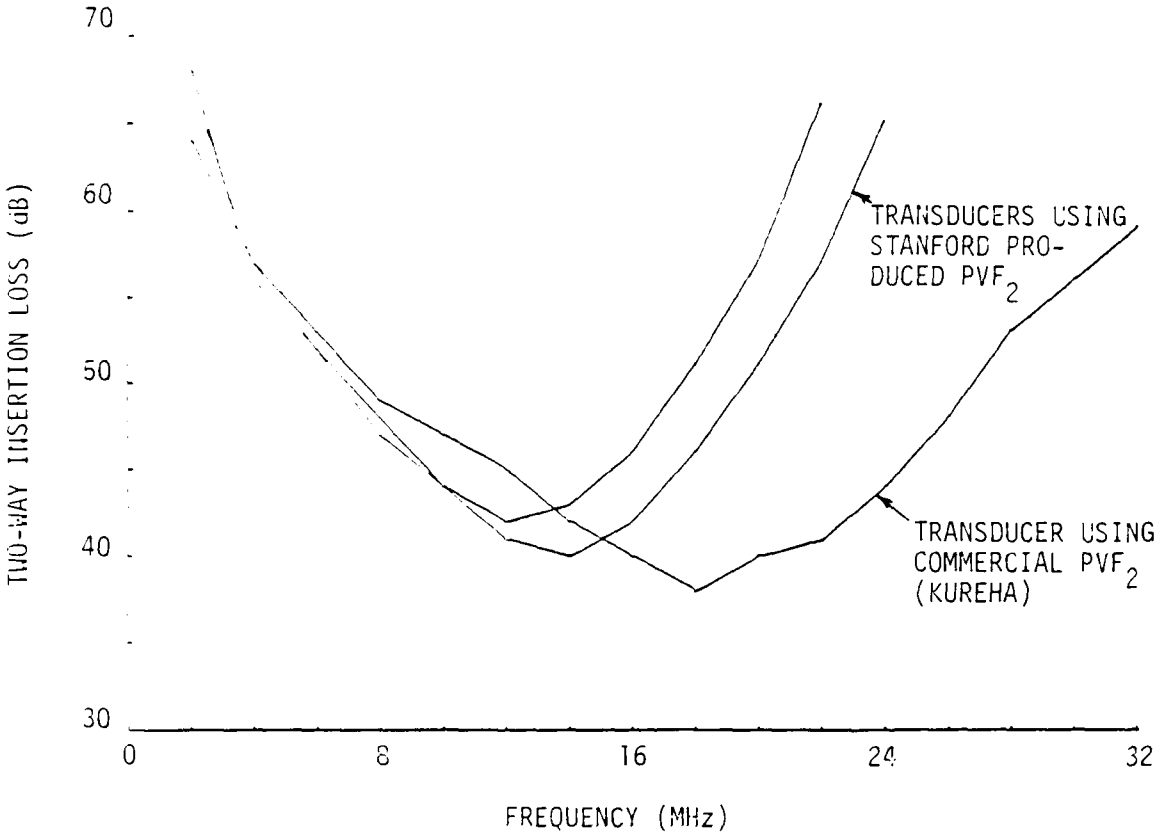

Fig. 28--Measured two-way insertion loss curves for transducers using Stanford and Kureha films.

We are interested in this subject because a small amount of these defects favor the production of the piezoelectrically active beta phase PVF_2 as opposed to the inactive alpha phase PVF_2. The synthesis program at Stanford has been examining the defect count of commercially available resins and is attempting to find the defect count that gives the optimum PVF_2 film.

This program has succeeded in synthesizing research quantities of PVF_2 from the monomer and is working on improving the process. One aim of this work is the development of PVF_2 with improved piezoelectric strength.

AD-A107 642 STANFORD UNIV CA EDWARD L GINZTON LAB OF PHYSICS F/G 20/3
PIEZOELECTRIC PVF2 POLYMER FILMS AND DEVICES.(U)
NOV 81 D G WEINSTEIN, H J SHAW N00014-77-C-0582
UNCLASSIFIED GL-3355 NL

2 OF 2
AD A
107642

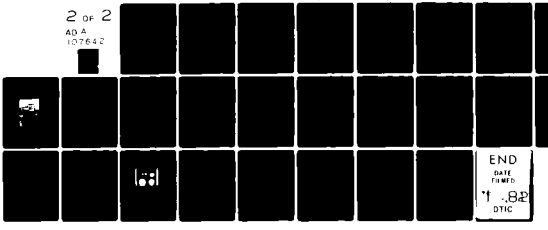

VIII. PVF_2 IMAGING ARRAYS

A. INTRODUCTION

In this section we apply the properties and techniques, developed in the preceding sections on bulk wave transducers, to the field of acoustic imaging. We describe a fully operational multielement ultrasonic imaging array using photolithographic integrated circuit techniques, and taking advantage of the unique combination of extreme accuracy and simplicity made possible through the use of PVF_2 film.

The system uses a phased array approach applied to a linear array of radiators. The array was tested in several ways. The uniformity of the individual elements was found to be excellent. The array was operated as a transmitter and used to image a test pattern placed in a water tank. The array was operated with an f-number of five. The focused beam was electronically scanned in one direction and mechanically scanned in a perpendicular direction, so as to produce a two-dimensional image. The resolution of the array measured during an actual 2-D imaging experiment was very close to the theoretical limit. The line response of the beam was also measured and found to be in excellent agreement with the calculated line response.

All critical tolerances are handled in the production of the deposition mask, which is easily done by photoreduction, while all bulk assembly operations are noncritical. The active array elements and the electrical connections to them are all made in one single deposition. Immediate extension to arrays having an arbitrary larger number of elements would be straightforward.

The sensitivity of PVF_2 arrays, although lower than that of PZT arrays, is adequate for a large number of purposes in nondestructive testing and related fields. It is expected that arrays of this type will find application in practical systems, where their high accuracy and low cost will be of importance.

B. TYPES OF IMAGING SYSTEMS

Acoustic imaging refers to the use of acoustic waves to "see" objects much as we perceive objects using electromagnetic waves and our eyes. However, acoustic waves can travel through many optically opaque materials. The transmission of these waves depends on structural properties of the test material. These properties, such as the density, sound velocity, and stiffness, are often of more interest than the optical properties of the material. Thus there are many valid reasons to use acoustic waves to examine test objects.

As early as 1917 Langevin in France used acoustic pulse-echo techniques in order to measure the depth of the ocean. Since that time the use of ultrasonic waves has expanded greatly. At present, ultrasound is employed in the fields of nondestructive testing and medical imaging. Material flaws (inclusions, voids, and cracks) in nuclear power plants and airplane parts are currently of great interest to those engaged in nondestructive testing. In the field of medicine, real time acoustic images of the heart are currently available. An advantage of acoustic waves in this area lies in their relative harmlessness to the patient as compared to x-rays.

There are many types of imaging systems. Many use some form of lens and are analogous to optical imaging systems. Acoustic holograms have also

been produced. The scanning laser acoustic microscope uses a laser beam to measure the pattern of the acoustic waves created by scattering from a flaw.

These various types of devices employ different signal processing techniques. The image information may be gathered point by point, or it may be processed in parallel, in a so-called "staring" system.

Most nondestructive testing and medical imaging systems use frequencies in the range of 1-20 MHz. However, acoustic microscopes operate up to several gigahertz.

In cases where some type of lens is required, several choices are possible. An actual physical lens may be used to provide the necessary time delays. Or, a set of delay lines can be used to accomplish the same task. Also, phase compensation (or phase delay) can be used to achieve the same objective. Chirp focussing is an example of this last type of lens.

Some devices use a single mechanically scanned and focused transducer. For other applications however, it is advantageous to use an array of elements. In order to scan at faster rates many systems use electronic focusing methods that can be scanned at high speeds The high scanning speed possible in electronically scanned systems can greatly decrease the costs of the testing procedure, both in nondestructive testing and medical applications.

The system to be described in this report consists of a one dimensional linear array and a cylindrical physical lens. The signals fed to the array elements are phase delayed so that the beam radiated by the arrays is focused in one dimension. The added action of the physical lens focuses the beam to a circular spot.

The beam is electronically scanned in one direction by quickly shifting the signals driving the elements. In order to produce a two dimensional

picture the array is mechanically scanned in the direction which is perpendicular to the electronic scan direction and parallel to the array face.

The performance of array transducers used in imaging systems is judged using several criteria. These include resolution, bandwidth, field of view, dynamic range, efficiency, uniformity of element response, cross-coupling between elements, and sidelobe and grating lobe levels. These points will be discussed with regard to our array in the following subsections.

C. MATHEMATICS OF IMAGING

Before going on to describe our PVF_2 array, we present a short section of theoretical analysis on the mathematics of simple phased array imaging. Results of this section will be used to compare our experimental results with predicted results. They will also help explain how the array is phase focused.

Consider a one dimensional array of acoustic transducers as shown in Fig. 29. The center-to-center spacing of the elements = d . The element width = ℓ . The total number of elements = N . Thus the total length, or aperture, of the array = $N \times d = D$.

Across the face of the array acoustic waves will be emitted. The magnitude and phase of these waves will vary with position, and can be described by the function $U(x)$. We wish to determine the field developed by the radiating array at a line a distance z from the array.

Starting from Huygen's principle it can be shown that the field developed at the object line is

$$U(x_1) = \frac{1}{j\lambda} \int U(x) \frac{e^{jkr}}{r} dx \qquad (26)$$

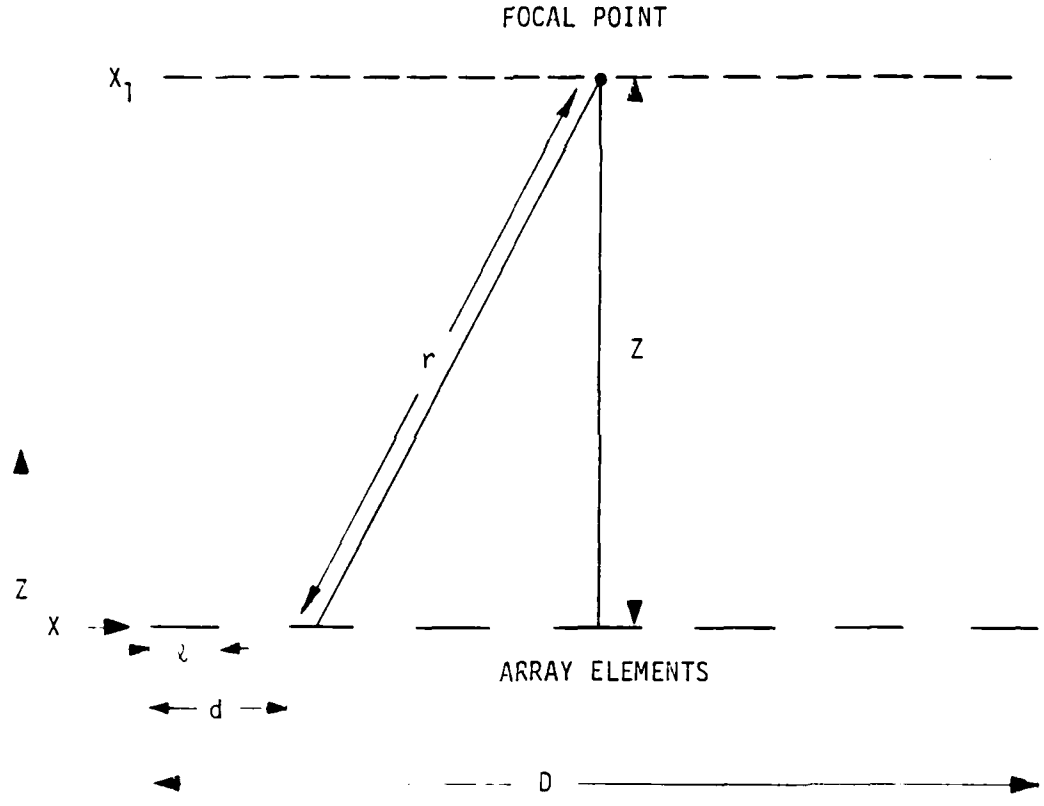

Fig. 29--Schematic diagram of phased array imaging. X is measured along the line connecting the array elements and X_1 is measured along the focal line.

where λ is the wavelength of the acoustic waves and r is as shown in Fig. 29.

The distance from the source points to the field points is r, and

$$r = \left[z^2 + (x - x_1)^2\right]^{1/2} \tag{27}$$

We now make the usual paraxial approximation, assuming that $z >> (x - x_1)$ and say

$$r \approx z + \frac{(x - x_1)^2}{2z} \tag{28}$$

We also replace the r in the denominator of Eq. (26) by z

Then we have

$$U(x_1) = \frac{e^{jkz + (jkx_1^2/2z)}}{j\lambda z} \int U(x)\, e^{(jkx^2/2z)}\, e^{j(kx_1 x/z)}\, dx \tag{29}$$

In many imaging systems, including ours, $U(x)$ is manipulated so that the term $\exp[jkx^2/2z]$ that appears in the integral of Eq. (29) is nullified. This is accomplished by the focusing mechanism of the system. Then the integral is in the form of a Fourier transform. The result is

$$|U(x_1)| \propto \frac{1}{\lambda^2 z^2} \int t(x)\, e^{-(jkx_1 x/2z)}\, dx \tag{30}$$

where $t(x)$ is the transducer shape, in this case, an array of rectangle functions

$$t(x) = \text{rect}\left(\frac{x}{D}\right)\left(\text{rect}\left(\frac{x}{\ell}\right) * \text{comb}\left(\frac{x}{d}\right)\right) \tag{31}$$

The output field is the Fourier transform of $t(x)$.

This can be shown to be

$$\left|U(x_1)\right| \propto \sum_{h=-\infty}^{\infty} \text{sinc}\left(\frac{n\ell}{d}\right) \text{sinc}\left(\frac{Dx_1}{\lambda z} - \frac{nD}{d}\right) \tag{32}$$

There are three main types of imperfections in this response as compared to a perfect impulse response. First, the main lobe has a finite width. It has a full width at its -4 dB points determined by the equation

$$\frac{Dx_1}{\lambda z} = 1 \quad \text{or} \quad \Delta x_1 = \frac{\lambda z}{D} = \lambda f_n \tag{33}$$

where f_n , the f number, is defined as z/D . Thus the resolution of the array is λf_n .

Secondly, there are sidelobes present next to the main lobe of the response. The sidelobes closest to the main lobe are -13 dB below the peak of the main lobe. These are located at a distance approximately $1.5\ \lambda z/D$ from the center of the response.

Thirdly, there are grating lobes which appear due to the discreteness of the array. These grating lobes are spaced in the x direction by a distance

$$\Delta x = \frac{\lambda z}{d} \tag{34}$$

Due to the earlier paraxial assumption, Eq. (34) is only valid if $x \quad z$. The grating lobes can actually be eliminated by moving them beyond the horizon seen by the array. For a system focused directly ahead of the array, choosing $\cdot d$ will eliminate the grating lobes. If the

array focus is being swept across the field of view the grating lobes will be eliminated when $d < \lambda/2$.

Since the resolution of a phased array is equal to λf_n it is advantageous to employ elements which have the ability to receive and transmit at large angles, as this allows the f number to be lowered, thus improving the system resolution.

Now consider a single rectangular radiating element of width w and an infinite length. Suppose that it is radiating bulk longitudinal waves of wavelength λ into an acoustic load. The far field radiation pattern is a scaled version of the Fourier transform of the aperture.[29] Therefore,

$$|U(\theta)| \propto \sin[\pi w \sin \theta/\lambda]/(\pi w \sin \theta/\lambda) \qquad (35)$$

where θ is the observation angle *from the normal* to the transducer. The equation above shows that if w is large compared to λ , the angular radiation pattern of the elements is small. To obtain a 30 degree angular width (to the 4 dB points) w must be smaller than λ . Most acoustic arrays operate with $w < \lambda$ without much trouble. Elements that are 10 mils wide allow operation in water up to 6 MHz before $\lambda = w$.

When used as receiving transducers, slotted array elements will have angular response patterns identical to their transmit responses. This is a consequence of the well known reciprocity theorem.

We have shown that acoustic beams focused under the conditions assumed have widths of λf_n , and that grating lobes are completely eliminated if $d < \lambda/2$. Sidelobes associated with the mainlobe are -13 dB lower than the main response in amplitude.

It has also been shown that acoustic array elements must be small in size (compared to an acoustic wavelength) if the elements are to have a

wide angular response as either receivers or transmitters.

D. DESIGN AND CONSTRUCTION OF THE PVF_2 BULK WAVE IMAGING ARRAY

Acoustic arrays are currently used to produce images for both industrial and medical applications. At the present time most of the arrays use PZT as their piezoelectric element. We have carried out the design and construction of an initial PVF_2 imaging array. The substitution of PVF_2 for PZT presents new tradeoffs and advantages in the construction and operation of an acoustic array. The purpose of this research was to explore these factors.

1. Description of the Physical Features of the Array

In this section we will describe the array dimensions and its physical characteristics. In later sections we discuss why we chose particular designs, and how the array was constructed.

Figure 30 is a schematic side view of the array. The individual elements are defined by deposited thin film electrode strips which are indicated in cross section by the dashed lines. They are deposited on a polished epoxy substrate.

The uniform PVF_2 film is electroded on one side only, (the bottom side in Fig. 30) with an electrically grounded, uniform electrode. The PVF_2 film is 25 microns thick with a 1" x 1" uniform electrode (50 Å Cr + 1000 Å Au) on one side. The non-electroded side of the film is in contact with the array pattern. We have shown in experiments with bulk wave transducers that there is no degradation of performance as a result of placing the counter electrode on the substrate, where it is separated from the PVF_2 by a thin layer of epoxy.

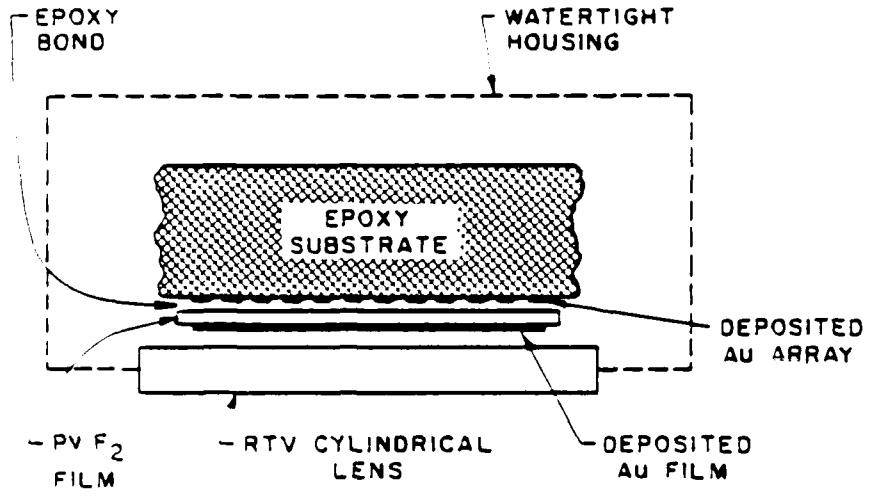

Fig. 30--Schematic cross-section of imaging array.

The substrate is a molded block of epoxy. The epoxy substrate is DER 332 resin with MPDA catalyst. It is 4" x 5" x 1", with one face having been lapped and polished before the electrode was deposited.

Figure 31 is an enlarged photo of the electrode pattern. The electrodes are parallel strips of 1000 Å gold on top of a flash of chrome. The finger widths and spacings are 5 mils, (.127 mm) and the finger length is 1 inch. There are a total of 80 identical electrodes, 40 of which connect to the electrically isolated bonding pads. The total array width is then 800 mils (20.3 mm). The remaining 40 elements are directly joined to the ground electrode which surrounds the entire pattern. A fan out from the active elements to the large bonding pads is included directly on the mask, so the leads can be easily connected to the external electronics.

To complete the structure, the array is enclosed in a watertight housing with a window in the form of a cylindrical lens. A lucite frame is epoxied against the substrate, surrounding the PVF_2. A cylindrical lens (focal length = 10 cm.) made of RTV silicon rubber is clamped in the lucite frame. Castor oil is used to couple acoustically between the PVF_2 and the lens.

Figure 32 is a photo of the principal parts of the array, shown unassembled.

2. Design Considerations

The most important point about our PVF_2 array design is that it uses photolithography to define the array elements. This allows us to take advantage of the ease of construction and simple mass replication capabilities of the photolithographic techniques commonly used in the electronics industry. We made this design choice specifically because we thought it would lead to easy, accurate construction. The choice was possible because

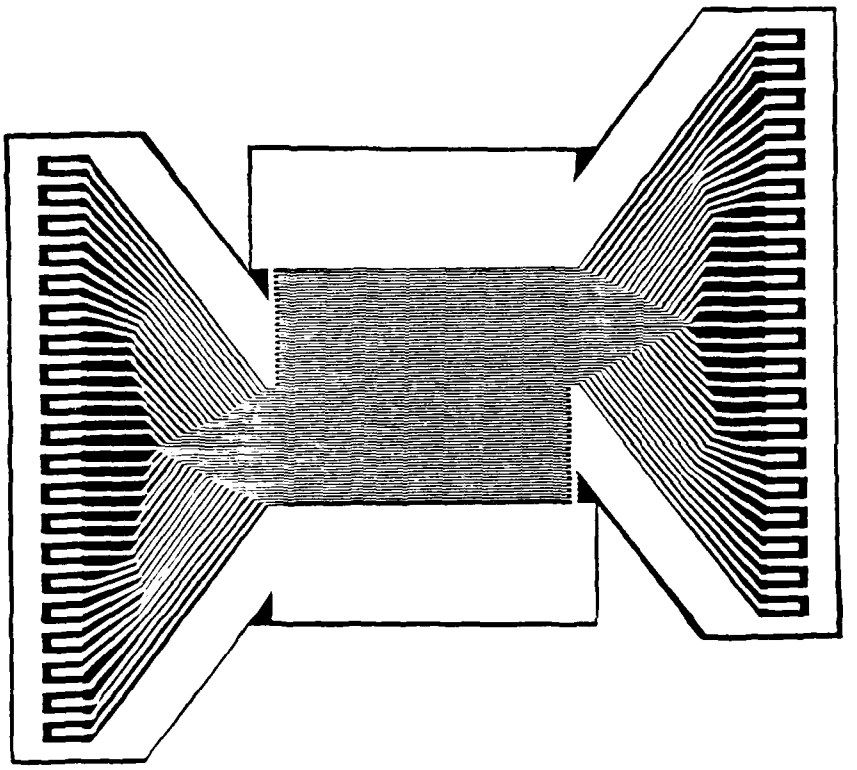

Fig. 31--Enlarged photo of deposition mask. Smallest line widths and spacings are 5 mils.

Fig. 32--Photo of nonassembled array parts.

of the unique physical properties of PVF_2.

In contrast to this, PZT arrays are usually slotted in order to define their array elements This is done in order to reduce acoustic and electrical cross coupling between elements. Such acoustic cross coupling occurs when sound waves reverberate in the PZT and scatter along the array, inducing electrical signals as they strain the PZT. Electrical cross coupling takes place when the high dielectric constant of the PZT ($\sim 830\ \varepsilon_0$) allows electrical signals on one element to induce signals on adjacent elements. Both these kinds of cross coupling degrade the imaging properties of the array. Cross coupling makes the array elements appear wider than they are, as erroneous signals propagate down the array. This effect can also seriously degrade the radiation patterns of the individual elements. A focused beam formed by an array consisting of such coupled elements can have high sidelobe levels and a larger beam spot size than for the uncoupled element case.

Slotting of a PZT slab plus matching layers is difficult and often leads to nonuniform element response. Slight variations in the depth of the slot cuts will introduce these element-to-element differences. These variations will also harm the quality of the images produced by the array. They also make electrical tuning of the elements a slow, tedious process, since each element must be tuned individually.

It is possible to avoid slotting the PVF_2 array because acoustic cross coupling is inhibited by the low mechanical Q of the PVF_2.[30] Electrical cross coupling is not as severe in PVF_2 as in PZT, because the low dielectric constant of PVF_2 ($8\ \varepsilon_0$) impedes electrical cross-talk between elements. Electrical cross coupling is also suppressed in our design by including ground electrodes on the deposition mask.

Furthermore, in part due to the low acoustic wave velocity of PVF_2, the acoustic elements have a fairly small thickness of 25 microns (1 mil). Thus they are five times as wide as they are thick. This ratio is large enough to allow the use of the thin disk model calculations described in Section IVB. Since the device is not slotted, there are no problems with lateral mode resonances interfering with the thickness mode resonances. This is another simplification arising out of our design.

Once we had decided to use photolithography to define the elements, we had another design choice. The most straightforward route was to deposit the electrodes directly on the PVF_2 surface. However, the state-of-the-art for accurate photolithography of multielement arrays directly on PVF_2 with good yield was not well developed. (PVF_2 is a difficult substrate, compared to say, silicon). Thus depositing the electrodes on the array backing, and then epoxying the bare side of the PVF_2 film against the electrodes was a preferred procedure. As stated before, we knew that a thin layer of epoxy between the electrodes and PVF_2 would not be harmful.

After this decision had been made the choice of backing materials was limited somewhat. For one, the substrate can not be a conductor since the array elements must be operated at different potentials during imaging.

The eventual choice was an epoxy backing which offered several favorable features. The material could be easily worked and accurately polished so as to insure high resolution, high yield photolithography. The low acoustic impedance (3.2) of the epoxy we used is also advantageous. As shown on Fig. 13, a PVF_2 transducer backed by a closely matched impedance will have an extremely large bandwidth. This allowed the array to be operated well below the resonance point of the film ($\sim$ 40 MHz). The large bandwidth would also be advantageous if the array were operated in a pulsed

mode. In that case, the matched backing would produce a very short, compact impulse response allowing excellent axial resolution. The epoxy backing also permits the array to have a wide angular response, as explained in Section VI-C.

The array design as so far described, is very simple and quite acceptable for some applications. However, its dynamic range and sensitivity could be improved by the addition of impedance transformers. These would be located close to the active array elements. These elements have high electrical impedances (several thousand ohms at 3 MHz) due to the combination of the low dielectric constant of PVF_2 and the small element areas.

When the array is in use as an acoustic transmitter, transformers will improve the transfer of electrical power from the power source to the array elements by impedance matching between the high impedance elements and the lower impedance signal lines (typically 50 ohms). This will increase the power output into the acoustic load.

For good sensitivity as an acoustic receiver the elements should be connected to amplifiers with high input impedances (high meaning large compared to the element impedances). Thermal noise considerations alone call for the highest impedance achievable in order to obtain the best signal-to-noise ratio. However, other sources of noise, such as transistor and coupled noises would be made worse by a high amplifier input impedance. Accordingly, there will be an optimum value of amplifier impedance that will result in the best signal-to-noise ratio.

We have not yet used either transformers or receiving amplifiers in our array. However, in order to derive the benefits of impedance matching listed above, the array housing was designed in such a way as to allow the addition of small toroidal transformers or IC preamps close by the array elements.

After the specifications of the necessary transformers and preamps have been calculated, impedance matching can be implemented in the allocated space.

3. Construction of the Array

Construction starts with the casting of the epoxy backing. The backing is then machined to the proper size. Next, one of its 4" x 5" faces is lapped and polished. The liftoff technique is used to deposit the electrode pattern on the polished face. The films deposited are 50 Å of chrome, followed by 1000 Å of gold.

Then the PVF_2, electroded uniformly on one side, is epoxy bonded on top of the electrode pattern. The lucite frame is then bonded around the PVF_2. The RTV-615 cylindrical lens is placed on the lucite frame. Leads are easily soldered from the array bonding pads to circuit boards within the array housing. The bonding pads are quite large, being 2 mm x .4 mm. This allows us to avoid the tedious bonding operations which are usually performed under a microscope during the construction of PZT arrays. Miniature coax cables travel from the pads to the controlling electronics.

This construction procedure requires no critical alignments during fabrication. This applies to alignment of the electrode mask on the substrate, and to alignment of the PVF_2 film, which can rotate or translate slightly during bonding without harm. Construction is simple to carry out, requiring only a few hours time. Three copies were made at the outset without difficulties.

Construction is completed by the addition of an aluminum watertight frame which encloses the entire structure, except for a sealed opening for the coax cables.

4. Conclusion

A PVF_2 acoustic imaging array has been constructed. The linear array elements are defined by electrodes deposited on the array backing using photolithographic methods. The fabrication procedure greatly simplifies the time and effort needed to construct the array compared to construction of standard slotted PZT arrays. A cylindrical lens made of RTV-615 is used in conjunction with the array elements to produce a focused beam.

E. EXPERIMENTAL IMAGING RESULTS

We have performed some initial tests on the array. First, calibration tests to measure array characteristics that are basic to its performance in any of various possible imaging configurations. Secondly, an initial imaging experiment using one particular configuration and a simple test pattern.

We will also first describe the electronic set-up used to control the system during these tests.

1. Array Electronic System

Figure 33 is a schematic of the relevant portion of the electronic system used to test the array. This system was developed under other programs in the lab. It was designed and tested by K. Bates,[31] and has since been expanded, upgraded and used with a variety of PZT arrays by K. Fesler. A multilevel digital section, referred to as a digital delay line, allows the operator to choose the amplitudes and phases of the cw rf signals in each of 128 separate channels. The amplitudes and phases are controlled by a microcomputer. Only certain quantized values of phases and amplitudes may be chosen. There are 16 available phase values, spaced by $2\pi/16$

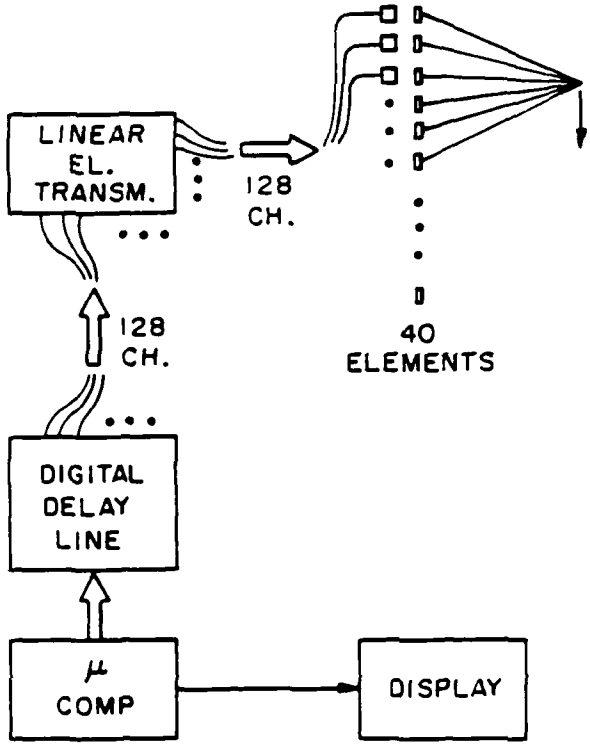

Fig. 33-Block diagram of electronic control system.

radians from each other. There are also 16 available amplitude levels. The largest provides an open circuit output of $\sim$ 15 volts, with the other values being linearly spaced from 15 volts down to 0 volts. The PVF_2 array makes use of 40 of the 128 total channels.

The system was designed to operate between 1 MHz and 10 MHz. We chose to perform our experiments at 2.25 MHz. The system had already been used at this frequency during tests of PZT arrays. Therefore we knew it was operational at 2.25 MHz. As the PVF_2 array was resonant in a $\lambda/2$ mode its resonant frequency was 40 MHz, well above the frequency used in the tests. Operation closer to the array resonant frequency will improve the dynamic range of the device.

The phases applied to the elements in order to produce a focused beam were determined by calculating the distance from each element to the spot where the beam was to be focused. This distance, d, also shown in Fig. 34, was then divided by λ and the remainder was recorded. In other words, dmod λ was calculated. If the remainder was 0, the phase level applied to that particular element was 0. If the remainder was $(1/2)\lambda$, the phase level applied to the element was 8, because phase level 8 is π radians, or $(1/2)\lambda$ ahead of phase level 0 in our system. As stated above there were only 16 possible phases to choose from. Since the exact phases needed to focus the beam were never exactly equal to the available phase level, that phase is chosen which is closest to the desired phase. This quantization of phase levels introduced only small aberrations in the beam shape and sidelobe levels, because there was a fine scale of quantization.[32]

The paraxial approximation was not used because the beam was sometimes scanned over a large angle and thus the approximation was not valid. Besides this fact, the method described above is more accurate than the paraxial

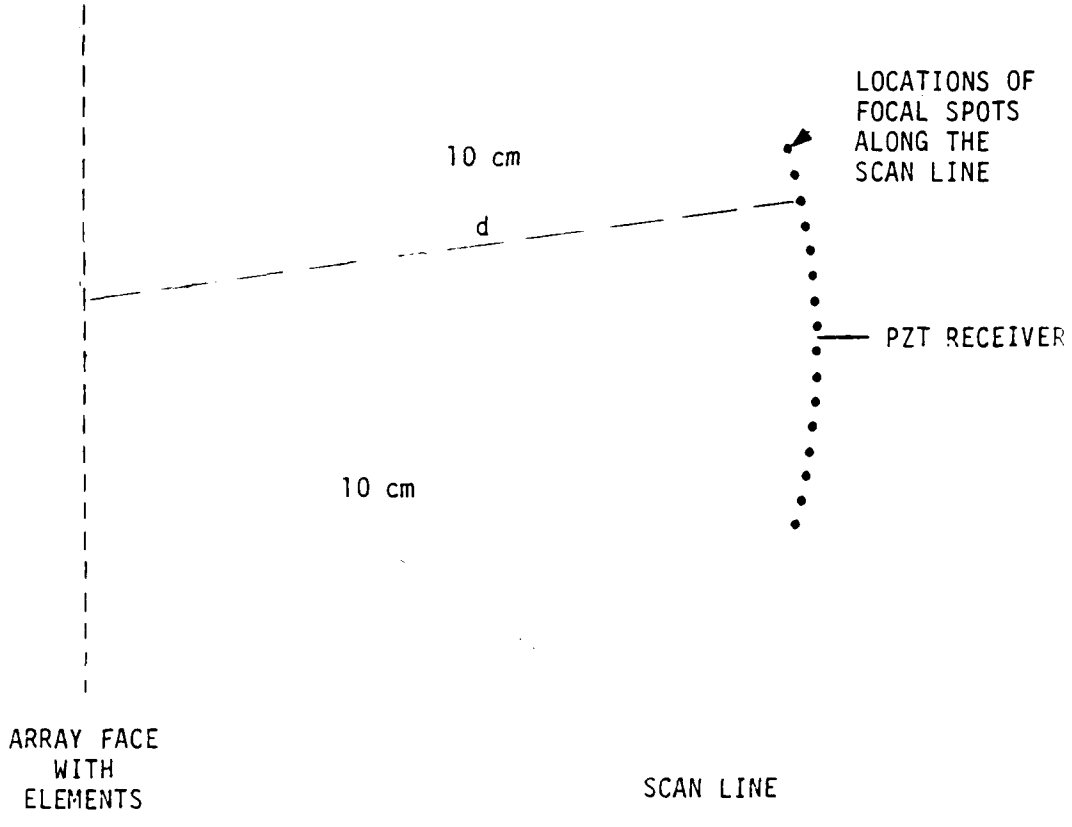

Fig. 34--Relative positions of the array, PZT receiver and image spots (not all shown) showing how the focal spot was scanned. Also shown, as an example of how the phasing information is calculated is the distance from an array element to a focal spot.

approximation even when the approximation is valid, and it is readily carried out on the microcomputer.

The 40 phases needed for focusing the beam at a particular spot in space were calculated for 100 equally spaced points lying on an arc of 10 cm radius centered at the middle of the array seen in Fig. 34. The phase information was stored before the scan was performed and fed to the computer when required.

The electronic system was not able to operate in a receive mode at the time of our experiments. Thus the array was operated as a transmitter.

2. Calibration tests

The first calibration test was that of element uniformity. This experiment was performed in a water tank, as were all the tests described here. The elements were first individually tested for acoustic response. A tone pulse at 2.25 MHz was applied to a single element while a small PZT transducer located 10 cm away measured the strength of the transmitted acoustic signal. The uniformity of the array was excellent. Thirty-nine of the elements were virtually identical in their acoustic output, falling within .3 dB of each other. (One channel in the electronics system was shorted and could not be used.) This level of uniformity is difficult to achieve with ceramic slotted arrays in which the element response is crucially dependent on the depth of cut.

The next calibration test was the measurement of the system point spread function. The width of this function is a direct measure of the focused beam width. (Here we will define the beam width as the full width at the half power points.)

This experiment was performed with the array transmitting into a water tank. The system was operated with an f number of 5 (the array aperture was 2 cm; the focal length was 10 cm). The voltage amplitudes applied to the array elements were constant from element to element and from scan to scan. The focused beam was swept in the 10 cm sector scan arc described earlier and shown in Fig. 34. The figure shows how 100 discrete points along the arc were imaged. The acoustic receiver was a .375 mm x 12 mm PZT transducer. The beam was swept across the face of the receiver. The small width of the receiver (.375 mm) relative to the beam size (several mm) meant that we did not have to perform a deconvolution of the measured point response with the receiving aperture.

Because the paraxial approximation was not used, the beam shape was not exactly that predicted in Section VIII-C. Furthermore, since the beam was scanned in an arc rather than being swept in a line, the array face was not exactly perpendicular to the beam direction. This aspect of the set-up also was not in agreement with the analysis of Section VIII-C. However, the data presented here were taken at small angles relative to the normal of the array face. In this case the formulas of Section 4C can be used without introducing any large errors.

The experimental line response is shown in Fig. 35. The line response has approximately classical shape, with a beam width of 3 mm, as expected from Eq (33). Also shown is the theoretical line response, $\mathrm{sinc}(Dx/\lambda z)$, with $D = 1.98$ cm, $\lambda = .066$ cm, and $z = 10.0$ cm. There is excellent agreement between theory and experiment.

3. Imaging Test

Following the measurement of the point spread function we performed an imaging experiment. The experiment was designed to be a test of the

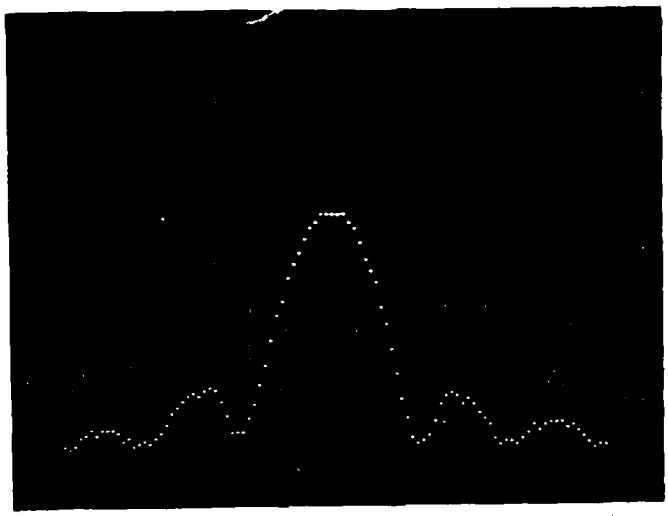

EXPERIMENTAL

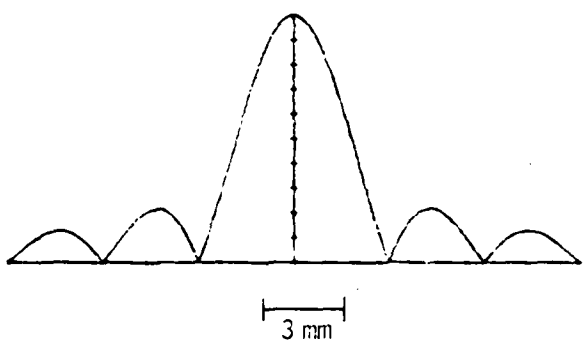

CALCULATED

Fig. 35--Line response function, both calculated and measured.

array under actual two dimensional imaging conditions. This was not an attempt to perform a nondestructive test measurement, but rather an initial test to further characterize the system using a test pattern.

The results obtained were taken with the system using the acoustic beam geometry of Fig. 36. Because we sector scanned the beam in an arc we required a set-up which compensated for the changing beam direction. A large, flat receiving transducer placed behind the objects to be imaged would not have produced the desired results. This is due to the fact that the phase fronts of the beam would have been constantly changing their direction relative to the face of the receiver as the sector scan progressed. Figure 37 shows this effect. When the incident phase fronts were aligned with the receiver a large signal would be produced. But as scanning misaligned the two, the output signal would have decreased, independent of any other effects. Thus some type of lens or shaped reflector is needed to provide a uniform field of view when a single localized receiving transducer is used.

This was provided by the set-up of Fig. 36. The beam scans in the plane of the paper. A cylindrical aluminum reflecting surface sends this sector scanning beam back to a small strip receiver located below the array. Because the receiver is quite small (.375 mm x 12 mm) no phase front alignment problems arise. Absorbing objects placed at the reflector surface are then imaged directly in an amplitude imaging mode. The array and reflector are mechanically tied together as a single assembly. Two-dimensional imaging is obtained by translating them as a single unit, perpendicular to the plane of the paper while the specimen remains fixed.

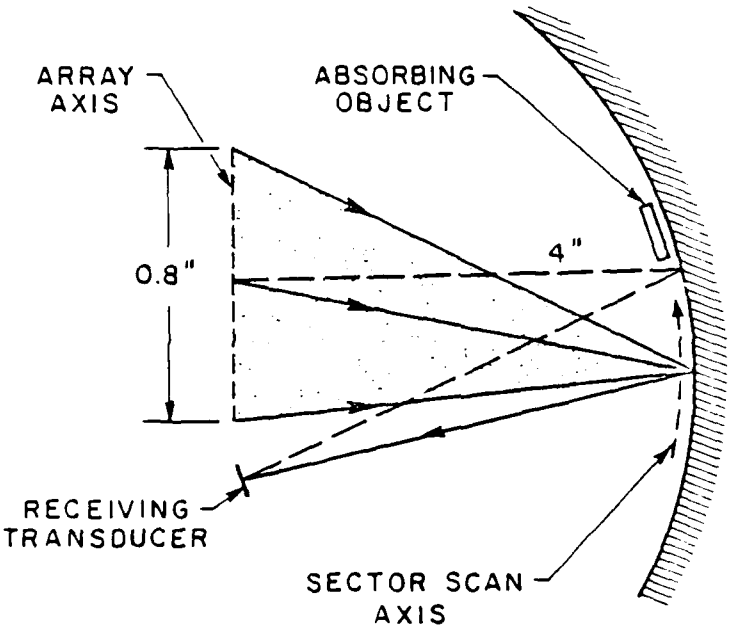

Fig. 36--Schematic of test set-up
for sector scan imaging.

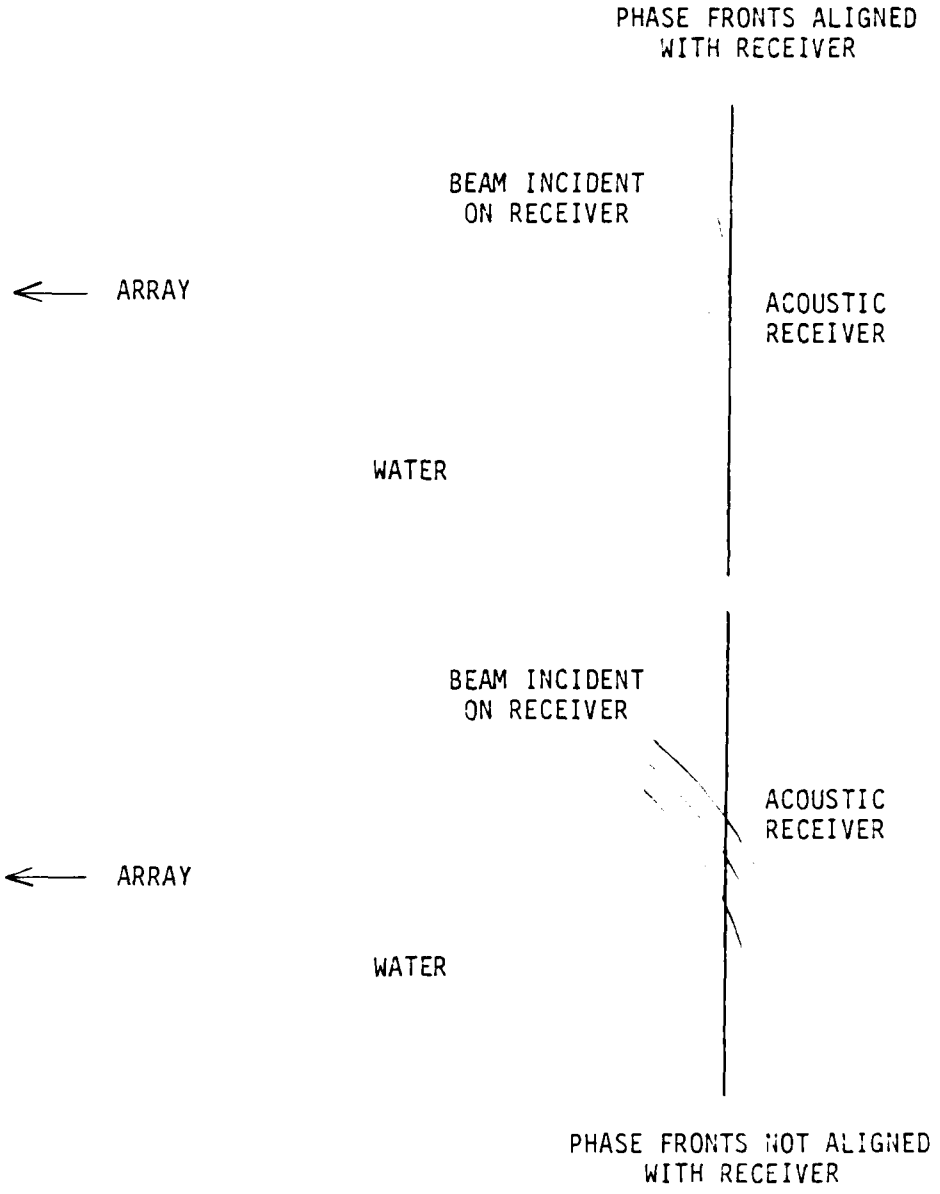

Fig. 37--Diagram showing both aligned and mis-aligned acoustic beam fronts incident on an acoustic receiver.

Figure 38 is a photo of the image of 5 rubber disks, having diameters of 12 mm, 9.5 mm, 6.4 mm, 3.2 mm and 3.2 mm. The separation of the edges of the two 3.2 mm disks was 3.2 mm. The acoustic wavelength in water at the operating frequency of 2.25 MHz is .67 mm, or about 1/5 of the diameter of the smallest disks. A small amount of signal processing was applied to the image. System variations in received beam intensity as a function of position along the electronic line scan direction (vertical) were removed by using the first few line scans to normalize all other line scans.

The theoretical resolution of the array is given by Eq. (33) as $\Delta x = (\lambda z/D)$, which equals 3.3 mm in this case. The 3.2 mm disks seen on the figure are clearly resolved. Thus the experimental result corresponds to the theoretical prediction.

Several general comments may be made regarding the results presented here. To begin, the dynamic range of the system can be estimated from the image of Fig. 38 and the point spread function of Fig. 35. In Fig. 35 the near-in sidelobes lie 13 dB below the peak of the response, while the extreme sidelobes are 18 dB below the peak. There is very little noise present on the response.

We have made an estimate of the noise level present on the sidelobes and compared this to the mainlobe peak response. The result is a dynamic range of 35:1, or 30 dB. In any case, the dynamic range of the array is large enough to allow useful imaging in a large number of cases of practical interest.

We should also like to mention that the field of view of the array can be increased in a straightforward manner. It can be easily demonstrated that the one dimensional fan-out of the array electrodes to the bonding pads can be replaced by a two dimensional stagger pattern that would allow unlimited

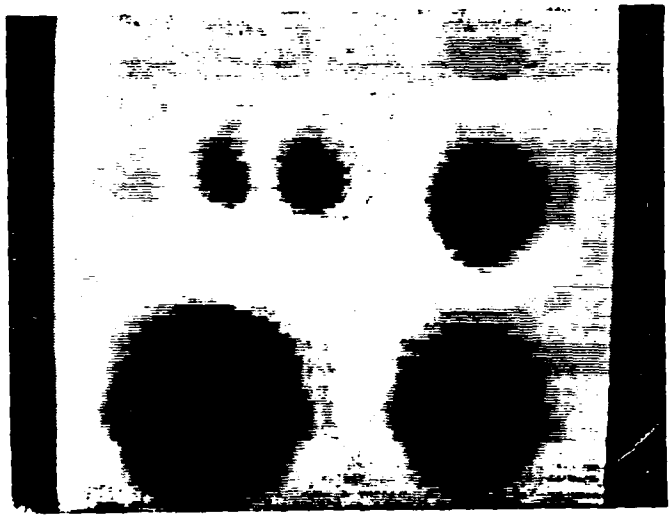

Fig. 38--Experimental images of flat rubber disk test objects. Disk diameters were 12.7 mm, 9.5 mm, 6.4 mm, 3.2 mm and 3.2 mm. The two 3.2 mm disks were separated by 3.2 mm edge to edge.

increase in the number of active array elements. This would not only increase the field of view of the array, but would also allow other, simpler scanning methods to be used.

For instance, a linear scanning mode could be employed, rather than the sector scan mode that we used in our experiments. In a linear scan only some of the active array elements radiate at any instant. These elements, which are located next to each other, produce a focused beam in the acoustic load. The beam is scanned in a straight line by successively stepping the acoustic beam profile one element at a time along the array.

In contrast to the sector scan approach, this method can be used with a large, flat acoustic receiver since the transmitted beam is always normally incident on the receiver. Furthermore, the calculation of the phase delays needed to focus the beam is quite simple, since the beam is always focused in the same place relative to the elements which are transmitting. This often allows faster scanning rates than are possible with sector scanned methods.

4. Conclusion

The PVF_2 imaging array has been tested in several ways. The uniformity of the individual elements was measured and found to be excellent. The array was also operated as a transmitter and used to image objects placed in a water tank. The array was operated with an f number equal to five. The focused beam was electronically scanned in one direction and mechanically scanned in a perpendicular direction, so as to produce a two dimensional image. The resolution of the array measured during an actual 2-D imaging experiment was very close to the theoretical limit. The line response of the beam was also measured, and found to be in excellent

agreement with the calculated line response. The tests of the PVF_2 array have shown it to be a dependable device which has a resolution close to the theoretical limit.

REFERENCES

1. Kawai, H., Japan J. Appl. Phys. 8, 975 (1969).
2. Ohigashi, H., J. Appl. Phys. 47, 949 (March 1976).
3. Sussner, H., et al., Phys. Lett. 45A, 475 (1973).
4. Fraser, J., Ginzton Laboratory Report No. 2973, Ph.D. Thesis, pp. 46-59 (May 1979).
5. Bui, L., Shaw, H.J., and Zitelli, L., Electronics Lett. 12, 393 (1976).
6. Bui, L., Shaw, H.J., and Zitelli, L., IEEE Trans. Sonics and Ultrasonics, SU-24, 330 (September 1977).
7. Solet General Information, Solvay and Cie Societe Anonyme, Brussels, Belgium.
8. Papadakis, E.P., J. of Adhesion 3 (1971).
9. Auld, B.A., Acoustic Fields and Waves in Solids, Vol. 1 (John Wiley and Sons, New York, 1973), pp. 326-336.
10. Sussner, H., Horne, D., and Yoon D., "A New Method for Determining the Pyroelectric Coefficient of Thin Film Polymer Films Using Dielectric Heating," IBM Research Laboratory Report, San Jose, CA (October 17, 1977).
11. Callerame, J., Tancrell, R., and Wilson, D., 1978 Ultrasonics Symposium Proceedings, p. 117.
12. Callerame, J., Tancrell, R., and Wilson, D., 1979 Ultrasonics Symposium Proceedings, pp. 407-411.
13. Auld, B.A., Acoustic Fields and Waves in Solids, Vol. 2 (John Wiley and Sons, New York, 1973), p. 318.

14. Kepler, A., and Anderson, R.A., J. Appl. Phys. 49(3), 1232 (1978).

15. Stanke, F., private communication.

16. Chou, C.H., Bowers, J., Selfridge, A., Khuri-Yakub, B.T., and Kino, G.S., 1980 Ultrasonics Symposium Proceedings, pp. 984-987.

17. Linvill, J., Stanford Electronics Laboratories Report No. 4834-3, page 71 (1978).

18. Omoto, R., private communication.

19. Bacon, D., 1980 Ultrasonics Symposium Proceedings, pp. 582-585.

20. DeReggi, A., and Harris, G., 1980 Ultrasonics Symposium Proceedings, pp. 598-599.

21. Auld, B.A., Drake, M., and Roberts, C., Appl. Phys. Lett. 25, 9, 478 (November 1974).

22. Whitman, R., Ahmed, A., and Korpel, A., Acoustical Holography (Plenum Press, New York, 1972), Vol. 4, p. 11.

23. Jacobs, J., IEEE Trans. Sonics and Ultrasonics, SU-15, 146 (July 1968).

24. DeSilets, C., Ginzton Laboratory Report No. 2833, Ph.D. Thesis, pp. 135-150 (June 1978).

25. Chen, W., Shaw, H.J., Weinstein, D., and Zitelli, L., 1978 Ultrasonics Symposium Proceedings, pp. 780-783.

26. Hunklinger, S., Sussner, H., and Dransfeld, H., Festkorperprobleme XVI, (1976), pp. 267-291.

27. Auld, B.A., Acoustic Fields and Waves in Solids, Vol. 1 (John Wiley and Sons, New York, 1973), pp. 176-182.

28. In the United States: Pennwalt, Polysciences, Aldrich and Kreha; Solvay (Belgium); Dynamit Nobel (Germany).

29. Bracewell, R., The Fourier Transform and Its Applications (McGraw-Hill Book Company, New York, 1965), p. 276.

30. Horvat, P., Gagnepain, J., and Auld, B., 1979 Ultrasonics Symposium Proceedings, pp. 511-514.

31. Bates, K., Carome, E., Fesler, K., Liu, R., and Shaw, H.J., 1979 Ultrasonics Symposium Proceedings, pp. 216-219.

32. Bates, K., Acoustical Imaging (Plenum Press, New York, 1980), pp. 239-263.

33. Fraser, J., Khuri-Yakub, B.T., and Kino, G., Appl. Phys. Lett. 32, 11, 698 (June 1, 1978).

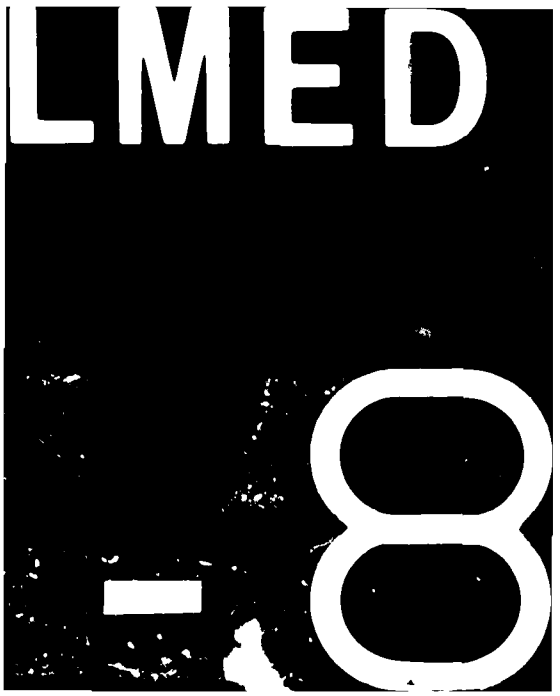
LMED
8